Single-Virus Tracking: From Imaging Methodologies to Virological Applications

Shu-Lin Liu,[#] Zhi-Gang Wang,[#] Hai-Yan Xie, An-An Liu, Don C. Lamb, and Dai-Wen Pang*

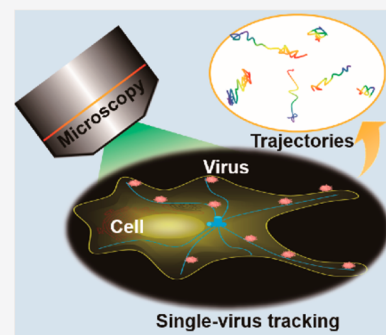Cite This: *Chem. Rev.* 2020, 120, 1936−1979

Read Online

ACCESS | Metrics & More | Article Recommendations

ABSTRACT: Uncovering the mechanisms of virus infection and assembly is crucial for preventing the spread of viruses and treating viral disease. The technique of single-virus tracking (SVT), also known as single-virus tracing, allows one to follow individual viruses at different parts of their life cycle and thereby provides dynamic insights into fundamental processes of viruses occurring in live cells. SVT is typically based on fluorescence imaging and reveals insights into previously unreported infection mechanisms. In this review article, we provide the readers a broad overview of the SVT technique. We first summarize recent advances in SVT, from the choice of fluorescent labels and labeling strategies to imaging implementation and analytical methodologies. We then describe representative applications in detail to elucidate how SVT serves as a valuable tool in virological research. Finally, we present our perspectives regarding the future possibilities and challenges of SVT.
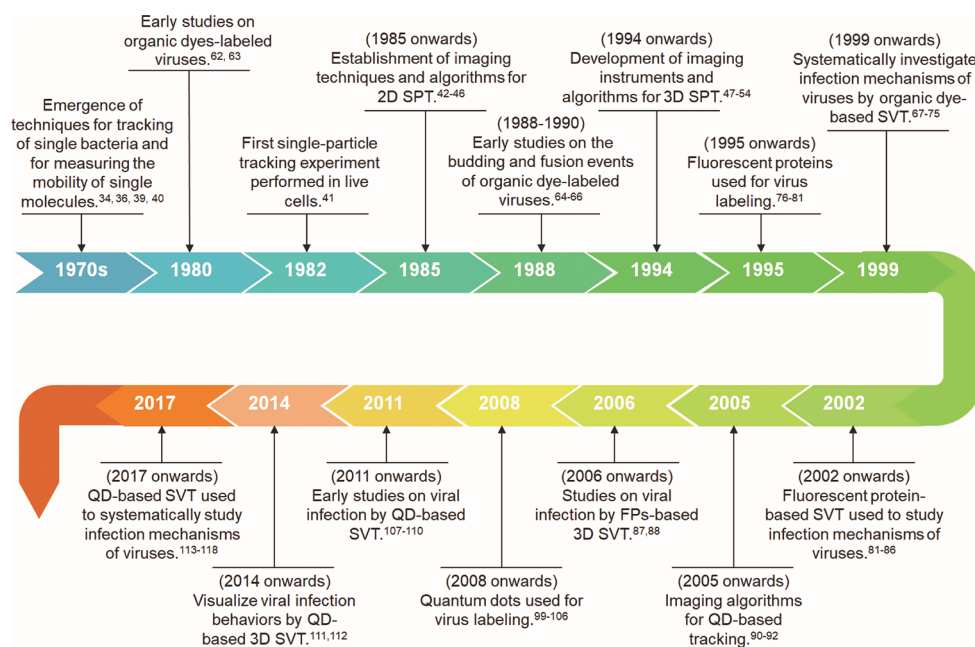
CONTENTS

Figure 1. Timeline of the key developments of the single-virus tracking technique.

1. INTRODUCTION

Viruses are intracellular parasites that rely on host cells for completion of their life cycles. Most viruses are composed mainly of nucleic acids (RNA or DNA), structural proteins (e.g., capsid), and a lipid membrane (for enveloped viruses). The primary function of any virus is to reproduce in host cells. For this purpose, viruses should accomplish two major tasks: (i) to break through the barriers that block virus entry and transport into cell cytosol and (ii) to release their genome at the preferred sites within the cells for viral transcription and replication.[1−4] The newly synthesized viral proteins and genomes are assembled in the infected cells to generate progeny viruses, which are then released to the extracellular space by exocytosis or by lysing the host cells. Additionally, viruses may take different pathways to infect host cells, and the complicated infection processes usually include multiple steps and intricate interactions between viral components and cellular structures.[5−7] Thus, it is important to understand the complicated infection mechanisms of viruses in time and space for fighting against virus infection and preventing viral diseases.

Early researchers mainly utilized transmission electron microscopy (TEM) and biochemical experiments to investigate viral infection mechanisms in cells. TEM has played an essential role in studying the infection pathway of viruses, but it can only acquire static images from the scenario of virus infection in live cells. *In vitro* biochemical experiments commonly use the samples isolated from organisms to conduct ensemble measurements and deduce the effects. Conventional methods lack the ability to acquire dynamic information on individual viruses during the infection process, since the cellular events occur in a stochastic manner across spatial and temporal scales. The biggest challenge is how to realize the visualization of infection processes directly and dynamically in live cells and thereby uncover the mechanisms of infection and proliferation.

Fluorescence microscopy has had a great impact on cell biology ranging from the molecular to the organism scale. Initially, fluorescence was mainly used to visualize the intracellular distribution of proteins in fixed cells via antibodies.[8,9] With improvements in microscopy, it has become possible to measure individual biomolecules as they perform their function in their native environment using single-particle tracking (SPT).[10−17] SPT has successfully solved many basic biological questions and greatly enhances our repertoire of research approaches for investigating, for example, membrane organization,[18−20] protein folding,[21−23] molecular motor dynamics,[24−26] and cell signal transduction.[27−29] Thereinto, single-virus tracking (SVT) allows researchers to follow individual viruses, visualize their transport behaviors, dissect their dynamic interactions with the host cells, and reveal the underlying mechanisms of viral processes.[30−33] In SVT studies, viruses are addressed independently, avoiding ensemble averaging and making it possible to investigate the dynamic behaviors of single viruses in their native, complex surroundings. Thus, time-dependent unsynchronized infection events can be monitored in real time. Hence, the SVT technique is a powerful approach for studying the real-time and *in situ* dynamics of viral processes in live cells, and it is attracting the attention of researchers. Until now, this method has revealed a variety of complicated infection mechanisms of various viruses including the mechanisms of viral entry, trafficking, and egress. SVT has also been used to follow the uptake and cellular distribution of artificial viruses and drug delivery carriers due to their similar nature.

In this review, we will first describe the historical retrospect of the SVT technique, and then discuss the fluorescent labels used for SVT, discuss the advantages and limitations of each kind of fluorescent labels, and describe how to use the fluorophores for virus labeling. Subsequently, we will elaborate on the various approaches for SVT, the imaging instruments, and data analysis methods for accurately extracting the dynamic information on virus infection from live-cell measurements. We then highlight a couple applications of SVT and finally propose the future possibilities and challenges of the SVT technique.

2. HISTORICAL RETROSPECT OF SINGLE-VIRUS TRACKING

Single-virus tracking is a new and growing technique. It originates from single-particle techniques, which have each become a remarkable tool in biological fields. These techniques add new insights beyond conventional ensemble methods by providing dynamic information regarding the biological processes. There are a number of methods used to monitor the mobility of particles including fluorescence recovery after photobleaching (FRAP), fluorescence correlation spectroscopy (FCS), and single-particle tracking (SPT). FRAP was established in the 1970s to measure the mobility of molecules via the recovery speed of fluorescence intensity after photobleaching a given region.[34,35] In the same decade, FCS was developed to detect and analyze the fluctuations of fluorescence intensity caused by fluorescent molecules entering and leaving the observation volume.[36] The dynamic parameters, such as diffusion coefficient and average residence time, could be extracted from the autocorrelation analysis.[37,38] Strictly speaking, FRAP and FCS measure the average behaviors of hundreds or even thousands of molecules, and the geometry of the photobleached volume or the point-spread-function (PSF) of the FCS excitation beam, respectively, needs to be known in detail. These techniques only provide limited dynamic information and do not truly reflect the kinetics of biological processes in time and space on the single particle level. SPT, however, is capable of monitoring the movements of individual molecules directly by optical microscopy, and it can detect subpopulations and event detection changes in diffusional behavior of a single particle. Hence, the technique is appealing for investigating dynamic events in live cells.

SPT dates back hundreds if not thousands of years. Galileo Galilei tracked the moons of Jupiter and contributed data that resulted in overturning the view of the universe at that time. SPT on the microscale began in the early 1970s, when Howard Berg built a microscope for tracking single bacteria.[39,40] The first subcellular tracking experiments were performed at the beginning of the 1980s, when Barak et al. tracked individual low-density lipoprotein (LDL)-receptor complexes in live cells.[41] These measurements opened up a new avenue for studying the dynamic mechanisms of individual biomolecules (Figure 1). Notably, advances in imaging instruments and algorithms greatly improved the imaging speed and accuracy of the SPT technique, which enabled the investigation of more complex processes with a better spatial-temporal resolution.[42−48] Since then, the applications of SPT had a dramatic increase in the biological field. A major breakthrough in three-dimensional (3D) SPT occurred in 1994. Using a modified epifluorescence microscope where a weak cylindrical lens had been placed in the detection path, Kao et al. successfully tracked individual fluorescent particles and determined z positions from the image shape and orientation with a peak detection algorithm.[49] Inspired by this research, many researchers made efforts to develop imaging methods and analyzing algorithms for 3D SPT.[50−57] In recent years, a number of 3D SPT methods have become available to track the dynamic behaviors of biomolecules in the 3D environment. For recent reviews, we refer the reader to refs58−61.

Viruses, due to their small size and the dramatic impact they have on human health, are an important and popular system for SPT experiments. Hence, SPT performed on viruses has

come to be known as single-virus tracking (SVT). Already in the 1990s, SVT techniques began to show their talent at probing the dynamic mechanisms of virus infection. Originally, organic dyes were used to label viruses by antigen−antibody interactions in fixed cells.[62,63] With the emergence and application of fluorescence video microscopy, organic dyes could be used to labeled viruses and the budding and fusion events of enveloped viruses monitored in live cells.[64−66] From the early 2000s, the SVT technique started to play a more and more important role in studying infection mechanisms of viruses.[67−75] One milestone in SVT was the experiments performed by the group of Bräuchle where they could follow the entry of adeno associated viruses labeled with a single organic fluorophore.[69] In live-cell measurements, care has to be taken when labeling viruses to ensure that the labeling does not interfere with the function of the virus and a single fluorophore is the ultimate limit for fluorescent labeling. The laboratory of Zhuang also contributed significantly to SVT with beautiful investigations that visualized the infectious behaviors of viruses and systematically dissected the dynamic mechanisms of virus entry, virus transport, and genome release.[72−74]

Almost contemporaneously, fluorescent proteins (FPs) came to the fore as fluorescent labels in the biological field. The key feature of FPs is that they allow specific cellular or viral proteins to be labeled by genetic engineering. Once a fortuitous location had been determined for virus labeling, it no longer became necessary to check after each sample preparation whether the labeling had affected the infectivity of the virus. For these reasons, the use of FPs emerged in virology and contributed immensely to the study of virus−cell interactions. In 1995, the green fluorescent protein (GFP)[76] was first introduced into the expression cassette of the potato virus X.[77] Subsequently, different kinds of viral components, including envelope protein, tegument, and capsid, were genetically labeled with FPs, and many subsequent attempts were made to monitor individual FPs-labeled viruses in host cells using SVT.[78−81] Especially the visualization of the transport behaviors of FPs-labeled viruses helped to accelerate our understanding of virus entry, fusion, and cell-to-cell transmission of human immunodeficiency virus (HIV).[82−86] Moreover, the advances made in SPT were quickly applied to SVT, and real-time 3D tracking of FP-labeled viruses provided more accurate information regarding viral processes in live cells.[87,88]

As an alternative to organic dyes and FPs, quantum dots (QDs) have also become an important tool for SPT and SVT and are heavily utilized in the fields of biology, virology, and medicine. The excellent brightness and superior photostability of QDs enable them to be tracked for extended periods of time with low laser intensity, making them particularly favorable for acquiring time-series images or z-stacks for 3D reconstructions. In the early 2000s, QDs were first utilized to track glycine receptors on the plasma membrane.[89] This stimulated the application of QDs in the SPT field and triggered the further development of imaging algorithms. In particular, special imaging algorithms were developed that overcome the drawbacks of QDs in SPT experiments, such as QDs blinking.[90−92] After that, QDs-based SPT made great advances in the investigation of dynamic processes occurring on the plasma membrane and in intracellular/intercellular environments.[93−97] In 2008, Joo et al. proposed a site-specific strategy to label the surface of lentiviruses with QDs, which pointed out a new way forward for QDs applications in virology.[98] Diverse

strategies emerged to label different viral components with QDs,[99−106] and QD-labeled viruses were implemented for the long-term tracking of individual viruses during virus infection.[107−110] Additionally, by combining QD-labeling strategies with 3D SVT, viral behavior could be followed over long time scales in three dimensions and new insights gained regarding virus infection.[111,112] These results again ignited the enthusiasm of researchers to study the infection mechanisms of viruses by SVT.[113−118] There is no denying that SVT has greatly improved our understanding of the infection mechanisms of viruses.

3. FLUORESCENT LABELS FOR SINGLE-VIRUS TRACKING

The first step necessary for performing SVT experiments is to label viral components with fluorescent labels. Viruses are typically densely packed structures, and there can be limitations on the size and location of the tags that can be used as to not inhibit the functionality or even assembly of the virus. Hence, particular care needs to be taken in choosing the correct labeling approach and location on the virus, and proper controls need to be performed to verify that the functionality and infectivity of the virus is not hampered. Also, the assembly of viruses occurs directly in the living host cells such that in cellular labeling approaches are needed to visualize the early stages of assembly. These limitations make the labeling of viruses particularly challenging in comparison to the labeling of other objects such as nanoparticles used for therapeutic applications. In addition, one wishes to acquire image sequences with high spatiotemporal resolution and high signal-to-background ratio, which depends on the number and type of fluorescent labels and the imaging instrument. There is an intricate relationship among the optical characteristics of fluorescent labels, the duration of imaging and the spatial resolution and the accessible temporal sampling of imaging instruments. The brighter the labels are, the faster the time resolution can be and the higher the spatial resolution that can be achieved. Moreover, the more photostable the label is, the longer the virus can be tracked. A fluorescent label is evaluated by the relevant spectroscopic features. High brightness is one of the important properties for any fluorescent label, which means that a good fluorescent label should possess a strong ability to capture photons, such as a large molar absorption coefficient and a high fluorescence quantum yield. Meanwhile, the high photostability is the essential property belonging to the good fluorescent labels, which can endure many excitation−deexcitation cycles prior to photobleaching. This is the principal criterion for fluorescent labels used in the SVT field. It should be noted, however, that in some cases, viruses have a large number of components that can be labeled without deleterious effects. For example, the Gag protein of HIV can be labeled with FPs in a ratio of 1:1 without significantly altering its structure and infectivity.[119] As HIV contains approximately 2400 Gag proteins, ~1000 FPs are coupled to a single viral particle and the lower photophysical properties of the FP are compensated for by the sheer number of fluorophores.[120]

There are several types of fluorophores that have emerged for labeling viral structures in the SVT field, including organic dyes, FPs, and nanoparticles (Figure 2). Each type of fluorophore has its advantages and drawbacks that the researchers need to balance according to the requirements of SVT experiments.[121] The focus of this section is to describe
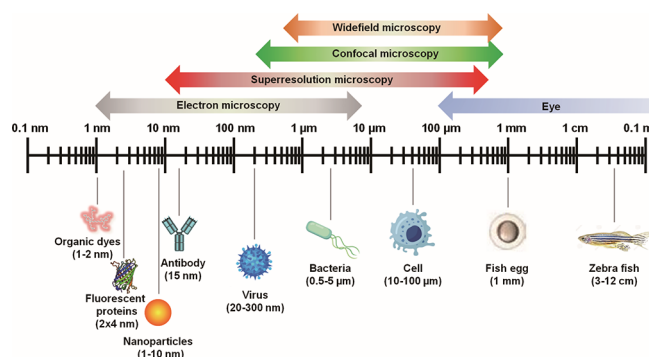

Figure 2. Comparison of the size scales of fluorescent labels and the spatial resolutions of biological imaging techniques.

the recent developments and features of existing fluorescent labels and to highlight the prospective applications for future research in the SVT field.
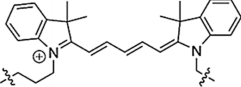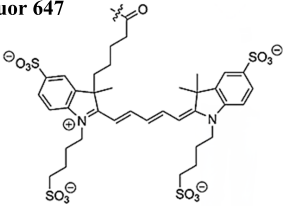
3.1. Organic Dyes

As small fluorescent labels (<1 kDa), organic dyes have proven indispensable for fluorescence labeling of biological systems.[122] The fluorescence properties of organic dyes are governed by both fluorophore structure and chemical environment and can be fine-tuned by elaborate design strategies. Beyond their small size, the major advantages of most organic dyes are their good photophysical properties, commercial availability, the availability of a multitude of reactive groups for various labeling strategies, and the wide spectral range of options.[123] Compared with FPs, organic dyes have several excellent properties, such as higher brightness, smaller size, better photostability, and a wider color palette,[10,122,124] which have been broadly used for single-virus imaging.[31,125−127] According to their inherent nature and characteristics, organic dyes can be classified into three categories for virus labeling: covalent labeling dyes, lipophilic dyes, and intercalating dyes.

3.1.1. Covalent Labeling Dyes. Many organic dyes can be used to bind viral components covalently. During the development of the SVT technique, several families of fluorescent dyes have been used for labeling viruses. The photophysical properties of these dyes for single-virus imaging vary widely. More detailed information regarding the properties of the covalent labeling dyes is shown in Table 1.

Cyanine dyes have received wide attention for biomolecular labeling applications due to their high absorption cross sections, leading to high brightness and photostability. They consist of two quaternized heteroaromatic bases joined by a polymethine bridge. Their emission profiles extend from about 450 to 1000 nm, which can be tuned by the length of the polymethine bridge.[147−149] Cy3 and Cy5 are the most popular cyanine dyes for SVT.[119,129−133] It is worth pointing out that an epoch-making progress happened in 2001,[69,150] when adeno-associated viruses (AAVs) labeled with a single Cy5 dye were tracked in real time to dissect the entry pathway of individual viruses in living cells (Figure 3). The detailed observation and quantitative description of viral behaviors paved a new road to illuminate virus−host cell interactions at single-virus level. Thereafter, the field paid more attention to the use of organic dyes to label various components of viruses for tracking. One also began to use environment-sensitive fluorophores, such as CypHer5, which is a pH-sensitive cyanine dye that has low fluorescence at basic pH and high fluorescence at acidic pH. Based on this property, it was

Table 1. Covalent Labeling Dyes for Virus Imaging

	Cy5							Alexa Fluor 647		

	Color[a]	λ_{ex}[b] (nm)	λ_{em}[c] (nm)	ε_{abs}[d] (M^{-1}cm^{-1})	Φ_f[e] (%)	τ_{fl}[f] (ns)	Sites	Virus	Refs
Cyanine dyes									
Cy3	Orange	550	570	150,000	15	<0.3	Envelope vRNP[g]	IV[h, 68, 128-129]	y
Cy5	Deep red	649	670	250,000	28	1.0	Capsid Envelope	AAV[i,69] SVV[j,130] PV[k,130-131] RABV[l,132] SFV[m,133]	y
CypHer5	Deep red	644	663	140,000	ND[w]	ND[w]	Envelope	IV[68, 128]	y
Alexa Fluor dyes									
Alexa Fluor 488	Green	495	519	71,000	92	4.1	Capsid Envelope	VSV[n,134] SV40[o,135] AAV[136] HPV[p,137]	x
Alexa Fluor 555	Orange	555	572	155,000	10	0.3	Capsid	FMDV[q,138]	x
Alexa Fluor 568	Red	578	603	91,000	69	3.6	Capsid Envelope	MPV[r,139] VSV[140]	x
Alexa Fluor 594	Red	590	617	73,000	66	3.9	Capsid Envelope	VSV[134] SV40[135, 141]	x
Alexa Fluor 647	Deep red	650	665	239,000	33	1.0	Capsid Envelope	CPV[s,142] VSV[134, 140] RV[t,143] SV40[135]	x
Other dyes									
Fluorescein	Green	494	518	75,000	92	3~4	Capsid Envelope	SV40[144] HPV[137]	x
Texas Red	Red	596	615	85,000	ND[w]	4.2	Capsid Envelope	SV40[67] UUKV[u,145] HAdV[v,146]	x
Atto 647N	Deep red	644	669	150,000	65	3.4	Capsid	CPV[142]	z

[a]The color of emitted light. [b]Maximum excitation wavelength. [c]Maximum emission wavelength. [d]Extinction coefficient. [e]Fluorescence quantum yield. [f]Fluorescence lifetime. [g]Viral ribonucleoprotein. [h]Influenza virus. [i]Adeno-associated virus. [j]Seneca valley virus. [k]Poliovirus. [l]Rabies virus. [m]Semliki forest virus. [n]Vesicular stomatitis virus. [o]Simian virus 40. [p]Human papillomavirus. [q]Foot-and-mouth disease virus. [r]Murine polyoma virus. [s]Canine parvovirus. [t]Reovirus. [u]Uukuniemi virus. [v]Human adenovirus. [w]Not determined. [x]Information from Thermo Fisher. [y]Information from GE Healthcare. [z]Information from Atto-TEC.

applied to monitor the viral movements from the plasma membrane to acidic endosomes. The double labeling of viruses with Cy3 and CypHer5 made it possible to simultaneously monitor the transport and acidification processes of viruses.[68,128]

The Alexa Fluor family of organic dyes are synthesized though the sulfonation and modification of certain well-known dye classes such as rhodamine, fluorescein, and cyanine dyes. Due to the sulfonation, Alexa Fluor dyes are normally negatively charged and more hydrophilic than their precursors. With the aid of additional modifications, Alexa Fluor dyes are more photostable and less pH-sensitive than the original dyes.[151,152] In the meanwhile, the emission spectra of the Alexa Fluor series span the visible spectrum and extend into the near-infrared region. These properties make them ideal for investigating the cellular uptake and endosomal transport of viruses. Thus, Alexa Fluor derivatives have been popularly applied to label viruses, including murine polyoma virus (MPV),[139] canine parvovirus (CPV),[142] vesicular stomatitis virus (VSV),[134] simian virus 40 (SV40),[135,141] human

papillomavirus (HPV),[137] foot-and-mouth disease virus (FMDV),[138] AAV,[136] and reovirus (RV).[143] For example, by labeling RV with Alexa Fluor 647, Kirchhausen et al. found that individual RV particles were captured and internalized by clathrin-coated pits and vesicles, illustrating RV required access to endosomes for successful infection.[143] Multiple-color imaging of Alexa Fluor-labeled VSV and a shorter, defective interfering particle indicated that the elongated shape of a VSV particle triggered the recruitment of actin filaments to complete the viral internalization process, and the cargo geometry was important for specifying the entry modes of the viruses (Figure 4).[140]

There are other organic dyes used for labeling viruses such as fluorescein, Atto dyes, and Texas Red. Fluorescein, as a classical fluorescent reagent in biological research, possesses relatively high brightness, strong pH sensitivity, and poor photostability. Owing to the pH-sensitivity of fluorescein, the fluorescence of labeled viruses is quenched and undetectable under acidic conditions. Using the pH sensitivity, investigators could distinguish internalized fluorescein-labeled viruses from
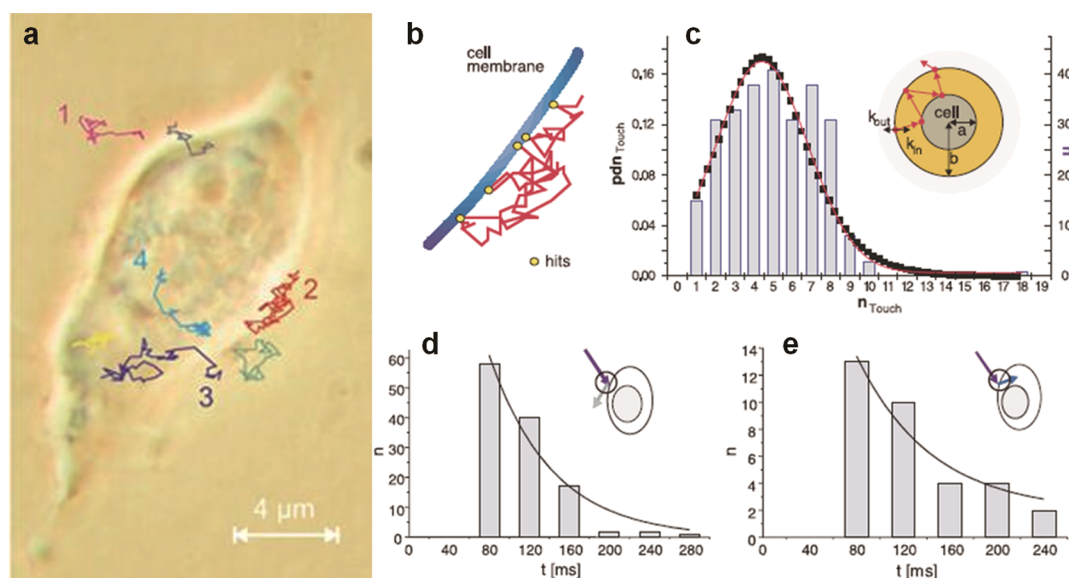
Figure 3. Uptake of Cy5-labeled adeno-associated virus (AAV) by a live HeLa cell. (a) Representative trajectories of AAV particles in cells at different stages of the infection. (b) Zoom in of trajectory 2 showing several membrane interactions of the AAV at the cell surface. (c) Mean number of consecutive cell interactions derived for viruses that did not dock. (d−e) Distribution of adsorption times for (d) 137 nondocking and (e) 42 membrane penetrating trajectories. Adapted with permission from ref 69. Copyright 2001 The American Association for the Advancement of Science.
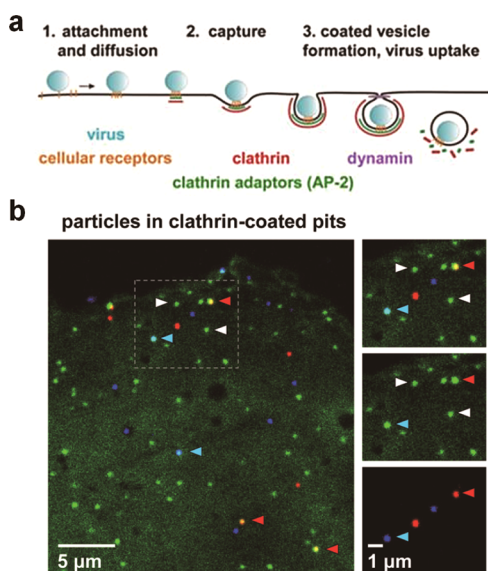

Figure 4. Clathrin structures capture vesicular stomatitis viruses (VSVs) and defective interfering particles (DI-T) with similar kinetics. (a) Schematic of the clathrin-dependent virus internalization pathway. (b) VSVs and DI-T particles captured by clathrin structures in the same cell. BSC1 cells stably expressing s2-eGFP (green) were inoculated with Alexa Fluor 647-labeled DI-T (blue, blue arrowheads) and Alexa Fluor 568-labeled VSV (red, red arrowheads). Adapted with permission from ref 140. Copyright 2010 Public Library of Science.

the extracellular viruses by changing the culture medium to pH 4.0.[137,139,144] Texas Red is a conventional red fluorescent dye, and its derivative, Texas Red-X (TRX) succinimidyl ester, is commercially available and readily reactive for conjugating to viruses.[67,145,146] Monitoring of TRX-labeled SV40 found that SV40 was internalized into cells by caveolae and transported to the endoplasmic reticulum by caveosomes.[67] Atto dyes have enhanced photostability and longer fluorescence lifetime than

either fluorescein or most cyanine dyes, and the emission profiles cover the visible and near-infrared wavelengths. These dyes have been used as fluorescent labels in a wide range of biological imaging experiments including SVT. For example, the unequivocal images of Atto 647N-labeled capsids of CPV demonstrated that CPV capsids had a relatively short residence time on the cell surface, which limited the efficiency of virus internalization.[142]

3.1.2. Lipophilic Dyes. The lipid membrane of enveloped viruses is derived from the plasma membrane or intracellular membrane of the host cells. Hence, virus labeling represents a significant application area for fluorescent membrane probes. Membrane probes include lipophilic organic dyes and fluorescent analogs of natural lipids. While some lipophilic dyes are particularly useful for SVT experiments, other lipid probes are scarcely used to label viruses. Lipophilic dyes are able to incorporate into the envelope of viruses by hydrophobic−lipophilic interactions (Table 2). For lipophilic dyes-based single-virus imaging, these dyes have an additional advantage in that they self-quench when they are incorporated into viral particles at high concentrations. At low pH levels or upon fusion where the viral and cellular membranes mix leading to a decrease in concentration, the lipophilic dyes dequench leading to a striking increase in fluorescence. Thus, the lipophilic dyes can detect the genome-release events of viruses, since the dequenching of the fluorescence signal could be considered as the sign of the occurrence of virus-endosome or virus-plasma membrane fusion. As one kind of early applied lipophilic dyes, rhodamine derivatives were used to study the kinetics of the virus-cell membrane fusion events on the membrane surface.[65,153,154,161] For example, R110-labeled influenza viruses were used to investigate the real-time hemifusion and the pore formation of influenza viruses on a lipid bilayer. The occurrence of the hemifusion was indicated by the transient brightening of individual viruses caused by the fluorescence dequenching of R110.[154]

Table 2. Lipophilic Dyes and Intercalating Dyes for Single-Virus Imaging

| | | Octadecyl Rhodamine B | | | | | | DiD | | |

	Color[a]	λ_{ex}[b] (nm)	λ_{em}[c] (nm)	ε_{abs}[d] (M^{-1}cm^{-1})	Φ_f[e] (%)	τ_{fl}[f] (ns)	Sites	Viruses	Refs
Rhodamine derivatives									
R18	Orange	556	578	125,000	ND[g]	ND	Envelope	IV[h, 65, 153] UUKV[i,145, 161]	t
R110	Green	498	520	ND	92	4.0	Envelope	IV[154]	t
Carbocyanine dyes									
DiO	Green	484	501	154,000	ND	~1	Envelope	HIV[j, 157]	t
DiI	Orange	553	570	134,000	7	~1	Envelope	EBOV[k, 158] HBV[l, 159] VSV[m, 160]	t
DiD	Deep red	650	670	247,000	ND	~1	Envelope	IV[68, 72, 74, 128] DENV[n, 73, 75, 162] HCV[o,71] ASLV[p,155] HIV[82-83] CHIKV[q,156]	t
Intercalating dyes									
Acridine orange	Deep red Green	460 500	650 526	53,000	ND	2.0	RNA DNA	PV[r,163-164]	165, t
Ribogreen	Green	500	525	67,000	0.65	ND	RNA	HRV[s,166-167]	168, t
Syto82	Orange	541	560	76,000	>0.4	ND	RNA	PV[99, 131]	169, t

[a]The color of emitted light. [b]Maximum excitation wavelength. [c]Maximum emission wavelength. [d]Extinction coefficient. [e]Fluorescence quantum yield. [f]Fluorescence lifetime. [g]Not determined. [h]Influenza virus. [i]Uukuniemi virus. [j]Human immunodeficiency viruses. [k]Ebolavirus. [l]Hepatitis B virus. [m]Vesicular stomatitis virus. [n]Dengue virus. [o]Hepatitis C virus. [p]Avian sarcoma and leukosis virus. [q]Chikungunya virus. [r]Poliovirus. [s]Human rhinovirus. [t]Information from Thermo Fisher.
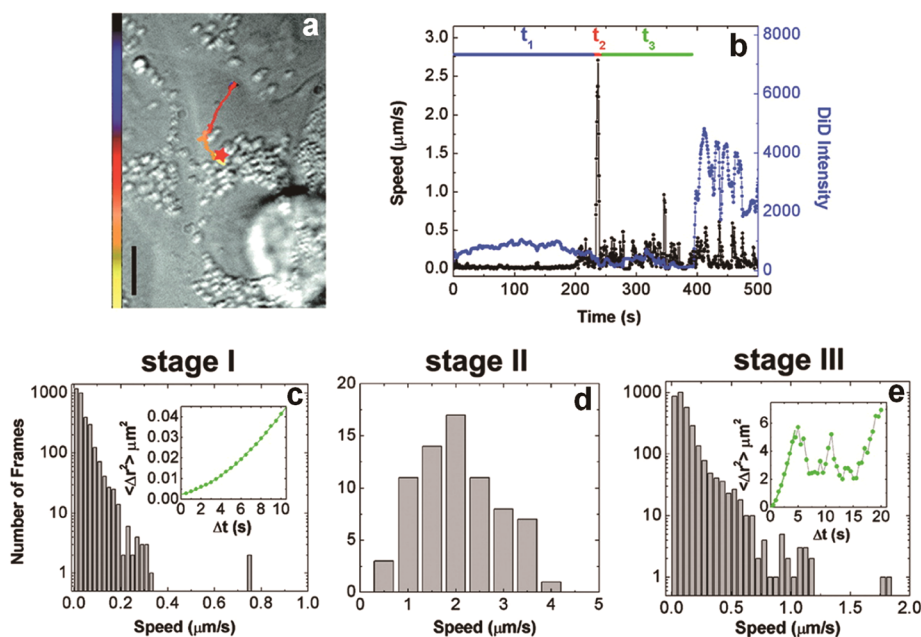
Figure 5. Tracking the transport and fusion of individual influenza viruses. (a) Trajectory of a DiD-labeled virus inside a cell. (b) Time trajectories of the velocity (black) and the DiD fluorescence intensity (blue) of a virus. (c−e) Histogram of the viral velocity in each stage. (Inset) Shown is the measured average mean square displacement ($\langle\Delta r^2\rangle$) vs time (Δt) for a virus. Adapted with permission from ref 68. Copyright 2003 National Academy of Sciences, U.S.A.

With the emergence and development of fluorescence microscopy, researchers began to observe individual fluorescent viruses for obtaining more intuitive information about virus infection. Long-chain dialkylcarbocyanines (e.g., DiD, DiI, and DiO) with varying fluorescent excitations and emissions were widely adopted to label individual viruses for

Figure 6. Characterization of near-infrared FPs. (a−c) Normalized excitation (a), emission (b), and full absorption spectra of different iRFPs. (d) Schematic representation of directed molecular evolution that led to iRFPs with distinct spectral properties. (e) Brightness of HeLa cells transiently transfected with iRFPs, normalized to the value for iRFP713-expressing cells. Adapted with permission from ref 181. Copyright 2013 Springer Nature.
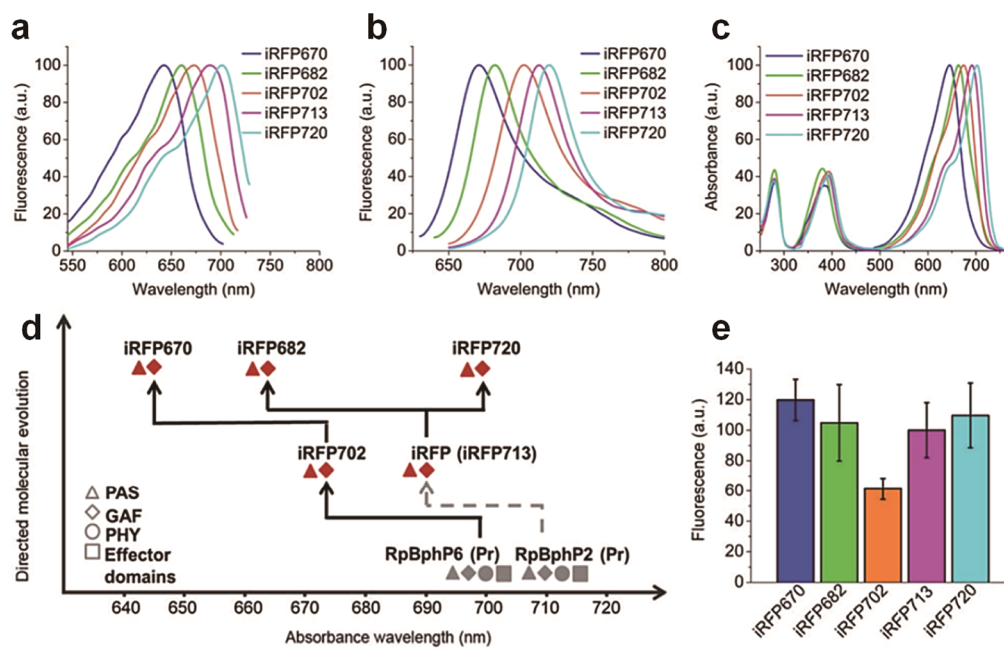
SVT. These dyes possess high extinction coefficients, moderate quantum yields, and short lifetimes in a hydrophobic environment. Their fluorescence is only detectable when they insert into lipid membranes. Owing to the strong autofluorescence of the cells (toward the blue end of the visible spectrum), the deep-red lipophilic dye (DiD) has been used extensively to track the infection behaviors and dissect the infection pathways of enveloped viruses, including influenza virus,[68,72,74,128] dengue virus (DENV),[73,75] hepatitis C virus (HCV),[71] avian sarcoma and leukosis virus (ASLV),[155] chikungunya virus (CHIKV),[156] and HIV.[82,83] The analogues of DiD, DiO (green) and DiI (red), have also been used to monitor the transport behaviors of viruses, such as HIV,[157] ebola virus (EBOV),[158] hepatitis B virus (HBV),[159] and VSV.[160] By quantitatively measuring the fluorescence intensity of individual viruses, the virus−endosome fusion events could be detected in real time (Figure 5).[68] However, detection of the actual release of the interior content of the virus, as a prerequisite for virus infection, still requires more accurate approaches. In addition, owing to the self-quenching of lipophilic dyes in viruses, the number of viral particles that can be fluorescently detected is very low.[73] When a large number of viruses bind to the cell surface, only 2% of viruses are indicated by DiD signals. This makes it challenging to efficiently and globally monitor the behavior of viruses in individual cells.[99]

3.1.3. Intercalating Dyes. Generally, the viral genome is encapsulated into the intact virus particle, which is not accessible for dye attachment. However, several intercalating dyes can penetrate the outer components of viruses to label the viral genomes to a certain extent (Table 2). Ribogreen is an intercalating dye with little fluorescence and negligible absorbance. The dye is fluorogenic, meaning that its fluorescence intensity amplifies by several orders of magnitude when it binds to nucleic acids. This dye has been used for detecting and quantifying both RNA and DNA. By incubating

ribogreen with the human rhinovirus (HRV), this dye contacted and bound with the viral genome during "capsid breathing".[166−168] Later, a metabolic labeling strategy was developed to label the viral genome during virus replication. For instance, acridine orange was incorporated into developing poliovirus (PV) to label the viral RNA.[163−165] However, these dyes could rapidly inactivate the viral RNA upon illumination. SYTO dyes are a kind of cell-permeable nucleic acid dye, which binds to nucleic acids by passive diffusion through the plasma membrane. Each of these dyes possesses different characteristics including optical properties, nucleic acid binding preferences, cell permeability, and DNA/RNA selectivity and can be used to stain DNA and RNA in both live and dead eukaryotic cells.[169] As an orange fluorescent nucleic acid binding dye, SYTO 82 has been successfully used to label the viral genome of RNA viruses, including PV and influenza virus.[99,131,170] $[Ru(phen)_2(dppz)]^{2+}$ showed its potential to label the viral genomes of DNA viruses during viral self-assembly.[171,172]

3.2. Fluorescent Proteins

Green fluorescent protein (GFP) was discovered and purified from *Aequorea victoria* by Osamu Shimomura in the early 1960s. It began to be utilized as a tool for molecular biologists when the nucleotide sequence of GFP was reported and expressed in *Escherichia coli* and *Caenorhabditis* in 1994.[173,174] The application of GFP as a genetically encoded fluorescence marker heralded a new era in cell biology.[175] Thereafter, a broad range of genetic variants of fluorescent protein were developed by mutagenesis, and the diversity of excitation−emission spectra was further extended.[76,176] In 2008, the Nobel Prize was awarded "for the discovery and development of the green fluorescent protein, GFP" to recognize the achievements of GFP labeling technology in the medical and biological sciences. More recently, GFP-like proteins from other species have been discovered with new optical properties, resulting in a

Table 3. Optical Properties of Representative FPs

Protein	$\lambda_{ex}{}^{a}$ (nm)	$\lambda_{em}{}^{b}$ (nm)	$\varepsilon_{abs}{}^{c}$ (M^{-1} cm^{-1})	$\Phi_f{}^{d}$ (%)	pK_a	Relative Brightness^{e} (% of EGFP)	refs
Sirius	355	424	15,000	24	<3.0	11	183
EBFP2	383	448	32,000	56	4.5	53	184, 185
TagBFP	402	457	52,000	63	2.7	98	185
mTurquoise	434	474	30,000	84	4.5	75	186
ECFP	434	475	32,500	41	4.7	40	187
TagCFP	458	480	37,000	57	4.7	63	188
mTFP1	462	492	64,000	85	4.3	162	187
EGFP	488	507	56,000	60	6.0	100	187
mWasabi	493	509	70,000	80	6.5	167	189
mNeonGreen	506	517	116,000	80	5.7	276	190
EYFP	514	527	84,000	61	6.5	153	191
Citrine	516	529	77,000	76	5.7	174	192
mOrange	548	562	71,000	69	6.5	146	178
mKO2	551	565	63,800	57	5.5	108	193
TagRFP	555	584	100,000	48	<4.0	143	194
mRuby2	559	600	113,000	38	5.3	128	195
mCherry	587	610	72,000	22	<4.5	47	178
mKate2	588	633	62,500	40	5.4	74	196
mNeptune	600	650	67,000	20	5.4	40	197
iRFP670	643	670	114,000	11	4.0	38	181
TagRFP675	598	675	46,000	8	5.7	11	198
iRFP702	673	702	93,000	8	4.5	23	181
iRFP713	690	713	98,000	6	4.5	18	181
iRFP720	702	720	96,000	6	4.5	17	181
pH-sensitive FPs							
Ecliptic pHluorin	495	511	ND^{f}	ND	7.1	ND	199
Super-Ecliptic pHluorin	495	512	ND	ND	7.2	ND	200
pHuji	566	598	31,000	22	7.7	20	200
pHoran4	547	561	83,000	66	7.5	163	200

^{a}Maximum excitation wavelength. ^{b}Maximum emission wavelength. ^{c}Extinction coefficient. ^{d}Fluorescence quantum yield. ^{e}The relative brightness values were calculated from the product of the molar extinction coefficient and quantum yield, divided by the value for EGFP. ^{f}Not determined.

further expansion of the color palette.[177,178] Nowadays, there are more than 1000 FP variants reported, which cover the color range from blue to near-infrared spectrum (Figure 6).[179−182] A representative list of FPs and their optical properties are given in Table 3.

FPs are genetically encodable such that the cells and organisms can label themselves.[201] Therefore, this method avoids additional procedures for purifying, tagging, and introducing labeled proteins into cells. However, the fluorescent intensity of FPs in live cells is not only relevant to the molecular brightness in themselves, but also to the number of FP molecules in their functional form. For GFP-like proteins, the fluorescence only can be observed after the chromophore has matured and the polypeptide chain has folded. Thus, the expression level is related to many factors, such as transcription and transfection efficiency, protein stability and folding, and chromophore maturation.[202,203] Thus, although the labeling efficiency is near "100%", the effective labeling can be much less. GFP and GFP derived proteins tend to have a high maturation efficiency (>85%), whereas red fluorescent proteins can be significantly lower, for example 40% for the case of mCherry.[204] For SVT experiments, FPs are a convenient tag for labeling the relevant cellular structures and viral components, especially the internal components of viruses. However, viruses are very dense structures, and the relatively large size of FPs can make it a problem when using them to label viral proteins. Hence, the correct location for adding the FP to the viral genome needs to

be found. Often, it is beneficial to spike the sample with a mixture of labeled and unlabeled components. In the case of adding a FP to the Gag protein of HIV-1, spiking with a ratio of 1:1 already restores wild-type like infectivity.[119]

To obtain FPs-labeled viruses, the recombinant gene technology should be used to fuse viral protein genes with FPs genes.[177,205] When the recombinant cDNA clone was transfected into live cells, the viruses could be detected via their fluorescence. For single-virus labeling, FPs can be divided into three classes: autofluorescent proteins, pH-sensitive FPs, and phototransformable FPs.

3.2.1. Autofluorescent Proteins. The main feature of GFP and GFP-like proteins is that its fluorescence is encoded in the sequence and is typically preserved when fused with other proteins. This is a major breakthrough for specific fluorescent tagging of proteins in live cells using simple molecular biology. This discovery aroused the enthusiasm of many researchers to create GFP mutants with better brightness, faster folding, less propensity to oligomerize, or different excitation and emission wavelengths. Enhanced green fluorescent protein (EGFP) was one of the first enhanced variants, exhibiting more desirable characteristics for the practical use in mammalian cells. Wild-type GFP has unsatisfactory properties with respect to brightness (due to the chromophore being often in a dark, protonated state), folding properties, and excitation spectrum. Numerous GFP variants always emit fluorescence in the magic range of 442 to 529 nm.[206] To break this limitation, efforts were devoted to

cloning similar FPs from other organisms. So far, the whole palette of autofluorescent proteins spans the emission wavelength from blue to near-infrared spectrum. Both the spectral range as well as photophysical properties of FPs are being continuously expanded.

One of the most important applications of FPs is site-specific labeling of viral components for single-virus imaging in live cells, including the envelope,[207−209] capsid,[209−212] matrix,[213] ribonucleoprotein (vRNP),[207] and other compo-nents.[82,84,214−216] For example, a GFP-labeled influenza virus was generated by carrying a GFP reporter in the NS segment to visualize the dynamics of infection progression (Figure 7).[217] Tracking double-labeled rabies viruses (RABV)
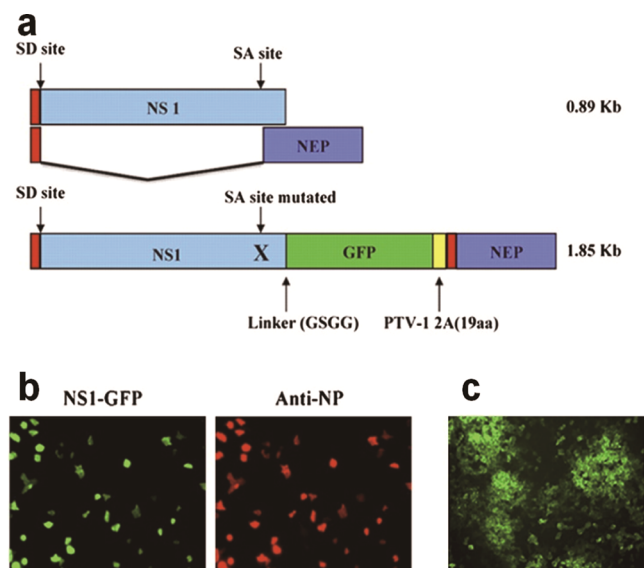

Figure 7. Generation of recombinant influenza viruses carrying a GFP reporter. (a) Schematic representation of the NS segment of WT PR8 virus and NS1-GFP virus. (b) A549 cells were infected with recombinant PR8 virus carrying NS1-GFP. At 10 h postinfection, cells were fixed and stained for NP. NP staining is shown in red and NS1-GFP is shown in green. (c) Fluorescent micrographs of NS1-GFP virus plaques taken at 20× magnification. Adapted with permission from ref 217. Copyright 2010 National Academy of Sciences, U.S.A.

comprising a RFP-labeled envelope and an EGFP-labeled vRNP found that RABV was transported as a cargo in neurites of neuroblastoma cells in the retrograde direction.[207]

3.2.2. pH-Sensitive Fluorescent Proteins. By muta-genesis, researchers discovered many extremely useful mutants of wide-type FPs, which have various optical properties and environmental sensitivities.[176,182] As protonation affects the photoproperties of the wild-type GFP chromophore, variants could be produced that were sensitive to the physiological pH in the cell and detect changes in pH. The optical parameters of representative pH-sensitive FPs are shown in Table 3. These proteins always display high fluorescence under neutral conditions, while the fluorescence signal markedly decreased under acidic conditions. Thus, they exhibit unique advantages for studying the transport mechanisms of endocytosis and exocytosis in live cells.[218] Since many viruses need to hijack the endocytic pathway of host cells to realize the genome release for virus replication, targeted expression of pH-sensitive FPs to viruses allows for the real-time analysis of the virus-endosome fusion events in live cells. Thus, the pH-sensitive FPs are

valuable fluorophores for investigating the virus infection mechanisms.[214,215,219] For example, pHluorin, a pH-sensitive GFP variant, has been used to label HIV. By labeling the Gag protein and altering the external pH of the medium, the fission of newly assembled HIV particles could be detected.[220] By labeling the surface of HIV, the fluorescent signal was used to monitor the uptake and delivery of HIV into acidic endosomes.[214] Meanwhile, Hogue et al. captured the earliest viral exocytosis events and elucidated the intracellular transport pathways and egress mechanisms of alpha herpesvirus.[221] Additionally, pHluorin and mKate2 (a pH-resistant FPs) were introduced to label the envelope and internal content of ASLV simultaneously. Live-cell imaging of infectious dual-labeled ASLV demonstrated the transport and fusion behaviors of ASLV were closely associated with early and intermediate endosomes (Figure 8).[215]
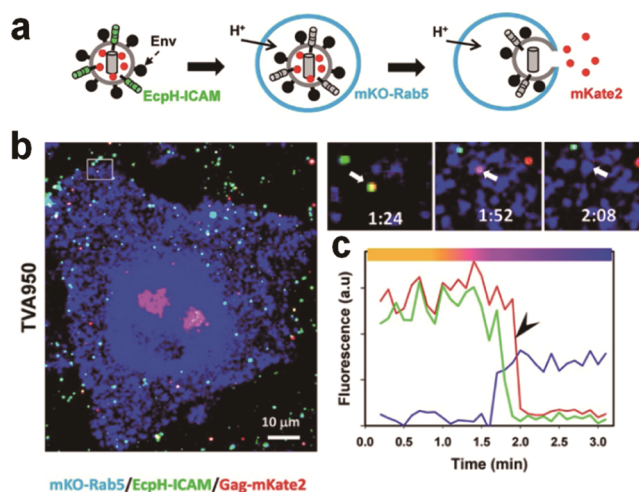

Figure 8. Single ASLV-A entry into acidic endosomes and virus-endosome fusion. (a) Schematic diagram illustrating virus labeling and how the endosomal pH drops and subsequent ASLV-A fusion is visualized. (b) ASLV-A (yellow) fusion with TVA950 cells transiently expressing mKO-Rab5 (blue). Pseudoviruses were labeled with EcpH-ICAM (green) and Gag-mKate2 (red). The right top image panels show consecutive snapshots of the boxed region showing the virus prior to internalization (left), immediately after entry into acidic Rab5-positive endosomes (middle), and after fusion with early endosomes (right). The graph in panel (c) shows the fluorescence intensities of mKO-Rab5 and the viral EcpH-ICAM (green) and Gag-mKate2 (red) signals as a function of time. Adapted with permission from ref 215. Copyright 2014 BioMed Central Ltd.

3.2.3. Phototransformable Fluorescent Proteins. Another extremely powerful functionality of some FPs is that they can be activated or spectrally shifted using light.[222,223] Phototransformable fluorescent proteins (PtFPs) have already attracted worldwide attention with their skyrocketing popular-ity for super-resolution microscopy in recent years.[222,224] In 2002, Kaede, a GFP homologue, was discovered that was photoconvertible from green-to-red fluorescence emission under UV illumination.[225] In the same year, using mutagenesis, a photoactivatable GFP variant (paGFP) was developed, which was initially irradiated by 413 nm light and then emitted strong fluorescence when excited with 488 nm light.[226] Nowadays, a wide range of PtFPs have been developed to satisfy the requirements for different colors and modes of conversion, including photoactivatable, photoconvertible, and photo-

switchable proteins. These proteins have been used for tracking the dynamics of cellular components in live cells (Figure 9).[224,227,228] For example, photoactivated-localization
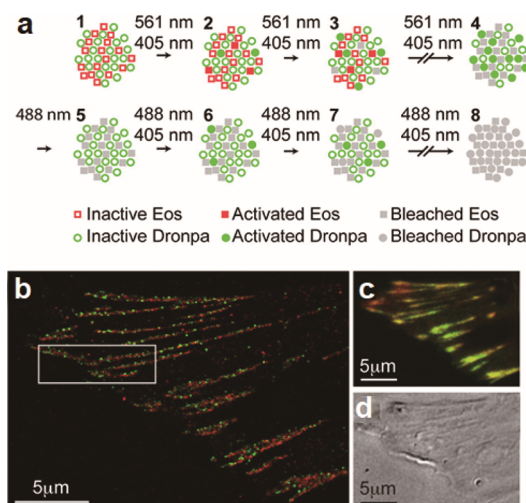

Figure 9. Use of PtFPs for investigating focal adhesions. (a) Protocol for dual-label super resolution imaging by PALM. (b) Dual-color PALM super resolution image overlay of paxillin (green) and zyxin (red). (c) Diffraction-limited, summed molecule, dual-color TIRF image. (d) DIC image. Adapted with permission from ref 228. Copyright 2007 National Academy of Sciences, U.S.A.

microscopy (PALM), as a kind of single molecule-localization super-resolution microscopy,[229] mainly relies on the amazing photophysical behaviors of PtFPs. This technique uses sequential activation of fluorophores and time-resolved localization to acquire high-resolution images,[180,230,231] which has facilitated the investigation of the mechanisms of virus infection.[232−234] Along with the development of SPT and SVT, which have provided subdiffraction resolution already in the 1980s, and superresolution microscopy, the combination of SPT and PALM (SPT-PALM) has been shown to be capable of visualizing multiple trajectories of viral proteins at high density in live cells.[235]

3.3. Fluorescent Nanoparticles

A major challenge in SVT is the development of fluorescent labels that combine small size with high brightness and photostability. To address this need and to enhance the imaging capabilities in SVT, researchers have pursued the development of biocompatible fluorescent nanoparticles for single-virus labeling. Compared with organic dyes and FPs, fluorescent nanoparticles usually show unique chemical and optical properties, such as higher brightness and photostability, which are highly preferable for single-virus tracking. Below, we will discuss commonly used nanoparticles: quantum dots and metal nanoparticles.

3.3.1. Quantum Dots. QDs, as a kind of semiconductor nanoparticles, have already attracted tremendous attention in biological applications.[236−240] This is mainly due to the excellent optical properties of QDs, such as high quantum yield, photostability, and size-tunable narrow emission spectra.[241−243] The spectral emission range of QDs covers the UV to infrared and can be adjusted by changing the size, shape, and composition of QDs.[123,244−246] The high brightness of QDs (10−100 times higher than organic dyes or FPs) facilitates the detection sensitivity and allows high-contrast

images to be obtained.[123,247] In addition, the excellent photostability of QDs (100−1000 times higher than organic dyes or FPs) makes it possible to track single viruses over several hours with high temporal resolution.[248] Moreover, QDs possess a wide excitation spectrum and a narrow emission spectrum, which makes them well suited for multicolor imaging where viral components and cellular structures can be tracked simultaneously.[249,250] Based on the prominent properties mentioned above, QDs are broadly used in biolabeling,[251−253] in bioimaging,[254,255] and subsequently for single-particle tracking.[256−259]

In SVT experiments, the most available QDs are made of CdSe cores coated with a ZnS shell,[260] which are usually prepared in the organic phase and covered with hydrophobic organic ligands (Figure 10). For biological applications, the
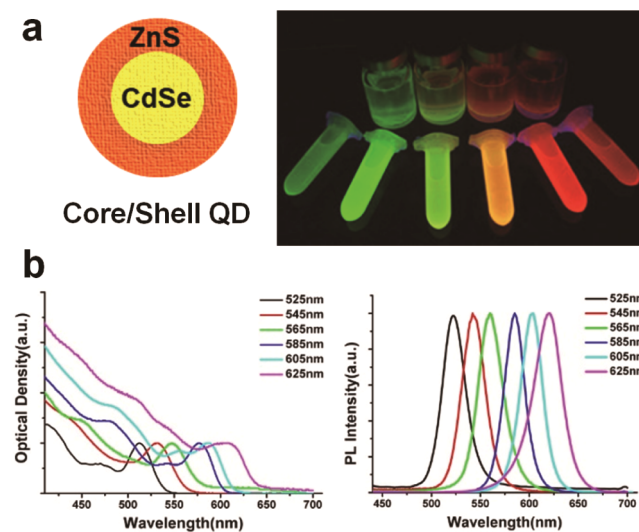

Figure 10. Properties of QDs. (a) Schematic drawing of a core−shell QD and fluorescent images of QDs of different sizes under UV light. (b) Absorption (left) and emission (right) spectra of CdSe/ZnS QDs. All QD samples and data were obtained in the group of Pang.

solubilization and biofunctionalization of QDs are essential steps owing to the hydrophobic surface of QDs. A substantial amount of pioneering research has been performed regarding these steps, which has led to a strong boost in the number and variety of applications of QDs in the fields of biology and biophysics.[237,243,260−263] So far, uniform, high-quality, bio-functionalized QDs are readily available via experimental synthesis or can be purchased commercially. In 2003, QDs were first applied to track individual glycine receptors on the neuronal membrane, which laid the cornerstone for exploring the dynamics of biomolecules in live cells by using QDs-based SPT.[89] After that, a huge number of QDs-labeled biomolecules of interest were tracked dynamically in a wide variety of biological systems.[94,238,264−267] In 2008, QDs were first successfully exploited to specifically label the envelope of viruses without significant effect on the infectivity of the virus, thereby allowing the uptake mechanism to be investigated in detail.[98] This was considered a watershed moment for SVT. With the further development of labeling strategies, different components of viruses could be labeled with QDs.[268] The detailed labeling strategies are described in detail in the section entitled Labeling Strategies for Nongenetically Encoded Fluorophores.

At present, QDs-based SVT techniques have acquired spectacular achievements and researchers have elucidated multifarious infection mechanisms of viruses. For example, Pang et al. utilized this technique to analyze the infection behavior of influenza viruses and dissect the transport mechanism of influenza virus trafficking at different stages of infection. The results indicated that influenza viruses underwent a previously unknown five-stage process from the cytomembrane to the perinuclear region along microfilaments and microtubules. A "driver switchover" mechanism was proposed to answer the question of how the transport of influenza viruses switches from microfilaments to microtubules.[108,110,114,115,118] In another example, Cui et al. designed QD-labeled transcription activator-like effectors to specifically target HIV proviral DNA sequences, and they identified single gene loci in the cell nucleus.[116] By encapsulating QD-conjugated RNAs into influenza viruses, they monitored the uncoating process of individual viruses and revealed the mechanisms of uncoating and vRNP trafficking of influenza viruses.[113]

3.3.2. Metal Nanoparticles.
In the middle of the 1980s, Brabander and colleagues visualized the movements of gold nanoparticles (AuNPs) with a size of 40 nm on the surface of live cells by using video-enhanced differential interference contrast microscopy.[42,46] This is the first experiment using AuNPs-based SPT in live cells. Over the years, numerous researchers dedicated their efforts to develop suitable methods for data processing and modeling, and then AuNPs-based SPT was increasingly utilized to study the dynamic organization and heterogeneity of the cell membrane.[269,270] One major advantage of AuNPs in SPT experiments is their high stability, because they have no photobleaching and less biodegradation. AuNPs possess unique optical properties due to the surface plasmon resonance and strong light scattering. The scattering light signal of AuNPs requires dark field microscopy or similar optical setup to be detected. The signal intensity is coupled to the illumination intensity, and thus good image contrast and high temporal resolution could be obtained. Experiments with AuNPs-labeled respiratory syncytial viruses (RSVs) demonstrated that the RSVs still maintain their virulence and could be successfully tracked over extended periods of time.[271] However, the ability to detect multiple species via scattering light is very challenging and the limited availability of multiple labels restricted their application for SVT.

Metal nanoclusters (e.g., Au, Ag) are composed of a small number of atoms and typically have sizes below 2 nm. The emission wavelength of fluorescent metal nanoclusters covers the visible to near-infrared region of the electromagnetic spectrum.[273,274] The fluorescence of metal nanoclusters can be tuned by a number of factors, such as size, composition, ligands, aggregation state, ionic strength, and pH value. Due to the unusual physicochemical and good optical properties, fluorescent metal nanoclusters have attracted increasing attention for biological and biomedical applications.[274−276] To date, there are a number of applications in virus detection,[277−279] but very few reports about virus labeling with nanoclusters. Marjomäki et al. developed site-specific protocols to target the enterovirus capsid with monodisperse gold nanoclusters (Figure 11). The end point dilution assay implied that the binding of gold nanoclusters to the viral surface did not lower the infectivity of the virus.[272] Thus, site-specific labeling of enteroviruses with nanoclusters could
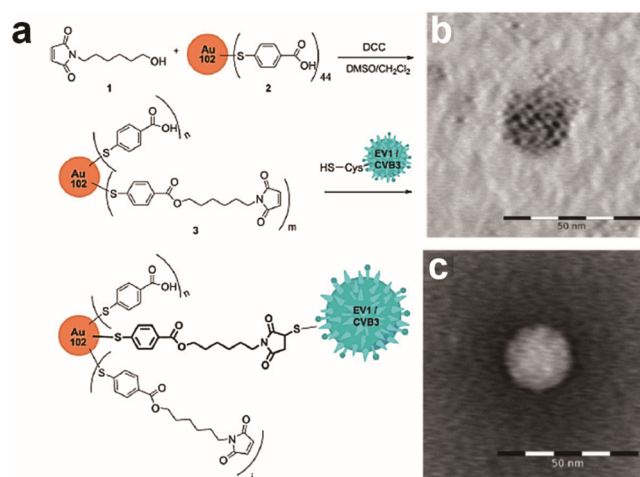

Figure 11. Gold nanocluster labeling of enteroviruses. (a) Synthesis of the maleimide functionalized $Au_{102}(pMBA)_{44}$ clusters and their site-specific conjugation to enteroviruses. (b−c) TEM images of CVB3 viruses treated with functionalized gold clusters. (c) Control TEM image with conventional negative staining of a virus sample incubated with nonfunctionalized clusters. Adapted with permission from ref 272. Copyright 2014 National Academy of Sciences, U.S.A.

facilitate the future structural studies of virus uncoating and become an important new tool for future SVT applications.

4. LABELING STRATEGIES FOR NONGENETICALLY ENCODED FLUOROPHORES

Organic dyes and nanoparticles, as nongenetically encoded fluorophores, can be advantageous over FPs owing to their superior brightness and photostability. However, most of these fluorophores can be used to target the viral components by direct chemical reactions or noncovalent interactions, but it is difficult to label viruses site-specifically. For many questions of interest, it is only necessary to label the viral particles and specific labeling of the virus is not important. Other questions require the labeling of specific viral components. For the following discussion of the several strategies that have been developed for attaching nongenetically encoded fluorophores to viral components, we will divide them into nonspecific and site-specific labeling approaches (Figure 12).

4.1. Nonspecific Labeling

In virtue of their intrinsic properties, it is possible to use hydrophobic−lipophilic interactions or intercalation for some organic dyes to label the viral envelope and genome, which have been described in detail in the previous section. For labeling the external components of viruses (including the envelope of enveloped viruses and the capsid of the nonenveloped viruses), many chemical labeling methods have been adopted for organic dyes and nanoparticles, such as cross-linking, click chemistry, and biotin−streptavidin interactions.

4.1.1. Cross-linking Reaction.
Cross-linking reaction is the simplest and versatile method for labeling viral components with organic dyes or nanoparticles, which mainly conjugate proteins and biomolecules with fluorophores by a covalent bond. Many cross-linking reagents (called cross-linkers) have been characterized and can be synthesized to combine two or more reactive groups within one molecule. The reactive elements can then chemically attach to specific functional groups of proteins and other molecules on the viral surface.
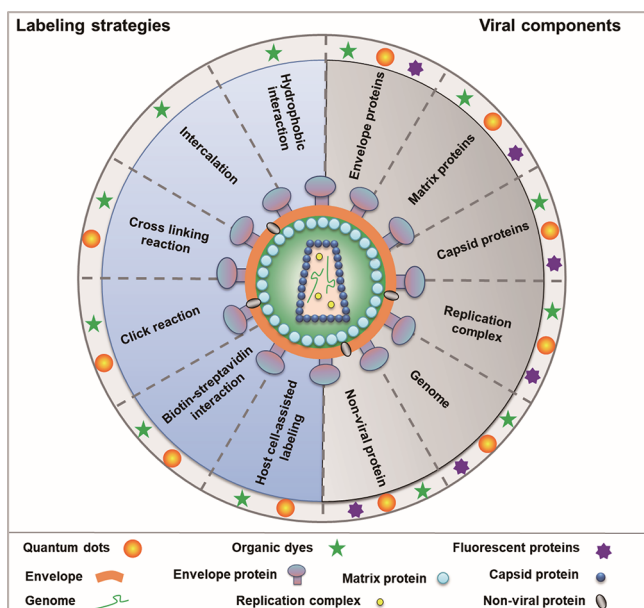
Figure 12. Labeling strategies and labeling sites for fluorescent labels in SVT.

Proteins are complex structures composed of a linear sequence constructed from 20 different amino acids. However, for labeling, there are typically only four functional groups of proteins that are targeted: primary amines ($-NH_2$), which exist at the N-terminus of each peptide and the side chain of lysine; carboxyls ($-COOH$), which exist at the C-terminal of each peptide and the side chain of glutamic acid and aspartic acid; sulfhydryl ($-SH$), which exists in the side chain of cysteine; carbonyls ($-CHO$), which can exist in oxidized glycoproteins.[280] Many chemical species can react with the four kinds of functional groups to form chemical bonds including isothiocyanates, acyl azides, N-hydroxysuccinimide (NHS) esters, sulfonyl chlorides, and imidoesters (Figure 13). A wide variety of cross-linkers are commercially available, which can be easily conjugated to proteins or other functional group-containing compounds based on the commercial
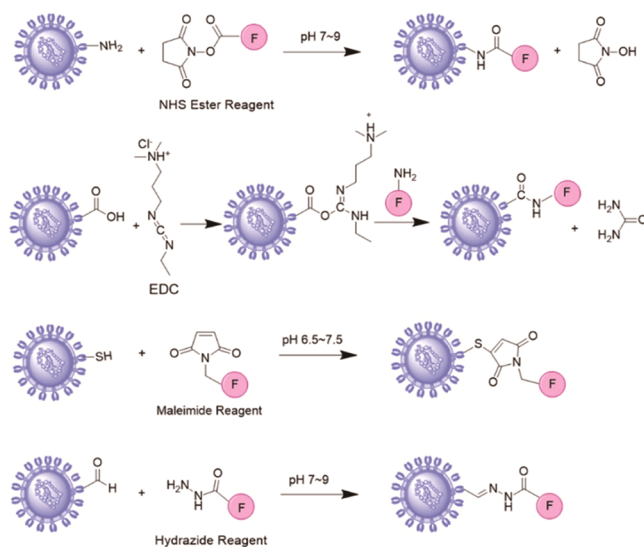

Figure 13. Cross-linking reactions for conjugating fluorescent labels to viruses.

protocols. Thus, any kind of viruses can be covalently labeled with organic dyes or nanoparticles by cross-linking techniques. Especially for nonenveloped viruses, where the capsid is exposed to the outside, covalent labeling is a desirable choice for labeling. For example, AAV was conjugated with QDs using an amino-carboxyl cross-linking reaction (Figure 14).[136] A
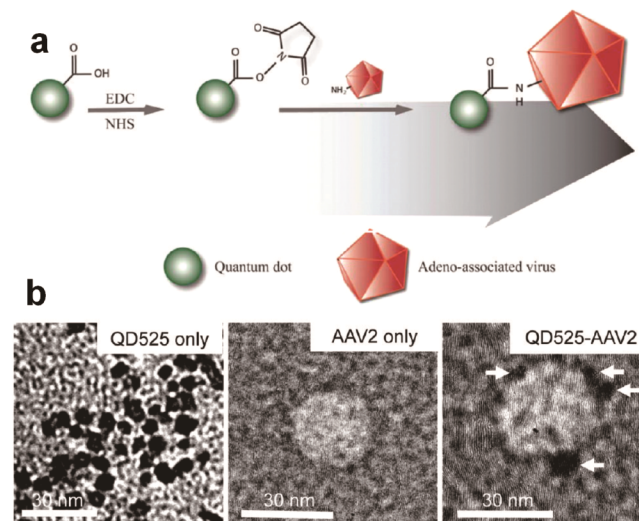

Figure 14. Covalent attachment of QDs to AAV and characterization of the QD-AAV conjugates. (a) QD-AAV networks are generated by an amide bond formation between the carboxylic source on QDs and the primary amines from lysine residues on the AAV capsid via carbodiimide chemistry. (b) Transmission electron microscope (TEM) images of (left) unconjugated QD525, (middle) AAV only, and (right) QD525-labeled AAV. Adapted with permission from ref 136. Copyright 2011 American Chemical Society.

mild and clickable reaction between hydrazine and aldehyde was also used to label envelope proteins of viruses with QDs.[101,281] The direct chemical labeling methods are flexible and easy to apply, by which QD-virus conjugates or organic dye-labeled viral particles are readily obtained for SVT experiments.

4.1.2. Click Reaction. "Click Chemistry" is a type of biocompatible small molecule reaction that is commonly used in bioconjugation with fast reaction rates, mild reaction conditions, high yields, simple procedure, and high selectivity. In 1963, Huisgen first discovered the unactivated azide−alkyne cycloaddition reaction, but this reaction was ignored for many years owing to the harsh experimental conditions.[282] The term "Click Chemistry" was first put forward by Kolb et al. in 1998 and fully described in 2001, where they also introduced Cu(I) as a catalyst to realize the azide−alkyne cycloaddition reaction at room temperature with high chemical yield.[283,284] The copper-catalyzed azide−alkyne cycloaddition reaction (CuAAC) is the most universal click reaction, but it is often incompatible with living systems due to the potential toxicity of Cu(I). Nowadays, there are several kinds of copper-free azide−alkyne cycloaddition reactions reported, such as the strain-promoted azide−alkyne cycloaddition (SPAAC),[285,286] thiol−ene reaction,[287] and strain-promoted inverse-electron-demand Diels−Alder cycloaddition (SPIEDAC).[288] The copper-free approaches opened up the possibility of labeling particular biomolecules in living systems with click reactions. For instance, to detect DNA synthesis *in vivo*, a thymidine analogue 5-ethynyl-2′-deoxyuridine was incorporated into

DNA during DNA replication, and the terminal alkyne group was labeled with a fluorescent azide by a click reaction.[289] Similarly, RNA synthesis was detected by using a click reaction between a uridine analog 5-ethynyluridine and fluorescent azide.[290] Researchers have also developed an unnatural sugar-based click labeling strategy.[291−293] The azido-sugars were added into the cell medium for cell culture. After metabolism, the azido groups were incorporated into the glycans on the cell surface, which could be used to bind with fluorophores by click chemistry.

The viral surface has potential targets for biofunctional modification, which can be functionalized to add clickable groups for virus labeling.[105,106,294,295] For example, Zhang et al. modified baculoviruses with a clickable group (4-dibenzocy-clooctynols) and then labeled viruses with azido-derivatized multidentate-imidazole polymer ligands-modified QDs by copper-free click chemistry.[106] Lin et al. established a site-specific click labeling strategy on the surface of hepatitis D virus (HDV). By incorporation of pyrrolysine analogues carrying various functional groups onto the envelope proteins of live HDV, they successfully exploited the subsequent click reaction to attach a biotin molecule onto the HDV surface (Figure 15).[296] Additionally, by introducing azide and vinyl
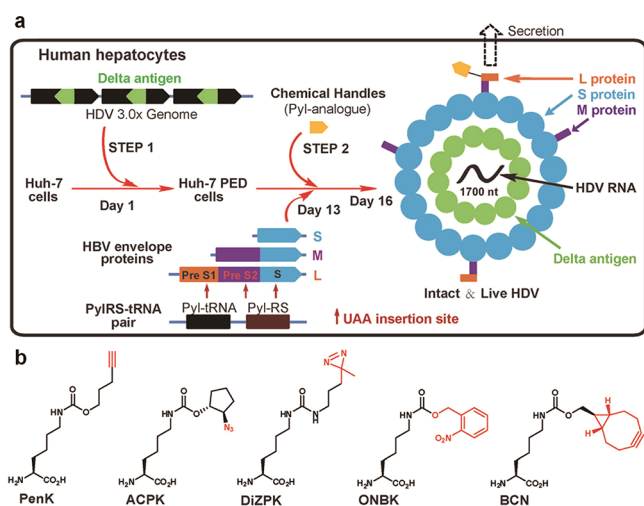

Figure 15. Engineering the hepatitis D virus (HDV) assembly process for site-specific incorporation of unnatural amino acids (UAAs) into its surface envelope proteins. (a) Two-step procedure for the assembly of intact HDV carrying site-specifically incorporated UAA-recognized non-natural amino acids in human hepatocytes Huh-7 cells. (b) Structures of five Pyl analogues used in this study: PenK (Nε-pent-4-ynyloxycarbonyl-L-lysine), ACPK (Nε-((1R,2R)-2-azido-cyclopentyl oxy-carbonyl)-L-lysine), BCN (bicyclo[6.1.0]non-4-yn-9-ylmethanol), DiZPK (3-(3-methyl-3H-diazirine-3-yl)-propaminocar-bonyl-Nε-L-lysine), and ONBK (o-nitrobenzyloxy carbonyl-Nε-lysine). Adapted with permission from ref 296. Copyright 2013 Wiley-VCH Verlag GmbH & Co. KGaA, Weinheim.

groups into proteins and the genome of viruses respectively, the envelope and genome of viruses could be labeled simultaneously via copper-free click chemistry and alkene-tetrazine ligation reactions.[297] Ethynyl-modified nucleosides have also been utilized to label newly synthesized DNA of vaccinia virus, adenovirus, and herpes virus by copper(I)-catalyzed click reactions for tracking the viral genome in host cells at the single-molecule level.[298]

4.1.3. Biotin−Streptavidin Interaction. The biotin-(strept)avidin system is one of the strongest noncovalent biological interactions present in nature, which also shows high selectivity, fast reaction speed, and good resistance to extremes of temperature or pH.[299] So far, this system has been used extensively in biomolecule detection, protein purification, and biological labeling, and there are a lot of biotinylation reagents available for developing different labeling methods. Therefore, the versatile approach is to covalently attach biotin to the biomolecule of interest and subsequently bind avidin, streptavidin, or neutravidin reagents. To label viruses with fluorophores, the viral components should be biotinylated chemically or enzymatically. Chemical biotinylation utilizes cross-linking reactions to generate nonspecific biotinylation of carboxylates, sulfhydryls, amines, and carbohydrates. Enzymatic biotinylation generates biotins in a specific lysine within a certain sequence of the viruses by a bacterial biotin ligase.[98,300] Details will be described in the following Site-Specific Labeling section. Based on the biotin−streptavidin interaction, two strategies have been developed for labeling viruses.

A one-step labeling approach to virus labeling is to directly obtain fluorescent-labeled virus conjugates by the interaction between biotinylated viruses and streptavidin-modified fluorophores. The conjugates could aid researchers in investigating the interactions between viruses and the plasma membrane in the early stage of virus infection. However, these one-step labeling methods require tedious purification procedures to remove free fluorophores, such as size exclusion and ultrafiltration. These cumbersome steps usually bring about a significant loss in virus and have deleterious effects on the integrity and activity of the viruses. Especially QDs-labeled viruses cannot be preserved for a long time, since viruses can be degraded at room temperature and QDs are unstable or precipitate below freezing. Thus, the method is not well suited for performing many parallel experiments for gathering statistics.

A so-called two-step labeling approach initially incubates the host cells with biotinylated viruses and then the streptavidin-modified fluorophores are added. For QDs labeling, the two-step labeling strategy has been broadly adopted for SVT experiments. After biotinylation, the viruses are added to cells at low temperature and allowed to bind to the viral receptors and then incubated with streptavidin-QDs to fluorescently label the viruses (Figure 16).[108,301,302] The whole process takes less than a half an hour and avoids tedious purification processes. A colocalization analysis indicated that nearly all viral envelopes could be labeled with QDs, and the infectivity of QDs-labeled viruses was still 86% of that of the native viruses.[99] Thus, this method is easy to perform with high efficiency and low damage to the virus infectivity and has been widely used for studying the infection mechanisms of viruses, including influenza viruses and infectious hematopoietic necrosis virus (IHNV).[99,107]

4.2. Site-Specific Labeling

The primary goal of viruses is to deliver their genome to the proper cellular compartment for transcription and replication. Only labeling external components is insufficient for following the whole infection pathway of a virus because the external components will be dissociated in the process of virus infection. Labeling the internal components of viruses is much more difficult, since fluorophores, especially fluorescent
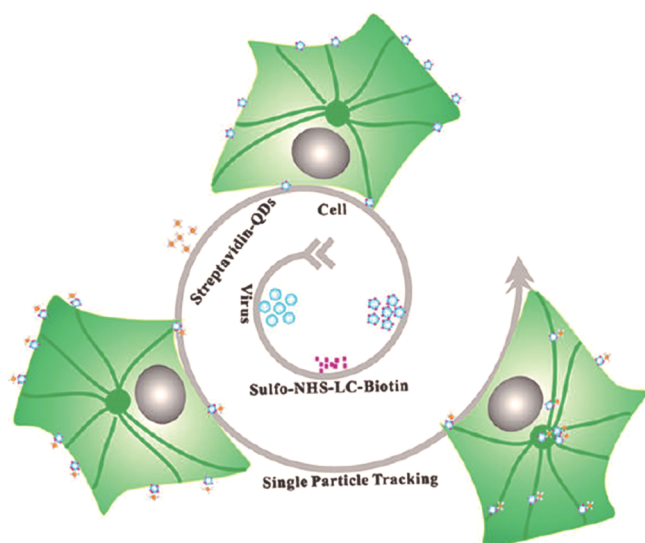
Figure 16. Schematic of a two-step labeling strategy of labeling virus with QDs via the biotin−streptavidin interaction. Adapted with permission from ref 108. Copyright 2012 American Chemical Society.

nanoparticles, are difficult to penetrate the external components of the viruses to enter the interior. This is where the use of FPs for fluorescence labeling has great advantages; when the appropriate location can be found that tolerates the tag, the viral genome can handle the increase in genomic size and there are enough copies to allow tracking over reasonable time periods. However, sometimes it would be great to combine the benefits of genetically encoded labels with the brightness and photostability of synthetic dyes or QDs. Thus, one big question is how to encapsulate nanoparticles or organic dyes into viruses and can it be done specifically.

In early 2006, Dixit and co-workers incorporated QDs into the capsids of the brome mosaic virus by self-assembly, and the generated virus-like particles (VLPs) had a similar size to the native virus.[303] Later, combining with site-specific labeling strategies, such as peptide tag-mediated labeling and oligonucleotide-guided labeling, host cell-assisted methods have been extensively developed in recent years, which are an alternative approach to label the internal and external components of viruses during virus assembly.[304−306] For virus labeling, the distinct advantage of host cell-assisted methods is that it is possible to avoid modification of the viral surface, thus minimizing the influence of labeling on the virus−receptor interactions. To date, host cell-assisted methods have played an important role in visualizing the infection behaviors in different infection stages of a variety of viruses including SV40, HIV, and PV.[131,290,307,308]

4.2.1. Peptide Tag-Mediated Labeling. Fluorescent proteins, as genetically encoded fluorescent labels, can be incorporated with high specificity but still suffer from relatively low brightness and poor photostability.[309] Organic dyes and nanoparticles typically have much better photophysical attributes but cannot realize site-specific labeling in live cells. To combine the best of both worlds, another class of genetically encoded proteins has been developed that can catalyze the autoattachment of fluorescent ligands inside living cells.[310] The proteins themselves are nonfluorescent but can be specifically labeled with fluorescent ligands.[311] These tags can be much brighter, more stable, color-tunable, and more chromatically diverse[312] and, similar to FPs, can also possess some specific properties such as environmental sensitivity and photoswitching but with better photophysical properties.[313,314] For imaging experiments, the labeling is controllable in space and time, and the color of the target protein can be selected according to the experimental requirements.[315] We will discuss two major site-specific approaches for labeling viruses with organic dyes or nanoparticles in live cells: self-labeling fusion tags and enzyme-targeted peptide tags (Table 4).[316]

4.2.1.1. Self-Labeling Fusion Tags. Self-labeling fusion tags have recognition domains that offer the specific attachment of fluorescent ligands to the target proteins in live cells. In this

Table 4. Tag-Mediated Site-Specific Labeling Methods

Tag	Size (amino acids)	Labeling reaction	Fluorophores demonstrated	Virus	Ref for Tag
Self-labeling fusion tags					
SNAP tag	182	Covalently binding with benzylguanine derivatives	TMR[a], SiR[b]	HIV[c,317,318]	319−321
CLIP tag	182	Covalently binding with benzylcytosine derivatives	TMR	HCV[d,322]	323
Halo tag	296	Covalently binding with haloalkane derivatives	TMR	PrV[e,324]	325
TMP tag	157	Engineered *Escherichia coli* dihydrofolate reductase noncovalently binding with trimethoprim (TMP)-fluorophore conjugates	Fluorescein, Atto dye	ND[f]	326−329
TC tag	6−10	Covalently binding with fluorogenic biarsenical compounds	FLAsH, ReAsH	HIV,[330] VSV,[g,331] IV[h,332]	333, 334
His tag	6	Noncovalently binding with Ni-NTA-functionalized fluorophores	QD[j]	Prion,[103] RSV[i,335]	336
Enzyme-targeted peptide tags					
AP tag	15	Covalently binding with biotin or ketone analogs of biotin	QD, Fluorescein, Alexa Fluoro	HIV,[98,116] Baculovirus[300]	337, 338
LAP tag	13−22	Covalently binding with lipoic acid derivatives	QD, Cy3, Alexa Fluoro	HIV[116]	336, 339, 340
Tub tag	14	Covalently binding with tyrosine derivative	Coumarin	ND	341, 342
S6/A1 tag	11	Covalently binding with coenzyme A derivatives	Texas red, Alexa Fluoro, Cy3	ND	343, 344

[a]Tetramethylrhodamine. [b]Silicon rhodamine. [c]Human immunodeficiency virus. [d]Hepatitis C virus. [e]Pseudorabies virus. [f]Not determined. [g]Vesicular stomatitis virus. [h]Influenza virus. [i]Respiratory syncytial virus. [j]Quantum dot.

approach, the target protein binds with a self-labeling fusion peptide or protein sequence. The protein is expressed in live cells and the specific fluorescent ligands are added for protein labeling. As the self-labeling fusion peptide or protein sequence is small, it is easy to create with a wide variety of fluorescent ligands, which can be optimized for the imaging instrumentation.

The SNAP tag, a 182 residues polypeptide (19.4 kDa), is an engineered version of human O^6-alkylguanine-DNA alkyltransferase (hAGT).[345] This protein catalyzes the attachment of O^6-alkylguanine or O^6-benzylguanine to one of its cysteines. To label the SNAP-tagged protein in live cells, the fluorescent membrane permeable O^6-alkylguanine substrates are added into cells having expressed proteins fused with SNAP-tag.[319,320] CLIP tag is a new variant of hAGT, which specifically reacts with O^6-benzylcytosine substrates.[323] The orthogonal relationship between the SNAP tag and the CLIP tag can be simultaneously exploited for dual-color labeling.[346]

The Halo tag is a modified haloalkane dehalogenase, which specifically binds the reactive primary alkyl halides and covalently attaches a modified fluorescent ligand to the active-site residue.[325,347] The trimethoprim (TMP) tag was developed on the basis of the strong interaction between the folate analogue TMP and the *Escherichia coli* dihydrofolate reductase (eDHFR). The protein of interest is fused with eDHFR, expressed in live cells, and then the fluorophore-modified TMP is added into the cells and binds with eDHFR with high affinity and selectivity.[326,348] So far, these tags have been widely used for protein imaging and trafficking in live cells. Based on reverse genetic technology, the halo-tag protein has been fused with the smallest pseudorabies virus (PrV) capsid protein VP26. The recombinant PrV was easily harvested and used directly for the virus tracking without further modification (Figure 17).[324] These labeling systems
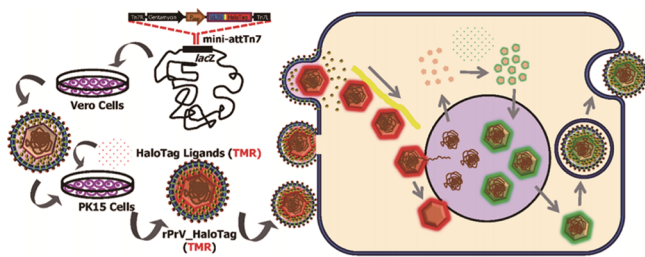

Figure 17. A schematic diagram for the generation of Halo tag-labeled pseudorabies viruses. Adapted with permission from ref 324. Copyright 2016 American Chemical Society.

have several obvious advantages. Fluorescence can be turned on when the fluorescent ligands are added into the cells and turned off using available blocking reagents. Alternatively, a ligand with a second dye can be added at a later time point such that the newly produced proteins of interest are labeled with a different color of dye.

One of the shortest peptide tags available is the tetracysteine (TC) motif (most commonly CCPGCC). The biarsenical dyes FlAsH (green fluorescence) and ReAsH (red fluorescence) specifically bind the TC tag in live cells. The TC tag is only 6 amino acids, and the protein of interest will fluoresce when the biarsenical dye binds. The smaller size and self-labeling capacity of the TC tag make it a very attractive tool for virus labeling. For example, Rudner et al. inserted a TC tag to the C terminus of HIV Gag and investigated the dynamic process of

HIV by two-color imaging analysis.[330] By fusing M protein with TC tags and P protein with EGFP, recombinant VSVs could be dually fluorescent-labeled. Time-sequence images confirmed the adsorption of VSV at the plasma membrane and illustrated that the entry and uncoating of VSV in the infected cells occurred with a half-life of approximately 28 min after virus adsorption.[331] However, due to the interactions with other thiol-containing proteins, the background signal is much higher, and time-consuming washing procedures are required before imaging.

The His tag consists of at least six histidine (His) residues and shows a high affinity and selectivity for Ni^{2+}. The $(histidine)_6$-Ni^{2+}-nitrilotriacetate (Ni-NTA) system has been widely utilized in protein purification. With the development of fluorescent Ni-NTA-based probes, the His tag has already been used for live-cell imaging.[103,109,349] For example, PEG-interspersed Ni-NTA-functionalized QDs were developed to label prion proteins expressed on cell surfaces.[103] Time-lapse imaging first demonstrated that the entire process of prion internalization could be divided into four discrete but connected stages and that lipid rafts played an important role in prion localization and internalization.[109] Further, by conjugating the viral surface with specific polypeptide containing histidine residues, Huang et al. developed a Ni-NTA based progeny virus labeling strategy, which is noninvasive and can be used to label other enveloped viruses budding from the plasma membrane (Figure 18).[335]
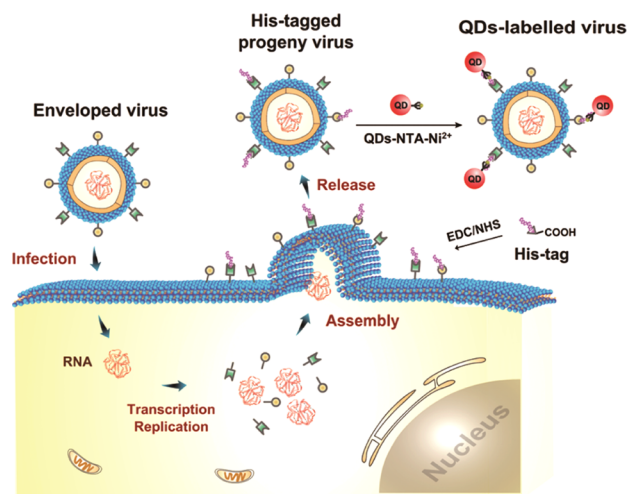
Figure 18. Scheme of the general strategy for *in situ* virus labeling during progeny virus assembly. The labeling procedure includes (1) infection of the host cells with the virus, (2) after 2 days' cultivation, the proteins on the host cell surface were conjugated with polypeptides containing his-tags and carboxyl groups, (3) progeny viruses assemble and are released from the cell surface, incorporating the his-tags in the process, and (4) the progeny viruses are further tagged with Ni^{2+}-NTA modified QDs. Adapted with permission from ref 335. Copyright 2016 The Royal Society of Chemistry.

4.2.1.2. Enzyme-Targeted Peptide Tags.
An alternative method for site-specific labeling is the use of enzyme-targeted peptide tags. The enzymes can catalyze the attachment of a specific peptide sequence to a fluorescent substrate. Thus, the enzymes could help to realize the modification of the peptides with high site selectivity. There are several kinds of enzymes used for protein labeling, such as ligases and transferases.

Ligases, including biotin ligase, tubulin tyrosine ligase, and lipoic acid ligase, can bind specific peptide tags to a recognizable sequence.[350] For example, the biotin acceptor peptide (AP)-tag, a 15 amino acids long peptide that is a substrate for biotin ligase (BirA), enables the conjugation of a biotin to a lysine side chain on the AP tag.[351] After the BirA-catalyzed biotinylation, fluorescent labeling of the protein of interest can be achieved using the biotin−(strept)avidin interaction. By taking advantage of this site-specific labeling strategy, the viral envelope incorporated an AP tag and subsequently, streptavidin-conjugated QDs were attached to the surface of virion after the biotinylation of the AP tag happened.[98,300] For example, the capsid protein VP39 of baculoviruses could be specifically labeled with streptavidin-modified QDs by modifying the protein with biotin by a genetic recombination technique during viral assembly in host cells.[102] It is worth noting that the various components of viruses will disassociate at different stages of the infection process. To dissect their whole infection pathway, it is a prerequisite for SVT to be able to simultaneously follow the related external and internal components of viruses. Pang et al. developed a cell-assisted strategy to simultaneously label the envelope, capsid, and genome of baculoviruses with QDs, EGFP, and SYTO 82, respectively. Such a triple-labeled virus makes it possible to visualize the dissociation process of key viral components in real time.[170]

Similarly, a short lipoic acid ligase (LplA) acceptor peptide (LAP) tag is a 22 amino acids long peptide, which can be catalyzed by LplA to conjugate with lipoic acid derivatives in an ATP-dependent manner.[352] The protein of interest can be fused with the LAP tag and labeled with fluorescent lipoic acid derivatives. The tub tag is a 14 amino acid hydrophilic recognition sequence. Using tubulin tyrosine ligase (TTL), it is possible to conjugate a tyrosine with the fluorescent tub tag.[353] Some of these tags have been utilized to label viral components during virus infection. For example, Cui et al. used a pair of QD-labeled transcription activator-like effectors (TALEs) to image single genomic loci of HIV-1 provirus in the cell nucleus. One of the TALEs was fused with LAP tag, and labeled by tetrazine-conjugated red QDs via Diels−Alder cycloaddition chemistry. The other TALE was fused with an AP tag, biotinylated, and labeled with streptavidin-modified green QDs. The fluorescence colocalization of the two QD-TALEs demonstrates that there is a single HIV-1 provirus loci in live cells (Figure 19).[116]

Transferases can transfer functional groups from a donor substrate to a specific amino acid in a peptide sequence. Phosphopantetheinyl transferases (PPTase), such as Sfp and AcpS, can catalyze the transfer of a phosphopantetheinyl group from coenzyme A (CoA) to a conserved serine. Sfp preferentially recognizes the S6-tag, and AcpS preferentially recognizes the A1-tag.[353,354]

4.2.2. Oligonucleotide-Guided Labeling. The base-pairing propensity of DNA and RNA oligonucleotides can be used to detect the presence of specific target sequences (i.e., complementary nucleic acid sequences) by hybridization. Short oligonucleotides can be synthesized and several different types of groups incorporated for fluorescently labeling the oligonucleotides. Organic dye- or QD-labeled oligonucleotides have been designed and transfected into infected host cells to bind the viral genome of interest in live cells. During virus assembly, fluorophores with oligonucleotides can be assembled into the interior of viruses. A paradigm is that QDs were
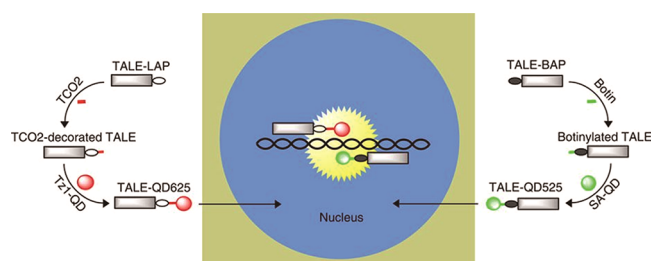

Figure 19. Labeling the HIV-1 proviral loci. Within the cytosol of a live cell, the TALEs fused with a short LplA acceptor peptide (LAP) are decorated with trans-cyclooctene and subsequently labeled with tetrazine-conjugated red QDs via Diels−Alder cycloaddition chemistry. The TALEs fused with an AP tag are biotinylated and labeled with streptavidin-conjugated green QDs. The two QD-TALEs bind to the target HIV-1 proviral DNA sequences, and their fluorescence colocalization demonstrates a single-copy HIV-1 provirus loci in the human chromosomes. Adapted with permission from ref 116. Copyright 2017 Springer Nature.

conjugated with QD-labeled guide RNAs containing the sequence of a packing signal of the viral genome, and then the functionalized QDs would be encapsulated into the capsid of VSV glycoprotein pseudotyped lentivirus (PTLV) in living cells (Figure 20).[355]
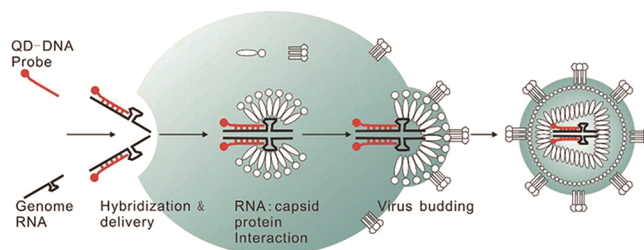

Figure 20. Working principle of encapsulating SA-QDs into HIV-based lentivirus in living cells. Adapted with permission from ref 355. Copyright 2013 American Chemical Society.

By labeling the viral oligonucleotides, it is possible to use SVT to follow the fate of the viral genome and where replication occurs. Several strategies have been developed to track the transport process of the viral genome in host cells. Fluorescence *in situ* hybridization (FISH) is a conventional nucleic acid recognition technique, which can be used to detect and localize endogenous or engineered DNA or RNA through Watson−Crick base pairing. However, FISH is performed in fixed specimens leading to a loss of dynamical information in comparison to tracking nucleic acids in live cells. For live-cell imaging, fluorescently labeled linear oligonucleotides were developed to visualize nucleic acids and allow investigations of trafficking or transient interactions. Using this hybridization approach, Molenaar et al. detected various endogenous nuclear RNAs in live cells without interfering with cell vitality.[356] Often, hybridization techniques suffer from a high level of background fluorescence due to the lack of effective approaches to remove unbounded probes. Here, using nucleic hairpin structures with a fluorescence quencher has been developed to minimize the background fluorescence from nonbound beacons. Upon binding to the target nucleic acid sequence, the hairpin opens and the fluorescence signal increases. One such approach uses fluorescence resonance energy transfer (FRET) to quench the fluorescence signal of

the donor and thus to significantly reduce the background fluorescence. Using FRET, a series of QD-labeled molecular beacons were developed with controllable QD valency. A nanobeacon with one conjugated DNA was favorable for labeling and imaging single RNA in live cells and was used for ultrasensitive detection of single HIV RNAs in HIV integrated cells.[357]

5. OPTICAL IMPLEMENTATIONS FOR SINGLE-VIRUS TRACKING

Many viruses are on the order of 100−200 nm in size, just slightly smaller than the diffraction limit of a high-end microscope. Hence, it is also potentially possible to monitor some viruses directly without the need for labeling them. One label-free approach that has been applied successfully for tracking HIV particles is interferometric scattering microscopy (iSCAT).[358] By using the interference of light reflected from the surface of the coverslip and that coming from the virus particle itself, it becomes possible to visualize the position of the virus and perform SVT with both high spatial and temporal resolution. Kukura and colleagues combined SPT with iSCAT to follow the diffusion of single Simian Virus 40 particles on supported bilayers with 8 ms temporal resolution and nanometer spatial resolution. By labeling the viruses with QDs, we could also measure the orientation of the virus and thus monitor the tumbling of the virus as it slides along the surface.[359]

Once viruses and/or viral components have been successfully labeled fluorescently, SVT measurements can be performed to investigate the various processes in the lifecycle of the virus. For this, fluorescence microscopy has become an indispensable tool. The basic function of a fluorescence microscope is to excite a sample with a specific band of wavelengths, separate the emitted fluorescence from the excitation wavelengths, and detect the fluorescence emission with high sensitivity. As only the emitted light reaches the observer's eye or the detectors, high-contrast fluorescence images can be recorded on a dark background. In the early part of the 20th century, the first fluorescence microscopes were built by the companies of Carl Zeiss and Carl Reichert.[360] Subsequently, Ellinger and Hirt developed "intravital microscopes" to visualize living organisms. They utilized UV light to excite the sample and put filters between the samples and eyes that would reflect the excitation light and transmit the emitted light. This provided the basic principle of modern fluorescence microscopy.[361] Nowadays, lasers are typically used for excitation of the sample instead of lamps. When usage continues with wave lasers or nonfemtosecond pulsed lasers, the excitation wavelength can be limited to a very narrow region of the spectra and emission filters can be produced to efficiency block that specific wavelength while not blocking much of the fluorescence emission. In addition, many lasers provide a high-quality beam profile that simplifies the construction of the excitation pathway. The recent developments in lasers, optics, and detectors as well as the broad spectrum of available fluorophores and various labeling methods have resulted in a revolution in fluorescence microscopy and the worldwide use of fluorescence microscopes in various fields including cell biology, virology, and biophysics.[33,362,363] There are several commonly used imaging modalities for single-virus tracking, which we will present below.[364,365]

5.1. Wide-Field Microscopy

The simplest optical implementation for SVT experiments relies on wide-field illumination and a highly sensitive camera. In wide-field microscopy, a large field of view is fully illuminated by the excitation light and the fluorescent structures of the sample can be captured quickly and easily by a single camera.[366] To acquire a high amount of signal, objectives with an NA > 1.2 are typically used along with sharp fluorescence filters having a high transmission (>80%). For detection, a fast frame transfer, high-quantum yield camera is essential for SVT. Conventional charge coupled device (CCD)-based cameras have high sensitivity but slow read-out speeds whereas complementary metal oxide semiconductor (CMOS) cameras offer very fast frame rates but a narrow dynamic range. An electron-multiplied charge coupled device (EMCCD) detector performs the electron amplification on chip before read-out to decrease noise and combines fast read-out speed with high quantum yield and optimum resolution. A newly developed scientific complementary metal-oxide semi-conductor (sCMOS) camera is based on a CMOS image sensor design and can also offer low noise, rapid frame rates, and high quantum yield. Both cameras are very suitable for quantitative measurements and dynamic imaging. For live-cell studies, an EMCCD camera is capable of obtaining discernible images with a lower number of photons. However, when fast, full-frame transfer rates are essential, sCMOS cameras are superior for fast imaging at speeds approaching or exceeding 1000 fps.[367−369]

The advantages of wide-field microscopy are the large excitation depth, large depth of focus, and low signal loss allowing the tracking of individual viruses in a large volume. However, there is no discrimination against out of focus light. For experiments with low autofluorescence and sparsely distributed fluorescence viruses, this approach works well. However, for experiments with a high background, such as investigations of the HIV assembly using FP-labeled Gag protein, the out-of-focus signals result in the low-contrast images.[370] In addition, owing to the large depth of field, this microscopy modality is rarely used to acquire 3D data over a certain depth of the sample. Thus, wide-field microscopy is mostly limited to 2D SVT tracking.[68]

5.2. TIRF Microscopy

In 1956, E. J. Ambrose first proposed the idea to illuminate cells that contact a glass surface by using total internal reflection. Total internal reflection fluorescence (TIRF) microscopy was first realized by Daniel Axelrod at the beginning of the 1980s.[371] The basic principle of TIRF microscopy is to use an evanescent wave to excite the sample near the glass−liquid interface. An evanescent wave is generated at the glass−liquid interface where the excitation light impinges on the glass-sample interface above the critical angle, at which point the light cannot physically propagate into the sample (typically buffer) and is thus totally reflected. The evanescent wave is a nonpropagating wave whose intensity decays exponentially with distance from the interface.[372−374] There are two main approaches to producing TIR excitation at the glass−sample interface (Figure 21). The original approach, prism-based TIRF, utilizes an optical prism to couple the excitation light to the upper surface of the glass (typically quartz)−sample interface. Upon the development of objectives with a numerical aperture above 1.4, it became possible to focus light onto the coverslip−sample interface such that the
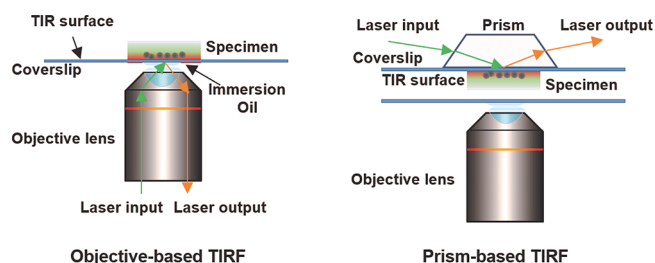
Figure 21. Schematic drawing of an objective-based TIRF and a prism-based TIRF.

incident beam reaches the glass−sample interface above the critical angle, creating an evanescent field.[375] When using an inverted microscope, objective-type TIRF leaves the sample above the objective free and is thus more convenient and easier to use. Objective-type TIRF is the common modality used for live-cell imaging.[376−379]

Due to the exponentially decaying intensity of the evanescent wave, TIRF microscopy is only suitable for exciting fluorescent samples within a depth of ∼200 nm from the interface.[371,377] Thus, TIRF largely reduces the thickness of the excitation plane and improves the image contrast significantly with respect to wide-field imaging (Figure 22). Combined with
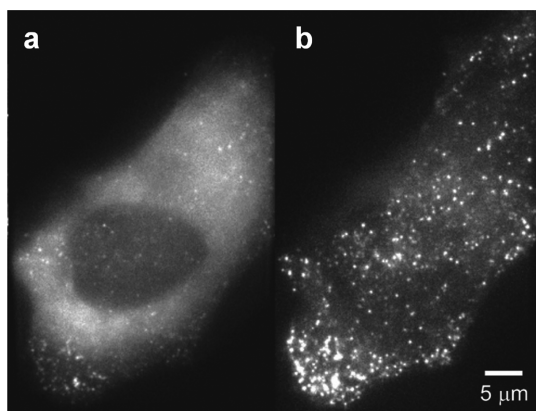

Figure 22. Live cell imaging of individual HIV-1 assembly sites. HeLa cell transfected with a mixture of pCHIV and pCHIV[eGFP] imaged at 25 h post transfection (a) in WF and (b) in TIRF mode. The scale bar represents 5 μm. Adapted with permission from ref 370. Copyright 2009 Public Library of Science.

ultrasensitive and fast detectors, TIRF microscopy has empowered researchers to visualize biological events occurring on the plasma membrane of living cells.[380] It is also possible to adjust the excitation beam such that it impinges on the sample just below the critical angle. The excitation beam then propagates into the sample at an inclined angle, which has the rough effect of only exciting a thin plane in the sample.[381] This technique, known as highly inclined and laminated optical sheet microscopy (HILO) or affectionately as poor man's TIRF, allows TIRF-like measurements to be performed internally in the cell.

Nowadays, most common SVT set-ups perform TIRF excitation by means of objective-based TIRF. In this configuration, it is easy to switch between wide-field to TIRF illumination modalities, even on a frame by frame basis.[370] TIRF microscopy is powerful for investigating dynamics at the plasma membrane, such as clathrin-mediated endocytosis of

VSV[134] and the fusion event between viral and cellular membranes.[382] A combination of TIRF microscopy and SVT identified different motional modes of MPV-like particles (VLPs) on the cell surface, and the particle trajectories provided new insights into the lateral mobility of membrane components and the heterogeneity of the plasma membrane.[139]

5.3. Confocal Microscopy

Marvin Minsky developed and patented the concept of confocal microscopy in the late 1950s with the aim of performing microscopy in thick tissues such as the brain. The basic principle of confocal microscopy is to use point illumination and a pinhole before the detector to eliminate the out-of-focus signals. For details regarding confocal microscopy, we refer the readers to ref 383. The excitation pinhole and the detection pinhole are both mounted in image planes of the microscope, thus "con-focal". In this way, only the fluorescence from the focal plane reaches the detector. This microscopy modality has a thinner depth of field and higher resolution compared to wide-field microscopy. One of the demands that Minsky had on confocal microscopy is that it could image in real time, which, according to Minsky, may have significantly delayed the acceptance of confocal microscopy.[384] Shortly after the development of the confocal microscope, lasers were invented. Lasers had high enough energy densities to perform confocal microscopy and, as light coming from the laser is collimated, an excitation pinhole was no longer needed. In addition to the laser, the development of computers and imaging software contributed to the rapid development of confocal microscopy and became commercially available in the late 1980s. There are two types of confocal microscopes (Figure 23).[385] The laser-scanning
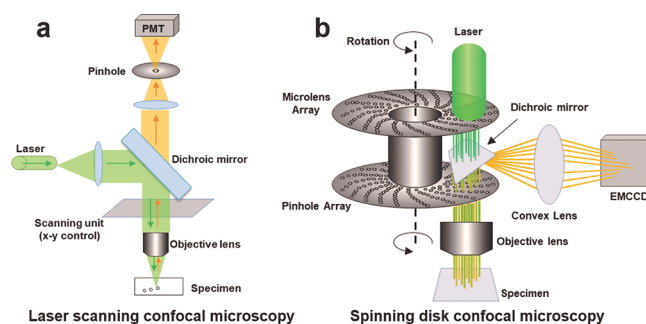
Figure 23. Schematic drawing of (a) a laser scanning confocal microscope and (b) a spinning disk confocal microscope.

confocal microscope (LSCM) scans the sample point-by-point. The sample can be scanned, typically using a piezo stage, or the excitation beam can be scanned using galvanometer mirrors (and nowadays also with resonant scanners) that can be used to increase the scanning speed. In either case, data is collected one pixel at a time and, even when the scanners have sufficient speed for imaging, one is often limited by the number of photons available per pixel. Thus, the typical image speed of a LSCM is limited to a couple of images per second and not suitable to track the dynamic behavior of quickly moving biomolecules in live cells. The second approach is to scan multiple volumes simultaneously, and a first apparatus was already built in the late 1960s.[386] This is done using a Nipkow disk and is referred to as spinning-disk confocal microscopy (SDCM).[385] The sample can be excited by multiple points

simultaneously in the focal plane and an area detector such as an EMCCD can be used to collect the detected signals. SDCM and similar approaches can significantly improve the imaging speed. Thus, SDCM has become an indispensable tool for investigating the dynamic events of biomolecules in live cells. Furthermore, combining SDCM with a fast piezo z-scan device allows recording of fast three-dimensional images and has been used for 3D single-virus tracking in live cells.[387,388]

5.4. Light Sheet Microscopy

To obtain cellular resolution imaging in intact or *in vivo* tissues, imaging methods must achieve optical sections of the tissue. Since single-particle experiments are extremely sensitive to background fluorescence and photobleaching, optical sectioning schemes such as TIRF and confocal microscopy have already been widely used for single-particle tracking in live cells. Owing to the limited imaging depth of TIRF, it is not suitable for single-particle tracking in extended 3D samples. Confocal microscopy has limitations in speed when used for 3D volumetric imaging. In addition, a good portion of the sample is always illuminated during confocal microscopy leading to photobleaching of the sample even out of the focal plane. To avoid this difficulty and to allow SVT in large biological objects in three dimensions, light sheet microscopy has been introduced. In light sheet microscopy (LSM), a focused thin plan of light is used to illuminate the sample and the emission light is collected orthogonally with a standard microscope objective and imaged.[389−391] The 3D volumetric image can be obtained by moving the coaligned excitation and detection plane relative to the sample.[392] Thus, compared with confocal microscopy, LSM is able to image thicker tissues (>1 cm) and has already successfully been utilized to image complex organisms at single-cell resolution in three dimensions, e.g. embryos of *C. elegans*, zebrafish, Drosophila, and even mouse embryos.[393−396] In addition, the plane that is illuminated by the light sheet is in the focal plane for detection and out-of-focus regions are not illuminated.

As the infection of viruses occurs in intricate 3D environments, the viral infection behavior exhibits diversified patterns *in vivo*, and consequently, the advent of light sheet microscopy will provide new insights regarding virus infection in living biological specimens.[397] Recently, inspired by LSM, Bosse and colleagues developed what they called a "Ring light sheet" and used it to reveal the remodeling of the nuclear architecture upon infection with herpes simplex virus allowing the nuclear herpes virus capsids to reach the nuclear membranes by diffusion.[398] Benefiting from the high spatiotemporal resolution provided by LSM, the tracking of rapid nuclear particle motility could be realized. The findings settled the question of how herpes virus capsids egress from the nucleus and illustrated a pathway for very large nuclear particles to cross the nuclear space by remodeling of the nuclear structure. Hoyer et al. developed a plane-scanning reversible saturable/ switchable optical transitions light-sheet nanoscope (RESOLFT), which circumvents the diffraction limit of the light sheet fluorescence microscope in the axial dimension.[399] It is believed that this charming microscopy will spark enormous interest notably in virus research because it is suitable for long-term three-dimensional imaging at high spatiotemporal resolution in living biological specimens.

5.5. SPT-PALM

In this review article, we have not discussed much about super-resolution microscopy in respect to SVT studies. One the one

hand, viruses, being often slightly smaller than the diffraction limit, are excellent objects that profit greatly from the increase produced in resolution by super-resolution techniques. As such, super-resolution methods will play an important role for viral studies. For example, PALM[229]/stochastical optical reconstruction microscopy (STORM)[400] microscopies were utilized to define spherical assembly sites of HIV (∼130 nm) in fixed cells, which is consistent with the size of mature virion particles[232,401−403] and to investigate the structure of the endosomal sorting complex required for transport (ESCRT) complex involved in the release of HIV.[404,405] On the other hand, SVT is, in a sense, a super-resolution technique as we are following a single object with nanometer spatial resolution. Thus, traditional SVT methods are more than sufficient for "super-resolution" tracking of individual viruses without the complications of the various super resolution methods, which typically have a low temporal resolution, have a high optical toxicity, and require heavy postacquisition processing. However, it should be noted that in recent years, super resolution techniques have already expanded to allow multi-color, three-dimensional single-particle tracking experiments in live cells.[406,407]

The one super-resolution approach that is of interest for SVT is SPT-PALM. By combining SPT and PALM, individual molecules present at high density can be tracked in live cells. In SPT-PALM, a small number of molecules are photoactivated in a live cell and followed using SPT. As the molecules are only sparsely activated, they can be easily tracked. After the molecules photobleach, new molecules can be photoactivated and tracked. SPT-PALM provides a large quantity of single-particle trajectories, though they are often very short due to the limited photostability of the photoactivatable FPs used for SPT-PALM. This technique has been successfully utilized to characterize the dynamics of biomolecules in a wide range of biological systems.[408−410] With respect to SVT, SPT-PALM has been used to track VSVG tagged with EosFP, providing several orders of magnitude more trajectories per cells as compared to traditional SVT methods. Thereby the authors could generate a spatially resolved map of single-molecule motility within the cell provided information regarding the heterogeneity of the cellular environment (Figure 24).[235]
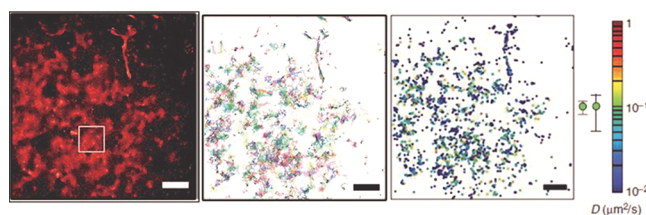
Figure 24. SPT-PALM imaging of VSVG in COS7cells. (left) PALM image of VSVG tagged with EosFP. (middle) All SPT-PALM trajectories of localized VSVG molecules. (right) Diffusion map of individual EosFP-VSVG molecules in the cell. Adapted with permission from ref 235. Copyright 2008 Springer Nature.

Unfortunately, owing to the poor photophysical properties of autofluorescent proteins, the trajectories of molecules are very short and the localization accuracy is much lower in SPT-PALM experiments. The acquisition time also has a strong influence on the localization accuracy of particles, which is associated with several factors such as imaging modality, brightness of the tags, detector sensitivity and speed, etc. Thus,
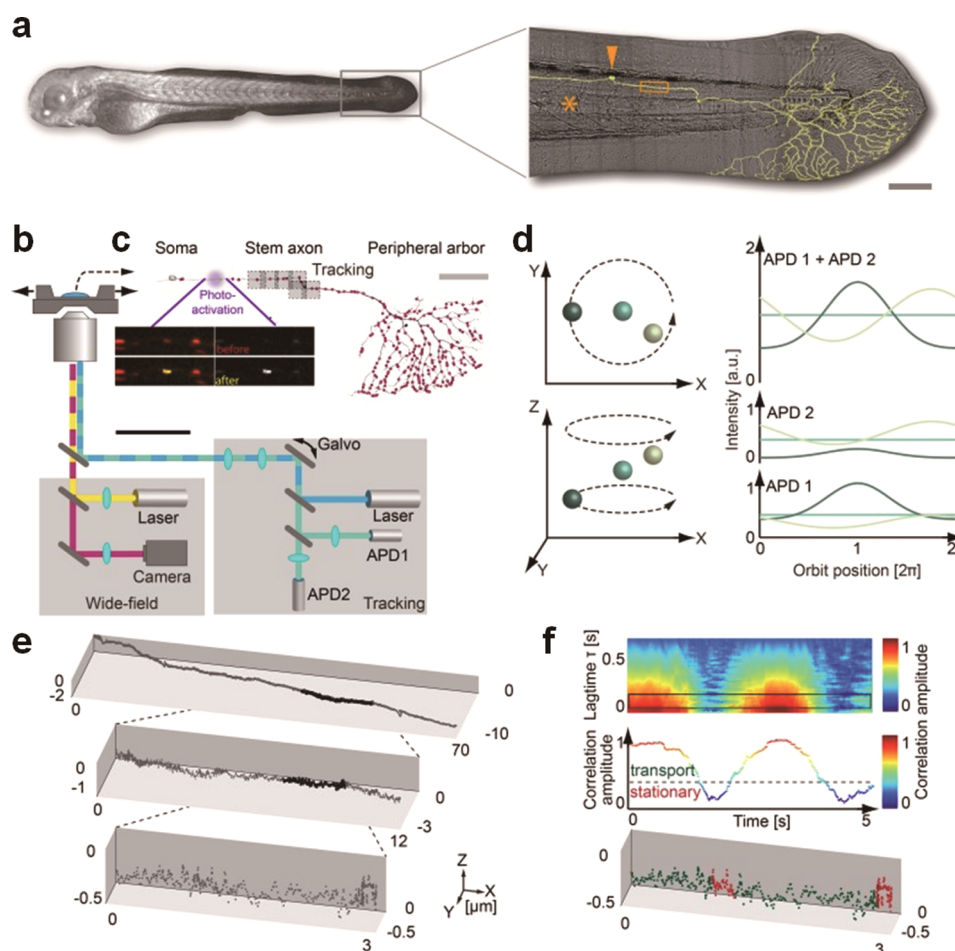
Figure 25. 3D orbital tracking. (a) Light microscopy transmission image of a zebrafish embryo and a zoom in on the tail with a typical Rohon−Beard neuron labeled by a membrane-targeted fluorescent protein (shown in yellow). (scale bar, 200 μm). (b) Schematic of the custom-built 3D real-time orbital tracking microscope consisting of a laser scanning confocal modality for tracking and a wide-field modality for simultaneous environmental observation. (c) (Upper image) Confocal reconstruction of a sensory neuron where both the membrane and the individual mitochondria are fluorescently labeled (scale bar, 100 μm). (Lower Image) Photoactivation of a single PA-GFP-labeled axonal mitochondrion (in yellow) (scale bar, 5 mm). (d) Schematic representation of the 3D orbital tracking approach. Different particle locations are indicated through spheres of varying color. Depending on the location of the particle, the phase and modulation of the signal vary. (e) Trajectory of an anterograde moving mitochondrion (100 Hz, 20,000 data points). (f) Autocorrelation carpet (top) of the angle between consecutive orbits and segregation of the trajectory into regions of directed transport (green) and stationary phases (red). Adapted with permission from ref 425. Copyright 2019 ELife Sciences Publications.

this technique is much more suited for detecting slow-diffusion events.

5.6. Orbital Tracking

Up until now, all tracking methods that we have been discussing involve *ex post facto* tracking. Movies are recorded in 2 or 3D and the tracking is performed afterward. These methods are mainly based on modified standard microscopes and achieve subpixel localization accuracy by 2D Gaussian fitting algorithm and 3D resolution using, for example, biplane[411] or multifocal plane detection,[54−56] a double-helix point spread function,[412−414] or astigmatic imaging.[415,416] Thanks to the emergence of spinning-disk confocal microscopy with high temporal resolution, it is also easy to implement z-stack imaging on a commercial confocal microscope.[417] A distinct advantage of the image-based approaches is that many fluorescent particles can be tracked at the same time. However, these methods have a lower temporal resolution.

There is a second class of SPT methods that track single particles in real time using a feedback loop. This includes

arranging four detection volumes in a tetrahedral geometry for locating the particle, championed by Werner,[418] a guided confocal microscope using prisms (for lateral tracking) and a pinhole (for axial tracking) from Yang,[419] or the newly developed MinFlux approach from Hell.[420] We utilize the orbital tracking approach proposed originally by J. Enderlein in 2000 to monitor fluorescent molecules motilities within a 2D membrane[421] and first realized in 2D and 3D by Gratton et al. in 2003.[57] In the orbital tracking approach, the laser beam is orbited in a circular path around the fluorescent particle. When the particle is in the center of the orbit, the fluorescence intensity will stay constant throughout the orbit. When the molecule moves from the center of the orbit, the fluorescence signal will modulate with the orbit and the x-y position can be obtained from the phase and the modulation of the periodic fluorescence signal using a fast Fourier transform.[422] For determining the z-position of the fluorescent particle, the difference is taken of the fluorescence intensity between two different z-planes separated by approximately half the axial width of the point-spread function. The localization method is

fast and can be utilized in a fast feedback mechanism where the orbit is recentered on the fluorescent particle and the location of the particle is written to disk. Thus, this approach allows us to track individual particles in three dimensions in real time.[58,423,424] The orbiting tracking system was used to monitor the assembly and egress of the matrix protein of Ebola virus. The researchers found that the actin coordinates the movement and assembly of VP40, a critical step in viral egress.[213]

Recently, Lamb et al. utilized a 3D orbital tracking microscope to track individual mitochondria in zebrafish embryos with nanometer precision and millisecond temporal resolution (Figure 25).[425] This demonstrates the possibility of following individual objects with high precision in living organisms. With respect to SVT, the uptake and transport of artificial viruses has also been followed using orbital tracking.[426] Orbital tracking exhibits several distinct advantages compared with image-based approaches. First of all, it has a very high spatial and temporal resolution (2−50 nm and 1−32 ms). Second, the fast Fourier transform as the localization algorithm is not sensitive to background noise and a single particle can be tracked in a scattering environment, although with a slightly lower precision. The main drawback of the orbital tracking approach is that it is not suitable to simultaneously tracking multiple particles in live cells. When particles are moving slowly, multiplexing can be performed, but in general, the approach only tracks one particle at one time. Thus, this approach is not convenient for collecting a high amount of statistics for rare events. On the other hand, as one is following the particle, one has the ability to measure various properties of that particle (e.g., spectra or lifetime[427]) or to photoactivate or manipulate that particle. In addition, the trajectory is written directly to disk in real time, which allows one to skip analysis steps 6.1 and 6.2 in the following section.

6. DATA ANALYSIS

The goal of SVT experiments is to quantitatively assess the dynamic properties of viruses during the infection process. After being able to fluorescently label the molecules and follow them using various SVT methods, the crucial procedure becomes how to extract the dynamic information from a time-series of diffraction-limited images of viruses acquired by fluorescence microscopy. For data analysis, the essential steps are to obtain the localization of each particle with subdiffraction resolution and then reconstruct single-virus trajectories by connecting the particle positions in each frame (Figure 26).[428−430] In this part, several advanced algorithms have been developed to perform precise and accurate localization and unbiased tracking.[365,431,432]

Once the trajectories have been determined, various analyses can be performed to uncover the underlying biological mechanisms in live cells. Generally, to interpret and classify the dynamics of viral behavior, the mean-square displacement (MSD) curves are calculated and fitted to models according to different types of movements.[270,433] The dynamic parameters obtained from curve fitting can be used to classify the types of the motional behaviors. As the type of motional behavior can also change, the instantaneous dynamic parameters (such as instantaneous speed and intensity) are also considered.[269]

6.1. Particle Detection

In SVT experiments, the raw data obtained by the various microscopy methods is typically a time series of diffraction-
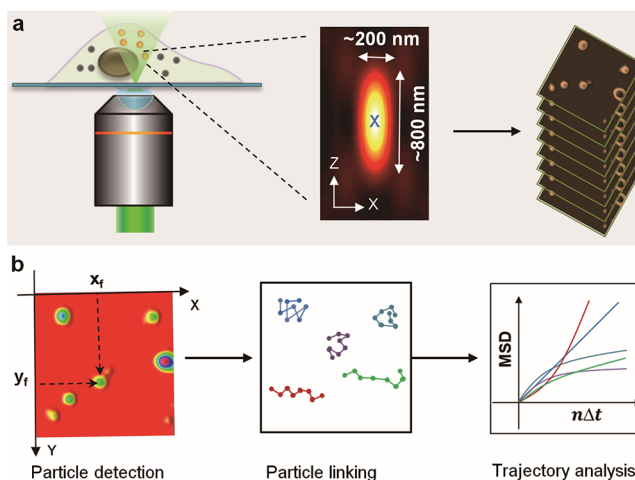

Figure 26. Schematic representation of single-virus tracking. (a) Time-series of images acquired using fluorescence microscopy. The optical spatial resolution is about 250 nm in the lateral direction and about 500 nm in the axial direction, although the localization of the particle can be determined with much higher precision. (b) Steps in SVT analysis. From the collected images, the location of the different particles is first determined, and then the same particle needs to be linked through the different frames. Once the trajectories have been determined, various analyses can be performed such as a mean-squared-displacement analysis.

limited images containing fluorescent particles. In each frame of the series, the blurred spots denote fluorescent particles. Upon detection of the individual particles, we would like to determine the location of the particle with high precision. With SPT, we typically know that the detected signal is coming from a single object. Hence, it is sufficient to locate the center of the diffracted limited spot or PSF, which can be done to a much higher precision than the width of PSF or diffraction limited resolution. To locate the center position, it is first important to understand the intensity profile of the PSF. The intensity of each particle is given by the convolution of the particle shape with the PSF. The 3D diffraction pattern of single particles can be described as a 3D PSF from the Born−Wolf model.[434]

$$PSF(x, y, z) = -\frac{2\pi i a^2 A}{\lambda f^2} e^{i\left(\frac{f}{a}\right)^2 u} \int_0^1 e^{-iu\rho^2/2} J_0(v\rho)\rho \, d\rho$$

where $u = \frac{2\pi}{\lambda}\left(\frac{a}{f}\right)^2 z$, $r = \sqrt{x^2 + y^2}$, $v = \frac{2\pi}{\lambda}\left(\frac{a}{f}\right)r$, $a/f = NA/n$, $\rho = r/a$. a, f, and r are the radius of the exit pupil, the focal distance of the objective, and the radial coordinate, respectively, n is the refractive index of the medium, λ is the wavelength of light, NA is the numerical aperture, $J_0(v\rho)$ is the Bessel function of zero order, and A is the amplitude.[435] Various algorithms have been developed to detect the particle center, which can be divided into two categories: geometric-based methods and PSF fitting methods.

The simple and most straightforward method is the centroid method, which finds the particle positions by calculating the intensity centroid of the bright region. It can be written as[50]

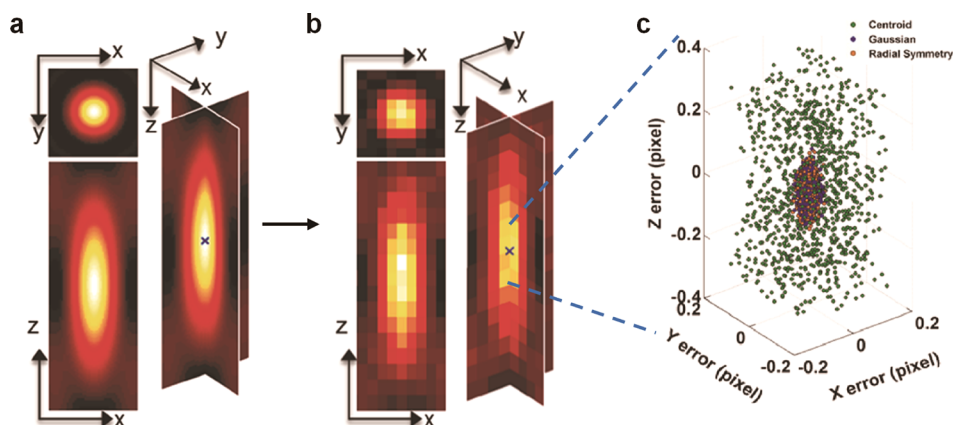$$x_f = \frac{\sum_{ijk} x_{ijk} I_{ijk}}{\sum_{ijk} I_{ijk}}$$

Figure 27. Detection of the accurate position of particles with subdiffraction resolution. (a) Image generated by sampling the point spread function (PSF) of wide-field microscopy on a 3D grid with a lattice size of 20 nm. (b) 3D CCD image simulated from the PSF image (a) with a signal-to-noise ratio of 20. The blue crosses indicate the true center of the 3D particle. (c) 3D scatter plots of the errors illustrating the error ranges of the centroid (green), Gaussian fitting (blue), and radial symmetry algorithm (red), respectively. Adapted with permission from ref 435. Copyright 2013 Springer Nature.

where x_{jik} is the coordinate of the pixel in the x direction and I_{ijk} is the intensity at the pixel (x_{ijk}, y_{ijk}, z_{ijk}). The formulas for the y and z centroid positions are analogous.

This method has the advantage that it is fast and easy to program. However, the obvious disadvantage of this method is that the localization accuracy is very sensitive to the background noise and the area selected region for the calculation.

Since the intensity of an object taken by a microscope can be described by PSF, PSF-fitting methods are widely used for particle localization. Hereinto, the Gaussian model is commonly used, since the Airy disk can be well approximated by the Gaussian distribution. In SVT, the most common fitting method is the Gaussian nonlinear least-squares fitting method. This method utilizes the iterative fitting to search for the parameters, which can minimize the weighted square error between the fit and the data.[59]

$$I(x, y, z) = B + A \exp\left[-\frac{(x - x_f)^2}{2S_x^2} - \frac{(y - y_f)^2}{2S_y^2} - \frac{(z - z_f)^2}{2S_z^2}\right]$$

where (x_f, y_f, z_f) is the actual position of the particle. S_x, S_y and S_z are the widths of PSF in the x, y, and z directions, respectively. A and B are the amplitude and background noise, respectively.[436]

The Gaussian nonlinear least-squares fitting method possesses very high localization accuracy and has been widely used in localization-based super-resolution techniques such as STORM and PALM.[432,437] However, this approach is very computationally expensive and not well suited for the large data volumes analyzed in 3D SPT. In addition, initial values are required to be set before Gaussian fitting, which can be very tedious, and inappropriate values can lead to a local minimum or, in the worst case, cause the calculation to crash.

The radial symmetry approach, as a new-type geometric-based method, has been proposed for localizing particle centers with subpixel resolution.[435,438] This method utilizes the fact that the gradient line at each pixel surrounding the signal from a single particle in a 2D or 3D image should theoretically intersect the true center of the fluorescent particle. Considering the influence of background noise and optical aberrations, the gradient lines do not intersect and the center

of the particle is estimated by selecting the point that minimizes the distance to all gradient lines. This method has no need for iterative, numerical fitting steps, so the computation speed of the method is about 2 orders of magnitude faster than that of the Gaussian fitting method and similar to that of the centroid method. Also, the radial symmetry approach has low edge sensitivity and subpixel accuracy, similar to that of the Gaussian nonlinear least-squares fitting method (Figure 27).[435] These features make our algorithm an intensely competitive method for 3D SPT applications.

6.2. Particle Linking

Once particles have been detected in the individual frames of a movie, the next step is to connect the localizations coming from the same particle from frame to frame and thereby reconstruct the particle trajectory. For data collected at low particle density, the nearest-neighbor algorithm is frequently used to identify localizations coming from the same particle in different frames. For each particle, the distances to all positions in the next frame are calculated and the minimum distance is taken as the most likely position for the same particle in the successive frame. These two positions are linked together. This procedure is repeated to link positions for as many particles in as many frames as possible and thereby obtain the entire trajectories for all the particles.[439] However, to achieve this last step, the tracking algorithm has to overcome a lot of difficulties such as temporary particle disappearance, particle merging, and particle splitting. Thus, the results acquired from this algorithm are not very reliable and usually require additional input.[440,441] In addition, it is always advisable to visually check the calculated trajectories and to manually correct them if necessary.

At high particle density, the occurrence of the interactions between particles greatly increases the difficulty of particle linking and makes the nearing-neighbor algorithms unsuitable for automatically reconstructing trajectories. Many algorithms have been developed to address tracking at high density and deal with the challenges caused by particle disappearance, merging, splitting, etc. Multiple-hypothesis tracking (MHT) is one of the most accurate methods to solve these problems.[442] All the trajectories are simultaneously constructed for the entire movie. An optimization strategy is used to select the
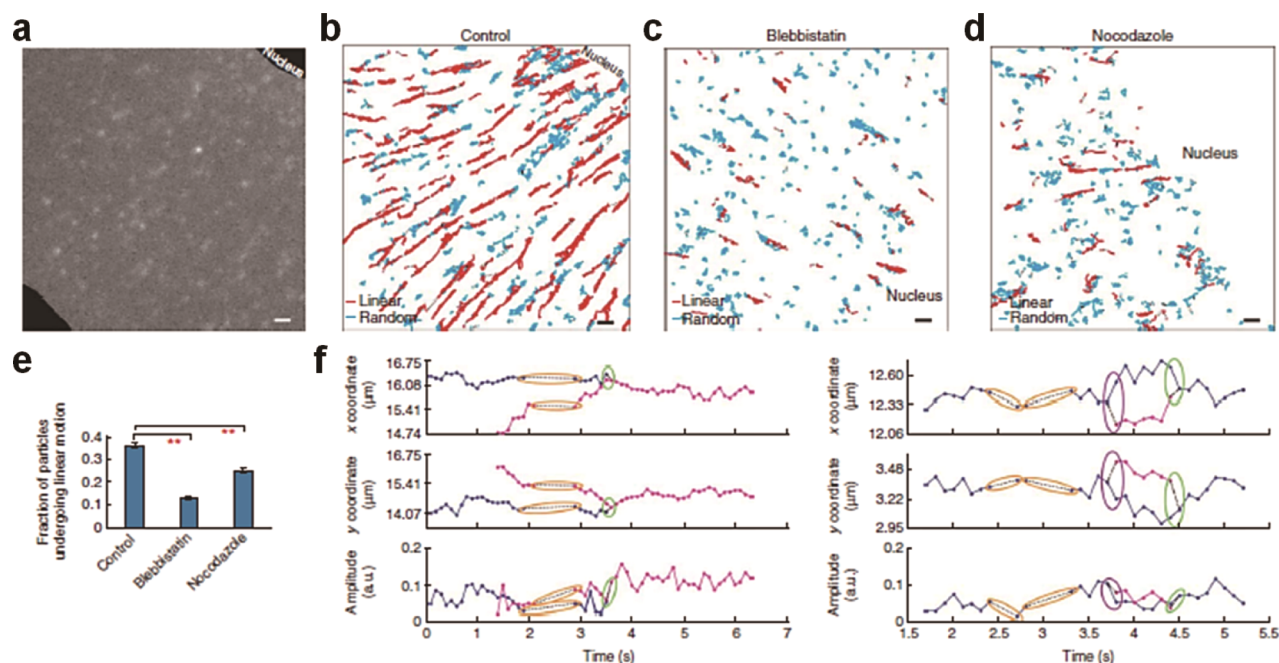
Figure 28. CD36 receptor aggregation activity depending on motion type. (a) Epifluorescence image of a macrophage where CD36 has been immunolabeled using a primary Fab fragment followed by a Cy3-conjugated secondary Fab fragment. (b) CD36 tracks in a control macrophage. (c and d) CD36 tracks in (c) a blebbistatin-treated and (d) a nocodazole-treated macrophage. Scale bars, 1 μm. (e) Bar plot showing the fraction of particles undergoing linear motion. (f) x coordinate, y coordinate, and amplitude of two sample trajectories as a function of time where merging events (green ovals), splitting events (purple ovals), and closed gaps (orange ovals) have been highlighted. Adapted with permission from ref 446. Copyright 2008 Springer Nature.

largest nonconflicting ensemble of trajectories where no two trajectories share the same position in any frame. This method is globally optimal in both time and space, but algorithms with high computational efficiency are required to just track a few tens of particles in a few tens of frames simultaneously. Therefore, several schemes have been developed to approximate the MHT solution.[53,443−445] It is worth mentioning that Jaqaman et al. have provided a robust tracking algorithm for SPT under high-density conditions that can solve all the challenges mentioned above with high accuracy and computational feasibility. Based on one mathematical framework, this method initially links the detected positions in successive frames and then connects track segments to close the gap and detect merge and split events (Figure 28).[446]

6.3. Trajectory Analysis

Once the individual trajectories have been collected, one can begin to extract the wealth of information such measurements provided. Some analyses are straightforward such as looking at colocalization and interactions between different cellular or viral components, or measuring the kinetics of viral assembly via the increase and saturation in fluorescence intensity. As mention in section 3.1.2, fluorescence intensity can also be used as a reporter of membrane fusion, especially when lipophilic dye-labeled viruses are used. Thus, the intensity vs time plot displays a distinct increase after fusion events.[68]

Other analyses can be performed to gain information with respect to the motional behavior of the viruses or viral components. The diffusion coefficient is determined by analyzing the mean square displacement (MSD), which is a measure of the spatial extent of random motion. The MSD is defined as

$$MSD(n\Delta t) = \frac{1}{N-n} \sum_{i=1}^{N-n} [r((i+n)\Delta t) - r(i\Delta t)]^2$$

where $r(\Delta t)$ is the particle position at the time point of Δt, Δt is the acquisition time of each frame, N is the total frames for the particle trajectory, and n and i are integers.[269,447,448]

How the MSD depends on the time lag ($n\Delta t$) depends on the motional behavior of the particle. For Brownian motion, the MSD depends linearly on the time lag:[12,449]

$$MSD(n\Delta t) = 2dDn\Delta t$$

where d is the space dimensionality and D is the diffusion coefficient. Hence, the diffusion coefficient can be determined from the slope of the MSD plot.

Pure random or Brownian motion is the simplest type of stochastic process. However, the cell is a crowded heterogeneous environment where many interactions can potentially happen.[12,17] In such a heterogeneous environment, particles often display anomalous diffusion. The relationship between MSD and $n\Delta t$ for anomalous diffusion is given by

$$MSD(n\Delta t) = 2dDn\Delta t^\alpha$$

where α is anomalous diffusion exponent ($\alpha < 1$).

Another type of motion that is often observed in live cells is confined diffusion. In confined diffusion, there is Brownian motion inside an enclosed environment from which the particle cannot easily escape. The dependence of MSD vs $n\Delta t$ is related to the shape of the confined region and the spatial dimensionality. The formula of this type of motion in 2D for confinement in a square is given by

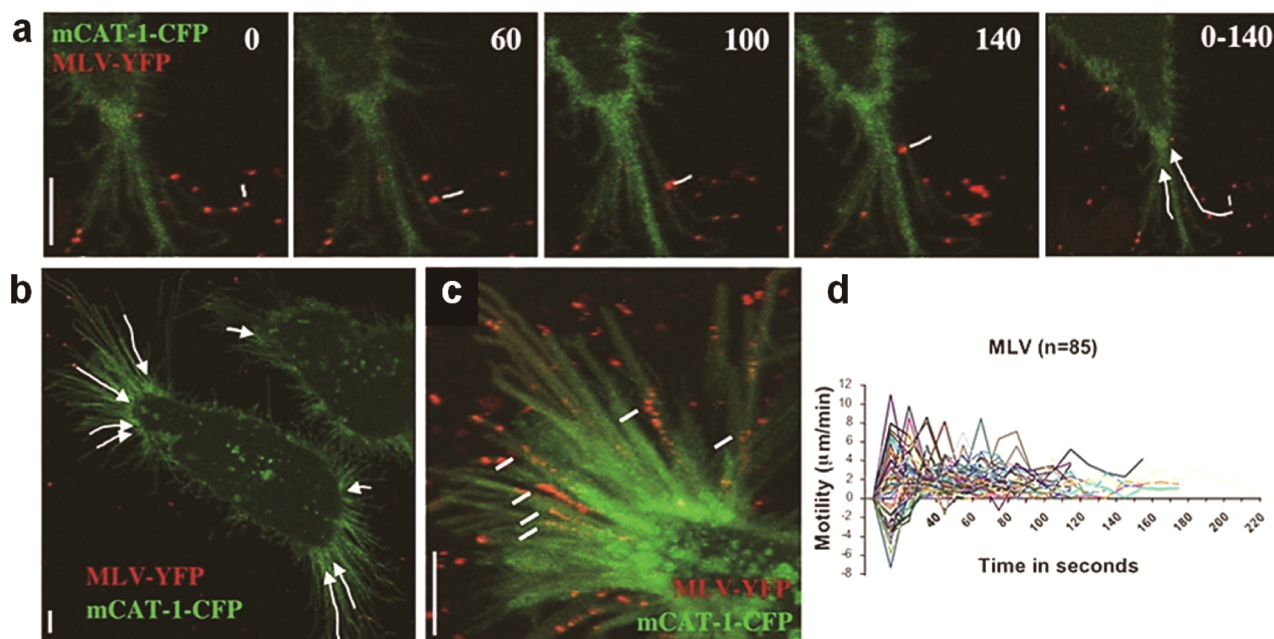$$MSD(n\Delta t) = \frac{L^2}{3}\left(1 - \exp\left(\frac{12Dn\Delta t}{L^2}\right)\right)$$

Figure 29. Virus cell surfing along filopodia. (a) Individual murine leukemia virus (MLV) labeled with YFP (red) surfing along the filopodium of a HEK 293 cell transduced with mCAT-1-CFP (green). The time in the upper righthand corner is given in seconds, and the motion from two particles is summarized as white arrows in the right-most panel. (b) Image summarizing the overall movement of selected particles on filopodia of a single HEK 293 cell. (c) Thirty-one frames from a recorded movie superimposed to show the transport and photobleaching of MLVs during the SVT experiment (moving particles are highlighted in white). (d) To quantify virus cell surfing, the motility of 85 individual MLV particles was plotted over time where time point 0 represents the moment the virus attaches to a filopodium. Adapted with permission from ref 208. Copyright 2005 The Rockefeller University Press.

where L is the length of the side of the square.[269,450,451]

In live cells, viruses are often transported along the cytoskeleton. The cytoskeleton, such as microfilaments and microtubules, is the highway of the cells. Several molecular motors walk along the cytoskeletal filaments and transport their cargo. For directed motion with a diffusional component, the MSD is given by

$$MSD(n\Delta t) = 2dDn\Delta t + (Vn\Delta t)^2$$

where V is the constant velocity for directed transport.[59] By fitting the MSD, the type of diffusional behavior can be determined as well other relevant information such as the diffusion coefficient, the velocity of directed transport, the size of confinement, or the degree of deviation from Brownian motion.

The MSD analysis is a statistical analysis and thereby very powerful but assumes the motional behavior is constant during the measurement. Often, viruses change their motional behavior, for example from 2D diffusion on the cell membrane to directed transport and then to 3D anomalous diffusion within the cytosol. In cases like this, the instantaneous speed of the particle is a useful way to characterize the transport behavior of the particle. It can clearly identify the obvious periods of directed transport of the particle and provide information on the types of motors involved in the transport process. Research has reported that the movements related to actin filaments have lower instantaneous speed in the range of 0.1−0.4 μm/s, and the instantaneous speeds associated with microtubules are one to several μm/s in live cells.[97,130,452,453] The particles may experience several different motional modes in one trajectory. By means of the dependence of instantaneous speed vs time, the different motions from a trajectory can be distinguished and analyzed separately.

7. VIRAL INFECTION MECHANISMS REVEALED BY SINGLE-VIRUS TRACKING

In the section below, we describe the current state of various applications of SVT in virology and elaborate the representative studies in detail to illustrate what information can be acquired and how SVT can be applied experimentally. The lifecycle of viruses, as obligatory intracellular parasites, is strongly coupled to interactions with the host cell. There are a number of processes that are needed for viral replication. The first encounter between viruses and host cells usually occurs via the attachment factors or receptors (such as a protein, an oligosaccharide, or a glycolipid, etc.) exposed on the cell surface. To overcome the barrier of the plasma membrane, numerous viruses hijack the endocytic pathway of host cells for internalization. Viruses are then trapped into membrane vesicles and transported to special regions for genome release. After the replication of viral components, new viruses are assembly and eventually egress to look for new cells to invade.[454,455] There is an extensive amount of excellent work in the literature, and it is not possible to highlight all articles that have made significant contributions to the field or deserve special attention.

7.1. Virus-Receptor Interactions

For virus infection, viruses primarily binding nonspecifically to attachment factors on the cell surface and migrate along the cell surface until they recognize and bind to the specific receptors. The virus-receptor binding will activate the downstream signaling and trigger the internalization of viruses.[3,5,454,456] The detailed processes of how viruses move on the cell surface to bind specific receptors is difficult to explore by conventional biochemical approaches. SVT can directly provide detailed kinetic information on this process
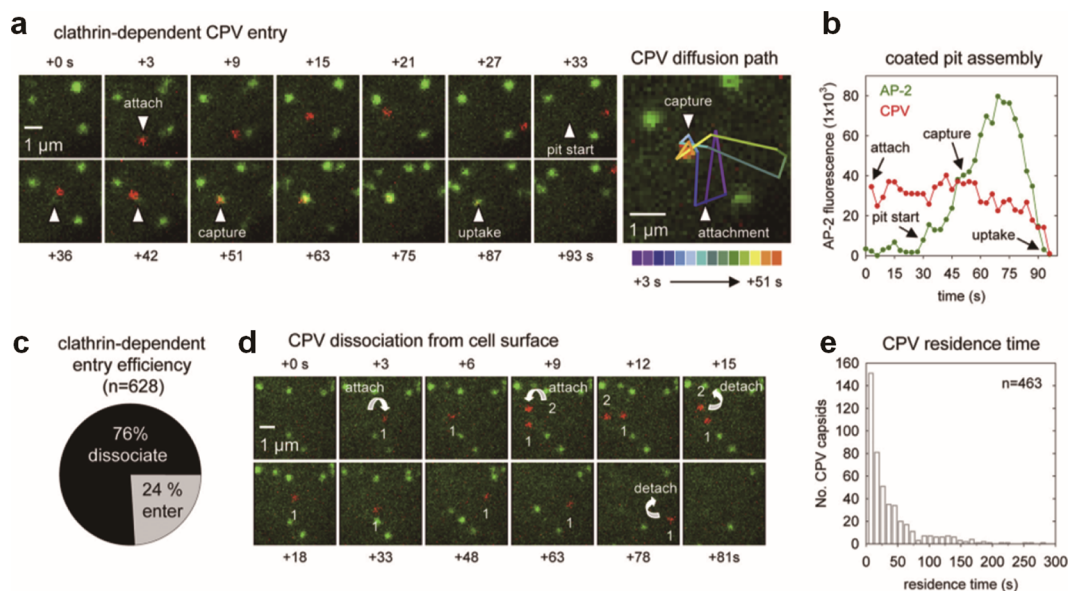
Figure 30. Real-time imaging of clathrin-dependent CPV internalization. (a) Example of clathrin-dependent CPV endocytosis. Left panels, CRFK σ2-eGFP cells (green, AP-2) were inoculated with fluorescent capsids (red) and imaged as before. Right panel, diffusion path of the capsid shown at left. A color-coded line trace of the capsid diffusion path is overlaid onto the t = 51-s image. (b) Plot of the background-corrected AP-2 (green) and capsid (red) fluorescence intensities with respect to time for the event in panel a. For frames prior to pit initiation, the AP-2 fluorescence intensity was quantified at the eventual site of pit initiation. (c) Efficiency of clathrin-dependent CPV entry. (d) Examples of CPV dissociation from the cell surface. Time-lapse images showing the attachment (downward-facing arrows) of two capsids (red; no. 1, no. 2) and subsequent capsid dissociation (upward-facing arrows). (e) Residence time of CPV capsids that dissociated from CRFK cells. Adapted with permission from ref 142. Copyright 2012 American Society for Microbiology.

and such studies have revolutionized our understanding of virus−receptor interactions.[59,457]

A recent study has highlighted the vital role of filopodia during virus infection.[458] Filopodia are actin-rich bundles protruding from the plasma membranes and participate in probing the extracellular environment, promote cell motility, and facilitate cell-to-cell interactions. More and more pieces of research reported that filopodia were exploited during the initial step of virus infection and visualized movements of different viruses along filopodia.[71,132,137,139,208,212,216] By tracking individual murine leukemia viruses (MLVs), the researchers found that MLV initially attached to the filopodia and underwent a rapid and actin-dependent lateral movement along the filopodia toward the cell body (Figure 29).[208] Meanwhile, by monitoring the lateral motility of HPV on the cell surface, four modes of HPV mobility were discovered, and only the directed movement along actin protrusions (such as filopodia or retraction fibers) enhanced HPV infection.[137] All these findings support the fact that viruses must bind to cellular receptors for promoting internalization into the cell body.

In addition, recent studies implied that viruses have different receptors for viral entry depending on cell types. The simultaneous tracking of ASLV and different receptors revealed that the infection efficiency was closely associated with the type of receptors the viruses bound to. Binding to lipid-anchored receptors may result in virus−cell membrane fusion where the genome is released into the cytosol. However, the transmembrane receptor accelerated virus uptake and provided a delay of the virus−endosome fusion event.[155] As another example, sialic acids act as receptors for many viruses, including human and avian influenza viruses. Human and avian influenza viruses preferentially bind to sialic acid linked to galactose by α-2,6 linkage and α-2,3 linkage, respec-

tively.[459,460] The binding specificity of sialic acid receptors is an important barrier in cross-species transmission. SVT was utilized to explore the dynamic mechanisms of different receptors in live cells. These observations indicated that the infection behavior of viruses was determined by the transport behavior of the sialic acid receptors.[112]

7.2. Virus Internalization

To infect and replicate, viruses must enter the intracellular environment of the host cells. After viruses bind to the receptors on the cell surface, there are mainly two strategies for virus internalization: endocytosis-independent and endocytosis-dependent internalization. In the first strategy, viruses bind to the receptors on the cell surface and then directly fuse with the plasma membrane to enter the cell. It has been known that certain enveloped viruses, such as herpes simplex virus (HSV) and Sendai virus, are internalized into cells by fusing with the plasma membrane directly at neutral pH.[454,461,462] It is considered an effective way for enveloped viruses to deliver viral genome into the cytosol. In this process, viruses first bind the specific receptors on the cell surface, which then promote the virus−membrane fusion event. On the other hand, endocytosis is hijacked by most viruses to enter the cells, which may occur via several different mechanisms, such as clathrin-mediated, caveolae-mediated, clathrin- and caveolae-independent endocytosis, and macropinocytosis.[456,463,464]

In the past, researchers investigated the endocytosis-dependent uptake of viruses by using conventional techniques such as TEM and inhibition experiments. A detailed understanding of the entry mechanisms and the dynamic processes involved in viral internalization is still lacking for most viruses. SVT has greatly contributed to our understanding of viral entry mechanisms in particular when combined with multicolor live-cell imaging. For example, by
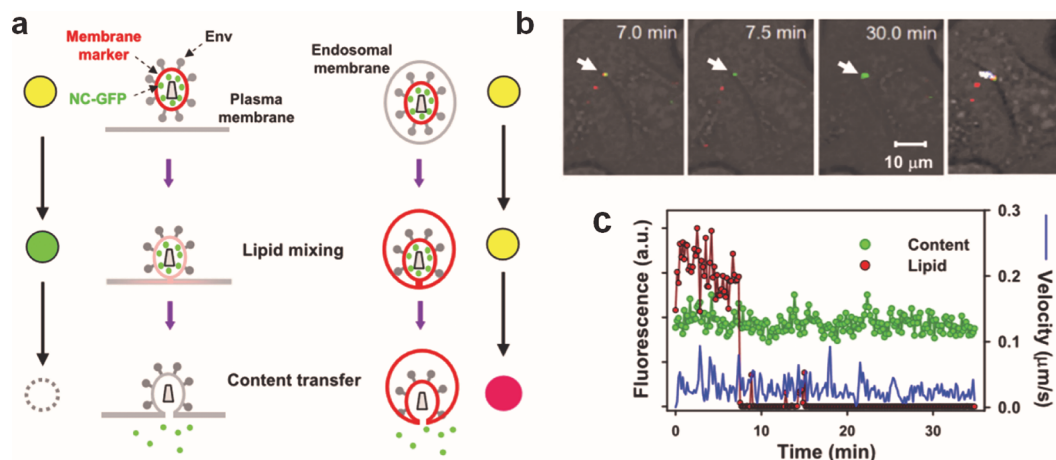
Figure 31. Identification of HIV-1 fusion sites by single-virus imaging. (a) Schematic presentation of redistribution of viral lipid and content markers upon fusion with a plasma membrane (left) and with an endosome (right). Viruses colabeled with membrane (red) and content (green) markers are pseudocolored yellow. (b and c) Partial fusion of JRFL with the plasma membrane of TZM-bl cells. The time from the beginning of imaging is shown. The two-dimensional projection of the particle's trajectory (cyan) is overlaid on the last image. Changes in fluorescence intensities (in arbitrary units) of membrane (red) and content (green) markers, as well as the instantaneous velocity (blue trace) of the particle, are shown. Adapted with permission from ref 83. Copyright 2009 Elsevier.

visualizing the interaction between the capsid of CPV and transferrin receptors on the cell surfaces, it became apparent that the interactions facilitate trapping of the viral capsid into clathrin-mediated endocytic structures by a rapid diffusion-based mechanism (Figure 30).[142] By tracking the infection behaviors of influenza virus in living cells, the entry of influenza virus followed two distinct pathways: a clathrin-mediated pathway, and a clathrin- and caveolae-independent pathway.[72] Simultaneous tracking of viruses and clathrin-coated pits indicate that most viruses promote the *de novo* formation of clathrin-coated pits around the viruses and exploit the clathrin-mediated pathway for virus internalization. In parallel, the remaining viruses enter the host cells by a clathrin- and caveolin-independent endocytic pathway with similar efficiency. Through the application of QD-based SVT and multicolor imaging, Pang's lab revealed that dynamin is involved in the clathrin-mediated pathway of influenza virus uptake and participates in the maturation and membrane fission of clathrin-coated pits in this pathway.[114] Macropinocytosis is usually considered as a nonspecific mechanism for virus entry. Several kinds of viruses have been reported to utilize macropinocytosis to infect the cells such as VV, HIV, and HSV.[462]

7.3. Virus Transport

As many viruses enter cells via an endocytosis pathway, they find themselves in intracellular vesicles and are transported to specific sites in the cell for genome release and replication. Endosomal transport along the cytoskeleton is assisted by several molecular motors including myosin, dynein, and kinesin. As a result, viral transport is a complex and multistep process, and viruses often follow several different pathways in the cytosol. With SVT, it is possible to monitor individual viruses in real time and dissect the infection behavior of each virus in living cells and thereby provide new mechanistic insights into the infection pathway of viruses. HIV has long been assumed to fuse at the plasma membrane and release the genome directly into the cytosol. However, by monitoring the early phase of viral infection, new evidence arose suggesting that the virus fused with endosomes in the cytosol of cells after receptor-mediated internalization (Figure 31).[83] Furthermore,

Cui et al. demonstrated that HIV was endocytosed and translocated into endosomes in a clathrin- and actin-dependent manner in macrophages and the viral core was released into the cytoplasm by endosomal fusion.[157]

There is plenty of evidence from SVT experiments that many viruses are transported in the cytosol in an actin filament- and microtubule-dependent manner, and microtubules assist viruses to move from the plasma membrane to the perinuclear region. This phenomenon has been reported for several kinds of viruses, including influenza virus,[68,108] DENV,[75,162] and adenovirus.[70,465] Viral transportation is a highly regulated process in live cells. For example, SVT results indicated that influenza viruses follow a five-stage process during trafficking inside the cell: viruses attach to the cell surface initially, move slowly along the actin filaments in the cell periphery, and travel rapidly toward the cell nucleus in a microtubule-dependent manner, followed by interacting and fusing with late endosomes for genome release.[108] Furthermore, the transport behavior of influenza viruses in the cytosol could be influenced by the microtubule structures. The microtubule configuration influences the destiny of individual viruses during viral transport in living cells.[110] QDs-based SVT and multicolor imaging illustrated that the retrograde motor proteins, myosin VI and dynein, were responsible for the seamless transport of viruses from microfilaments to microtubules during virus transport.[118] 3D tracking of influenza virus demonstrated that the distinct transport behaviors of viruses were associated with early and late endosomes, and the transition from early to late endosomes occurred in the perinuclear region.[111] Multicolor tracking of individual viruses and autophagosome provided an unambiguous dissection of the autophagic trafficking of viruses. Roughly one-fifth of the viruses found to enter the host cells did so through the autophagic pathway. The results provided dynamic and distinct insights into the relationship between autophagy and virus entry.[115]

7.4. Fusion and Genome Delivery of Viruses

After viruses are internalized into cells, the viral genome needs to be released into the cytosol for replication. Enveloped viruses usually enter cells via endocytosis, which has the

advantage that they can easily be transported toward the nucleus, but they need to find a way to escape the endosomes. The fusion proteins of most viruses are commonly activated under acidic pH. For instance, in late endosomes, the acidic environment induces a conformational change in the hemagglutinin, a fusion protein of influenza viruses, which mediates virus−endosome fusion for genome release.[466] Of course, not all viruses undergo pH-dependent release; nonenveloped viruses can escape the endosome for genome release through a fusion-independent manner and even for enveloped viruses. There are several pH-independent pathways and the molecular mechanisms underlying this portion of the virus life cycle remain only partially understood.

Some viruses fuse directly at the plasma membrane or can fuse either with the plasma membrane or with endosomes. Prototype foamy virus is thought to enter via both pathways. Using a dual-labeled variant of PFV, Lindemann and co-workers could visualize the fusion event in real time. Here, the envelop protein was labeled with mCherry and the capsid with eGFP. Before fusion, the virus was observable in both the eGFP and mCherry channels. Upon fusion, the eGFP from the capsid was observed to separate from the mCherry signal and was then transported into the cytoplasm (Figure 32).[467]
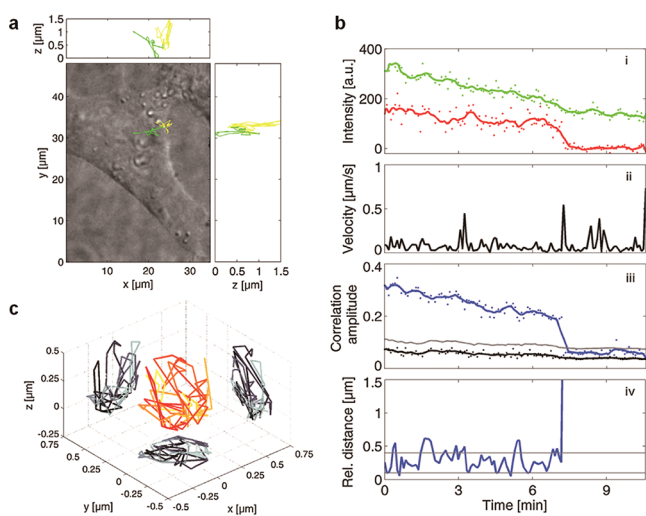

Figure 32. Fusion of PFV. (a) Bright field image of a cell overlaid with the trajectory of a dual-color PFV virus during fusion at or near the plasma membrane. The dual-color signal is shown in yellow and the single-labeled capsid in green. (b) Tracking image correlation (TrIC) analysis of the fusion event observed in panel (a). (upper panel) The fluorescence intensity of the Gag-eGFP signal (green) and mCherry-Env (red) signal, (second panel) instantaneous velocity, (third panel) cross-correlation amplitude (blue) and randomized cross-correlation signal (black), and (lower panel) relative distance between the Gag-eGFP and mCherry-Env signals plotted as a function of time. (c) 3D relative trajectory of the Env-labeled envelop with respect to the Gag-capsid showing movement in the order of hundreds of nanometers between the two labels before the completion of the fusion process. Adapted with permission from ref 467. Copyright 2013 Elsevier.

By virtue of multicolor labeled HIV viruses, Melikyan et al. found that complete viral fusion occurred in endosomes and not at the plasma membrane.[83] By labeling HIV integrase, Charneau and co-workers showed that cytosolic HIV complexes moved directly toward the cell nucleus in a microtubule and actin-dependent manner, then docked near

the nuclear membrane, and eventually diffused inside the nucleus.[87] In the case of PV, time-lapse imaging analysis indicated that the virus enters the host cell via a tyrosine- and actin-dependent endocytic pathway, and the genome release of PV occurs in the endosomes near the plasma membrane.[131] This result settled a long-lasting debate regarding where PV releases its genome.

SVT measurements of the dynamic uncoating of individual influenza viruses indicated that approximately 30% of influenza virus particles undergo uncoating through fusion with late endosomes. After viral fusion and uncoating, vRNPs are released separately into the cytosol and, following a three-stage transport process, reach the vicinity of the cell nucleus. Visualization of the intranuclear dynamic behavior of the vRNPs revealed two diffusion patterns within the nucleus. Thus, SVT significantly contributed to our understanding of the uncoating and vRNP trafficking mechanisms of influenza virus (Figure 33)[113] in particular and is helping to disperse the enigma of genome delivery in general.

Furthermore, the viral genome of influenza virus is generally replicated in the cell nucleus and exported to the cytosol as vRNPs and transported to the plasma membrane for virus egress with an uncertainty.[468,469] Live-cell tracking of fluorescent vRNPs showed that the cytoplasmic vRNPs accumulated in the recycling endosome vesicles with a Rab11 and microtubule-dependent manner[470,471] and in the vRNP/Rab11 hotspots.

7.5. Assembly and Egress of Viruses

After genome replication and protein synthesis, the goal of virus infection is to assemble and release progeny virus particles. The newly synthesized components are transported to a specific site for virus assembly, and the progeny viruses can be released from the host cells by a variety of mechanisms such as exocytosis, lysis of the cell, or budding from the plasma membrane. Compared to virus entry and transport processes, it is more challenging to investigate the dynamic mechanisms of virus assembly and egress since it is hard to label newly synthesized viral components with fluorescence. Here, FP-labeling of individual components is powerful and, with labeled constructs, fluorescence fluctuation spectroscopy can play an important role where the motional behavior of a small number of proteins can be analyzed to gain insights into mobility and interactions between viral components or between virus and cellular components. Hendrix and co-workers used a number of correlation methods to elucidate the early cytosolic steps in HIV assembly.[472] Nevertheless, there are also situations where SVT can be used to elucidate the molecular location, dynamics, and mechanisms during viral assembly and egress.[473]

Many enveloped viruses such as HIV are assembled and released from the plasma membrane of the host cell by the abscission of the viral envelope.[474] The Gag proteins of HIV are necessary for the assembly and release of virus particles. Time-lapse imaging showed that HIV Gag is initially distributed in the perinuclear region of the cytosol and then travels to the plasma membrane.[475] Using the photon counting histogram approach as well as a quantitative PALM analysis, the size and density of the HIV-Gag cluster during the assembly of virions could be calculated.[476−478] To investigate the dynamic process of HIV genome packaging, HIV RNA was labeled with a photoconvertible Eos protein. TIRF imaging results indicated that the presence of the Gag protein distinctly increased the dwell time of HIV RNA near the plasma
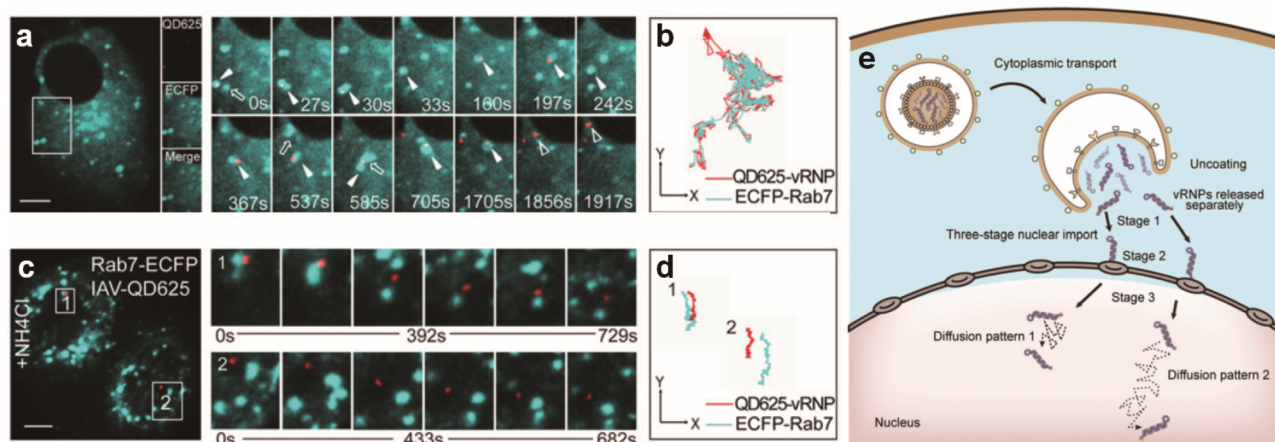
Figure 33. Real-time imaging of vRNP of influenza A viruses (IAV) release from a Rab7-positive endosome. (a) A fluorescence movie of a cell containing QD625-labeled influenza viruses (red) and Rab7-ECFP labeled endosomes (cyan) was recorded and SVT was performed. (b) Trajectories of the QD-labeled influenza virus colocalizing with the fluorescently labeled endosome from panel a. (c) Fluorescence image of an infected cell treated with NH4Cl. (d) Trajectories of the QD625 and ECFP fluorescent signals in NH4Cl-treated cells. (e) Model for IAV uncoating and vRNP dynamics. An IAV virion enters the host cell via endocytosis. Individual vRNPs finally undergo a three-stage active transport process to arrive at the cell nucleus and display two diffusion patterns within the nucleus. Adapted with permission from ref 113. Copyright 2019 National Academy of Sciences, U.S.A.
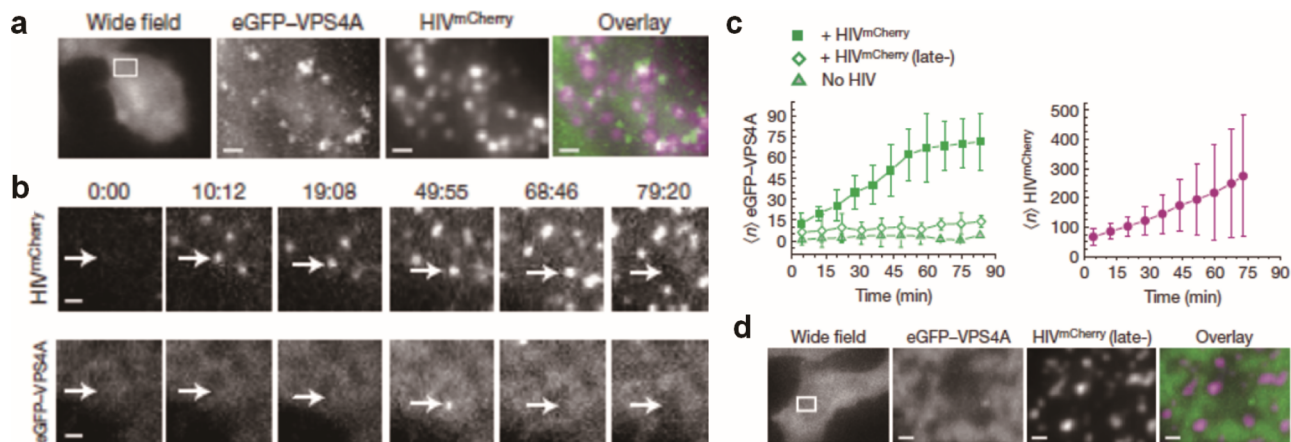

Figure 34. Recruitment of VPS4A to HIV assembly sites. (a) Wide-field image and time projections (5,926 s) from a TIRFM image series exemplifying frequent colocalization of eGFP-VPS4A bursts (green) with nascent HIV particles (magenta). (b) TIRFM images of the assembly and release of a HIV particle (top panel, arrows) and the corresponding eGFP-VPS4A channel (bottom panel, arrows). (c) Number of VPS4A bursts detected within 528 s (200 frames) in the presence of the indicated HIV derivatives (left) and number of HIV budding sites detected (right). (d) Wide-field image and time-projected TIRFM image of cells coexpressing eGFP-VPS4A (green) and the nonbudding HIV late minus mutant (magenta). All scale bars, 800 nm. Adapted with permission from ref 481. Copyright 2011 Springer Nature.

membrane.[479] Furthermore, simultaneous measurement of F-actin and HIV particles revealed that there is no characteristic pattern nor transient recruitment of F-actin during the viral budding process. The result demonstrated that the actin filaments-dependent transport pathway was dispensable for HIV Gag assembly on the plasma membrane.[480] By combining wide-field and TIRF microscopy, the assembly of the HIV protein shell was observed within ~8−9 min after nucleation of an assembly site and virus particles were formed individually. HIV release occurred ~25 min after nucleation of the viral assembly site.[370] Moreover, the transient recruitment of the ATPase VPS4 (vacuolar protein sorting 4) to nascent HIV particles at HIV budding sites on the host cell plasma membrane was observed before viral release, indicating that VPS4A played a distinct role in membrane scission for HIV-1 release (Figure 34).[481]

7.6. Cell-to-Cell Transmission of Viruses

Upon release of new viruses, the life-cycle continues with the infection of a new host cell. One mechanism for infection is cell-to-cell transmission. Nascent viruses reach a new host cell through direct cell−cell contacts, a pathway for infection that has been estimated to be 100−1000 times more efficient than the spread by cell-free dissemination.[482,483] Significantly, this spread pathway is less susceptible to the external surroundings (e.g., neutralizing antibodies, antivirus drugs, etc.). Virological synapses,[86,205,484] cell filopodia,[208,212,458,485,486] and membrane nanotubes[487−490] are three typical physical connections between cells which dramatically augment cell-to-cell transmission of many viruses. By means of SVT, the cell-to-cell transmission process can be visualized and the underlying mechanisms further uncovered by the dynamic evidence.

For instance, many viruses including HIV, HSV, and human T-lymphotropic virus (HTLV) tend to establish virological
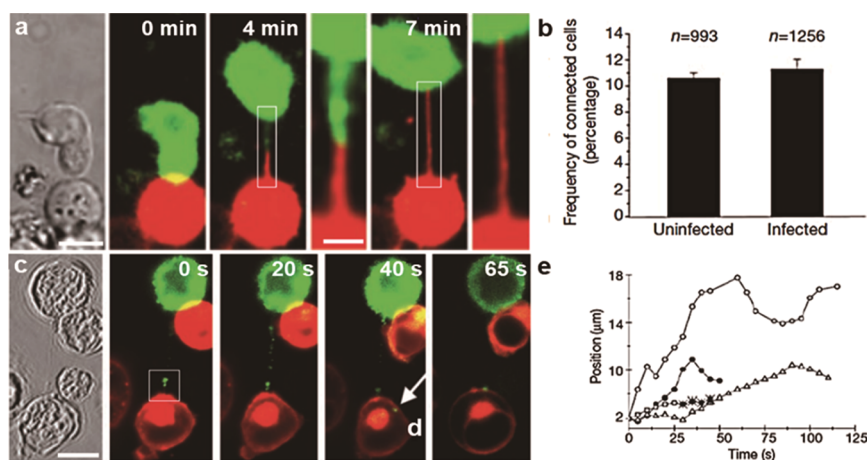
Figure 35. Membrane nanotubes present a novel route for HIV-1 to spread between T cells. (a) Membrane nanotubes were formed after intercellular contact between an infected Jurkat T cell (red) and an uninfected Jurkat T cell. (b) The frequency of membrane nanotubes formed between uninfected and infected Jurkat T cells or between two populations of uninfected Jurkat T cells. (c) Time-lapse imaging of Gag-GFP (green), expressed in the context of the fully infectious virus, along a membrane nanotube connecting infected with uninfected Jurkat T cells (red). (d) The arrow indicates Gag-GFP within the cytoplasm of the initially uninfected T cell. (e) The position of Gag-GFP is plotted against time showing generally directed movement from uninfected to infected cells. Adapted with permission from ref 489. Copyright 2008 Springer Nature.

synapses between infected donor cells and uninfected target cells through cell-to-cell transmission.[491−494] The direct translocation of HIV across the virological synapse was captured by continuous time-lapse monitoring of HIV. The dynamic information provided by quantitative, high-speed three-dimensional video microscopy indicated that HIVs dissemination between cells may be enhanced by virological synapse-mediated cell adhesion coupled with viral endocytosis.[486] Additionally, retroviruses could establish filopodial bridges by connecting infected cells with noninfected cells, and virus particles budding from infected cells would move along the outer surface of the filopodial bridge toward noninfected cells.[485] The whole process of transmission was visualized by SVT and clearly demonstrated that the cell filopodia could be exploited by retroviruses for the purpose of viral spread. Membrane nanotubes, as recently discovered membranous tethers between cells, facilitate direct intercellular communication, signaling, and the spread of pathogens.[96,489,495,496] Compared with filopodial bridges, membrane nanotubes usually span over longer distances, which means that these structures can aid the spread of virus rapidly and efficiently. The movements of GFP-fused recombinant HIVs on nanotubes were recorded, indicating that the viruses moved along the nanotubes from the infected toward uninfected cell. The process of HIVs transported along membrane nanotubes was receptor-dependent with a speed of 0.08 ± 0.03 μm/s. The results showed that membrane nanotubes presented a novel route for the rapid spread of HIV between T cells (Figure 35).[489]

8. CONCLUSIONS AND PERSPECTIVES

Single-virus tracking is a powerful tool for investigating complex dynamic processes of viruses and has become a standard lab technique now in the field of virology. The evolution and development of SVT in the past decades shed light on the mechanisms involved in the life-cycle of a variety of viruses including virus internalization, virus transport, genome delivery, and virus assembly. As an interdisciplinary technique, SVT required consecutive efforts from experts in chemistry, biology, virology, and physics. With the develop-

ment of new fluorescent tags, better labeling strategies, and novel optical instruments, SVT is continuously undergoing rapid expansion. In this review, we have given practical considerations of how to perform SVT experiments in live cells, including the choice of fluorescent tags, labeling strategies, imaging instrumentation, and data analysis, and have demonstrated the power of SVT by mentioning a few applications.

SVT has been established nearly two decades ago, and this booming technique shows no signs of slowing down. However, there are still several issues that need to be ironed out for SVT in the future. First of all, the sizes of different kinds of viruses (10−300 nm) vary largely and fluorescent tags may impair the virus infectivity in varying degrees. To reduce the influence of fluorescent labeling, only a limited amount of fluorescent tags can be used to attach to the viral components. New organic dyes and FPs with better photophysical properties are being developed and will contribute to improve SVT. Even so, monitoring the viral infection processes continuously with high temporal resolution over the entire infection process remains a big challenge. QDs, with their excellent optical brightness and photostability, are a great option and have the potential of tracking the whole infection process of individual viruses in living cells. However, QDs also have some limitations such as their larger size, photoblinking, and potential interference with the functionality of the virus. Fortunately, in many cases, QDs have been shown to have minimal influence on the virus characteristics and do not affect the viral infectivity, although to what extent QDs labeling may affect the real behavior of viruses in living cells is unclear. SVT will certainly profit from the development of new-types of QDs with small size and nonblinking to circumvent these limitations.[497−499] Smaller QDs will also most likely minimize any deleterious effects of the labeling process.

Second, the process of virus infection involves a vast number of interactions between host cells and viruses. Interactions often occurred between a small number of viral and cellular molecules. One of the future challenges will be visualizing these interactions. Here, multicolor labeling will be necessary. One possibility, as discussed above, is fluorescence fluctuation

spectroscopy. A second approach is super-resolution imaging, which has developed extensively over the past ten years and allows researchers to delineate the cellular processes on the nanoscale.[500] Super-resolution methods are commercially available and have pushed the optical resolution into the 20−100 nm range.[230,501,502] This opens the avenue for investigating the virus infection mechanisms within a subcellular environment and with subviral resolution thereby making it possible to uncover the underlying mechanisms of virus infection. New imaging techniques are still in demand to combine single-virus tracking and super-resolution microscopy for capturing and quantitative understanding of the fundamental processes involved in virus infection at nanometer spatial resolution.

Lastly, single-virus tracking is currently only limited to investigations of the infection mechanism of viruses in cultured cells, which is a simplified model system. *In vivo* experiments are needed to fully comprehend the mechanisms of virus infection. By tracking individual viruses in live tissue and animals, it may be possible to dissect the processes involved in the cell-to-cell transmission of viruses and learn how viruses break through the defense barriers of the host. To date, several groups reported the noninvasive visualization of viruses in mice,[503,504] but the real-time tracking of individual viruses *in vivo* still remains a challenge because of the limitations of current bioimaging techniques. Although optical microscopy has been a fundamental tool for biological researchers for more than three centuries, *in vivo* imaging is still restricted by light scattering. Recent advances in optical imaging techniques and *in vivo* microscopy allow images to be acquired at high resolution and unprecedented depths.[505,506] Additionally, the use of near-infrared fluorescent tags allows researchers to enhance tissue penetration of light and minimize the interference of tissue autofluorescence *in vivo*.[507−509] A series of near-infrared QDs were recently synthesized with an emission range from 800 to 1600 nm.[244,510,511,512] Of particular interest are the ultrasmall near-infrared QDs with a size of ∼2 nm and low toxicity generated via quasi biosynthesis, for example by utilizing the GSH enzymatic pathway.[245,246] Thus, enabled with these novel tools, new opportunities are becoming available for SVT to probe the dynamic interactions of viruses *in vivo* and thereby elucidate the mysteries of the infection processes.

AUTHOR INFORMATION

Corresponding Author

Dai-Wen Pang − *Nankai University, Tianjin, P. R. China, and Wuhan University, Wuhan, P. R. China;* orcid.org/0000-0002-7017-5725; Email: dwpang@whu.edu.cn

Other Authors

Shu-Lin Liu − *Nankai University, Tianjin, P. R. China, and China University of Geosciences, Wuhan, P. R. China;* orcid.org/0000-0002-1043-4238

Zhi-Gang Wang − *Nankai University, Tianjin, P. R. China;* orcid.org/0000-0002-3461-4014

Hai-Yan Xie − *Beijing Institute of Technology, Beijing, P. R. China;* orcid.org/0000-0002-6330-7929

An-An Liu − *Nankai University, Tianjin, P. R. China*

Don C. Lamb − *Ludwig-Maximilians-Universität, München, Germany;* orcid.org/0000-0002-0232-1903

Author Contributions

[#]S.-L.L. and Z.-G.W. contributed equally to this work.

Notes

The authors declare no competing financial interest.

Biographies

Shu-Lin Liu obtained her B.S. degree from Zhengzhou University (2007) and obtained her Ph.D. degree (2013) in Analytical Chemistry from Wuhan University. She worked as a postdoctoral researcher at University of Illinois at Chicago (2013−2017). After that, she worked as a professor at China University of Geosciences and now is a professor in Chemistry Department of Nankai University. Her research interests are mainly focused on single-virus tracking, lipid-mediated cell signaling, and developing new techniques for biological applications.

Zhi-Gang Wang received his B.S. degree (2005) and M.S. degree (2008) from the Department of Chemistry at Zhengzhou University. He obtained his Ph.D. degree (2014) in Analytical Chemistry from Wuhan University and finished his postdoctoral research at University of Illinois at Chicago during 2014−2017. Currently, he is an associate professor at School of Medicine, Nankai University. His main research interests include bioapplication of nanoparticles, single molecule/particle tracking, and signaling pathway and biosynthesis of QDs.

Hai-Yan Xie is a professor in the School of Life Sciences, Beijing Institute of Technology, China. She received her Ph.D. in Analytical Chemistry from Wuhan University in 2004. From 2013 to 2014, she worked as a visiting scholar in Stanford University. Her research focuses on the interdisciplinary work on biorthogonal chemistry, nanotechnology, and biomimetic biology for disease diagnosis and treatments.

An-An Liu received her bachelor's degree from Nankai University in 2008 and her Ph.D. in analytical chemistry from Wuhan University in 2016. Then she carried out postdoctoral research on single molecule imaging at Kyoto University and Okinawa Institute of Science and Technology Graduate University in Japan. She joined Nankai University in 2019 as an assistant professor. Her research focuses on developing nanomaterials and nanoprobes for bioimaging.

Don C. Lamb is Professor for Biophysical Chemistry at the LMU Munich. He obtained his Ph.D. degree from the University of Illinois at Urbana−Champaign and was a research fellow at the Harvard Medical School, an Alexander von Humboldt Research Fellow at the TU Munich, a member of the Laboratory for Fluorescence Dynamics at the University of Illinois at Urbana−Champaign, and a visiting scientist at the University of Ulm. His research focused on ultrasensitive fluorescence methods, advanced microscopy methods, protein function and dynamics, fluorescence fluctuation spectroscopies, live-cell imaging, single particle tracking, single virus tracing, and DNA nanodevices.

Dai-Wen Pang graduated with a B.S. degree in chemistry from Wuhan University in 1982 and received his Ph.D. degree in electrochemistry from Wuhan University in 1992. He was a professor at Wuhan University from 1996 to 2018 and now is a distinguished professor at Nankai University. His research interest focuses on biomedical-used quantum dots (BioQDs, especially ultrasmall biocompatible NIR-

fluorescent semiconductor nanocrystals), including space-time coupled living-cell synthesis of QDs, quasi-bio synthesis of QDs, single-virus tracking with QDs, photoluminescence mechanism of luminescent nanomaterials, and also backlight display with QDs. He was the Head of the Creative Research Group for Biomedical Probes of the National Natural Science Foundation of China (2006–2012) and 973 Chief Scientist appointed by the Ministry of Science and Technology of China for two projects of the National Key Scientific Program (2006–2015). He is now the Director of the Research Center for Analytical Sciences of Nankai University, member of the National Steering Committee for Nanotechnology, member of the Editorial Advisory Board of Analytical Chemistry, and Associate Editor for *New Journal of Chemistry*.

ACKNOWLEDGMENTS

REFERENCES

(1) Smith, A. E.; Helenius, A. How Viruses Enter Animal Cells. *Science* **2004**, *304*, 237–242.

(2) Greber, U. F.; Way, M. A Superhighway to Virus Infection. *Cell* **2006**, *124*, 741–754.

(3) Marsh, M.; Helenius, A. Virus Entry: Open Sesame. *Cell* **2006**, *124*, 729–740.

(4) Gruenberg, J. Viruses and Endosome Membrane Dynamics. *Curr. Opin. Cell Biol.* **2009**, *21*, 582–588.

(5) Sun, E.; He, J.; Zhuang, X. Live Cell Imaging of Viral Entry. *Curr. Opin. Virol.* **2013**, *3*, 34–43.

(6) Pelkmans, L.; Helenius, A. Insider Information: What Viruses Tell Us about Endocytosis. *Curr. Opin. Cell Biol.* **2003**, *15*, 414–422.

(7) Conner, S. D.; Schmid, S. L. Regulated Portals of Entry into the Cell. *Nature* **2003**, *422*, 37–44.

(8) Horan, P. K.; Melnicoff, M. J.; Jensen, B. D.; Slezak, S. E. Fluorescent Cell Labeling for in Vivo and in Vitro Cell Tracking. *Methods Cell Biol.* **1990**, *33*, 469–490.

(9) Giepmans, B. N. G. The Fluorescent Toolbox for Assessing Protein Location and Function. *Science* **2006**, *312*, 217–224.

(10) Alcor, D.; Gouzer, G.; Triller, A. Single-Particle Tracking Methods for the Study of Membrane Receptors Dynamics. *Eur. J. Neurosci.* **2009**, *30*, 987–997.

(11) Cang, H.; Shan Xu, C.; Yang, H. Progress in Single-Molecule Tracking Spectroscopy. *Chem. Phys. Lett.* **2008**, *457*, 285–291.

(12) Levi, V.; Gratton, E. Exploring Dynamics in Living Cells by Tracking Single Particles. *Cell Biochem. Biophys.* **2007**, *48*, 1–15.

(13) Shen, H.; Tauzin, L. J.; Baiyasi, R.; Wang, W.; Moringo, N.; Shuang, B.; Landes, C. F. Single Particle Tracking: From Theory to Biophysical Applications. *Chem. Rev.* **2017**, *117*, 7331–7376.

(14) Xia, T.; Li, N.; Fang, X. H. Single-Molecule Fluorescence Imaging in Living Cells. *Annu. Rev. Phys. Chem.* **2013**, *64*, 459–480.

(15) Manzo, C.; Garcia-Parajo, M. F. A Review of Progress in Single Particle Tracking: from Methods to Biophysical Insights. *Rep. Prog. Phys.* **2015**, *78*, 124601.

(16) Miller, H.; Zhou, Z.; Shepherd, J.; Wollman, A. J. M.; Leake, M. C. Single-Molecule Techniques in Biophysics: A Review of the Progress in Methods and Applications. *Rep. Prog. Phys.* **2018**, *81*, No. 024601.

(17) Wieser, S.; Schutz, G. J. Tracking Single Molecules in the Live Cell Plasma Membrane-Do's and Don't's. *Methods* **2008**, *46*, 131–140.

(18) Kusumi, A.; Tsunoyama, T. A.; Hirosawa, K. M.; Kasai, R. S.; Fujiwara, T. K. Tracking Single Molecules at Work in Living Cells. *Nat. Chem. Biol.* **2014**, *10*, 524–532.

(19) Kusumi, A.; Shirai, Y. M.; Koyama-Honda, I.; Suzuki, K. G. N.; Fujiwara, T. K. Hierarchical Organization of the Plasma Membrane: Investigations by Single-Molecule Tracking vs. Fluorescence Correlation Spectroscopy. *FEBS Lett.* **2010**, *584*, 1814–1823.

(20) Kusumi, A.; Fujiwara, T. K.; Chadda, R.; Xie, M.; Tsunoyama, T. A.; Kalay, Z.; Kasai, R. S.; Suzuki, K. G. Dynamic Organizing Principles of the Plasma Membrane That Regulate Signal Transduction: Commemorating the Fortieth Anniversary of Singer and Nicolson's Fluid-Mosaic Model. *Annu. Rev. Cell Dev. Biol.* **2012**, *28*, 215–250.

(21) Suzuki, K. G.; Kasai, R. S.; Hirosawa, K. M.; Nemoto, Y. L.; Ishibashi, M.; Miwa, Y.; Fujiwara, T. K.; Kusumi, A. Transient GPI-Anchored Protein Homodimers Are Units for Raft Organization and Function. *Nat. Chem. Biol.* **2012**, *8*, 774–783.

(22) Zhang, W.; Jiang, Y.; Wang, Q.; Ma, X.; Xiao, Z.; Zuo, W.; Fang, X.; Chen, Y. G. Single-Molecule Imaging Reveals Transforming Growth Factor-Induced Type II Receptor Dimerization. *Proc. Natl. Acad. Sci. U. S. A.* **2009**, *106*, 15679–15683.

(23) Kasai, R. S.; Kusumi, A. Single-Molecule Imaging Revealed Dynamic GPCR Dimerization. *Curr. Opin. Cell Biol.* **2014**, *27*, 78–86.

(24) Courty, S.; Luccardini, C.; Bellaiche, Y.; Cappello, G.; Dahan, M. Tracking Individual Kinesin Motors in Living Cells Using Single Quantum-Dot Imaging. *Nano Lett.* **2006**, *6*, 1491–1495.

(25) Nishikawa, S.; Arimoto, I.; Ikezaki, K.; Sugawa, M.; Ueno, H.; Komori, T.; Iwane, A. H.; Yanagida, T. Switch between Large Hand-over-Hand and Small Inchworm-Like Steps in Myosin VI. *Cell* **2010**, *142*, 879–888.

(26) Pierobon, P.; Achouri, S.; Courty, S.; Dunn, A. R.; Spudich, J. A.; Dahan, M.; Cappello, G. Velocity, Processivity, and Individual Steps of Single Myosin V Molecules in Live Cells. *Biophys. J.* **2009**, *96*, 4268–4275.

(27) Liu, S. L.; Wang, Z. G.; Hu, Y.; Xin, Y.; Singaram, I.; Gorai, S.; Zhou, X.; Shim, Y.; Min, J. H.; Gong, L. W.; et al. Quantitative Lipid Imaging Reveals a New Signaling Function of Phosphatidylinositol-3,4-Bisphophate: Isoform- and Site-Specific Activation of Akt. *Mol. Cell* **2018**, *71*, 1092–1104 e5.

(28) Sheng, R.; Chen, Y.; Yung Gee, H.; Stec, E.; Melowic, H. R.; Blatner, N. R.; Tun, M. P.; Kim, Y.; Kallberg, M.; Fujiwara, T. K.; et al. Cholesterol Modulates Cell Signaling and Protein Networking by Specifically Interacting with PDZ Domain-Containing Scaffold Proteins. *Nat. Commun.* **2012**, *3*, 1249.

(29) Komura, N.; Suzuki, K. G.; Ando, H.; Konishi, M.; Koikeda, M.; Imamura, A.; Chadda, R.; Fujiwara, T. K.; Tsuboi, H.; Sheng, R.; et al. Raft-Based Interactions of Gangliosides with a GPI-Anchored Receptor. *Nat. Chem. Biol.* **2016**, *12*, 402–410.

(30) Liu, S. L.; Wang, Z. G.; Zhang, Z. L.; Pang, D. W. Tracking Single Viruses Infecting Their Host Cells Using Quantum Dots. *Chem. Soc. Rev.* **2016**, *45*, 1211–1224.

(31) Brandenburg, B.; Zhuang, X. Virus Trafficking–Learning from Single-Virus Tracking. *Nat. Rev. Microbiol.* **2007**, *5*, 197–208.

(32) Huang, L. L.; Xie, H. Y. Progress on the Labeling and Single-Particle Tracking Technologies of Viruses. *Analyst* **2014**, *139*, 3336–3346.

(33) Parveen, N.; Borrenberghs, D.; Rocha, S.; Hendrix, J. Single Viruses on the Fluorescence Microscope: Imaging Molecular Mobility, Interactions and Structure Sheds New Light on Viral Replication. *Viruses* **2018**, *10*, 250.

(34) Axelrod, D.; Koppel, D. E.; Schlessinger, J.; Elson, E.; Webb, W. W. Mobility Measurement by Analysis of Fluorescence Photobleaching Recovery Kinetics. *Biophys. J.* **1976**, *16*, 1055–1069.

(35) Simons, K.; Gerl, M. J. Revitalizing Membrane Rafts: New Tools and Insights. *Nat. Rev. Mol. Cell Biol.* **2010**, *11*, 688–699.

(36) Magde, D.; Elson, E.; Webb, W. W. Thermodynamic Fluctuations in a Reacting System-Measurement by Fluorescence Correlation Spectroscopy. *Phys. Rev. Lett.* **1972**, *29*, 705–708.

(37) Hess, S. T.; Huang, S.; Heikal, A. A.; Webb, W. W. Biological and Chemical Applications of Fluorescence Correlation Spectroscopy: A Review. *Biochemistry* **2002**, *41*, 697–705.

(38) Haustein, E.; Schwille, P. Ultrasensitive Investigations of Biological Systems by Fluorescence Correlation Spectroscopy. *Methods* 2003, 29, 153−166.

(39) Berg, H. C. How to Track Bacteria. *Rev. Sci. Instrum.* 1971, 42, 868−871.

(40) Berg, H. C.; Brown, D. A. Chemotaxis in Escherichia Coli Analysed by Three-Dimensional Tracking. *Nature* 1972, 239, 500−504.

(41) Barak, L. S.; Webb, W. W. Diffusion of Low Density Lipoprotein-Receptor Complex on Human Fibroblasts. *J. Cell Biol.* 1982, 95, 846−852.

(42) De Brabander, M.; Geuens, G.; Nuydens, R.; Moeremans, M.; De Mey, J. Probing Microtubule-Dependent Intracellular Motility with Nanometre Particle Video Ultramicroscopy (Nanovid Ultramicroscopy). *Cytobios* 1985, 43, 273−283.

(43) Lee, G. M.; Ishihara, A.; Jacobson, K. A. Direct Observation of Brownian Motion of Lipids in a Membrane. *Proc. Natl. Acad. Sci. U. S. A.* 1991, 88, 6274−6278.

(44) Gelles, J.; Schnapp, B. J.; Sheetz, M. P. Tracking Kinesin-Driven Movements with Nanometre-Scale Precision. *Nature* 1988, 331, 450−453.

(45) Geerts, H.; de Brabander, M.; Nuydens, R. Nanovid Microscopy. *Nature* 1991, 351, 765−766.

(46) Geerts, H.; De Brabander, M.; Nuydens, R.; Geuens, S.; Moeremans, M.; De Mey, J.; Hollenbeck, P. Nanovid Tracking: A New Automatic Method for the Study of Mobility in Living Cells Based on Colloidal Gold and Video Microscopy. *Biophys. J.* 1987, 52, 775−782.

(47) Inoué, S. Imaging of Unresolved Objects, Superresolution, and Precision of Distance Measurement with Video Microscopy. *Methods Cell Biol.* 1989, 30, 85−112.

(48) Saxton, M. J. Single-Particle Tracking: Models of Directed Transport. *Biophys. J.* 1994, 67, 2110−2019.

(49) Kao, H. P.; Verkman, A. S. Tracking of Single Fluorescent Particles in 3 Dimensions-Use of Cylindrical Optics to Encode Particle Position. *Biophys. J.* 1994, 67, 1291−1300.

(50) Patwardhan, A. Subpixel Position Measurement Using 1D, 2D and 3D Centroid Algorithms with Emphasis on Applications in Confocal Microscopy. *J. Microsc.* 1997, 186, 246−257.

(51) Peters, I. M.; van Kooyk, Y.; van Vliet, S. J.; de Grooth, B. G.; Figdor, C. G.; Greve, J. 3D Single-Particle Tracking and Optical Trap Measurements on Adhesion Proteins. *Cytometry* 1999, 36, 189−194.

(52) Bacher, C. P.; Reichenzeller, M.; Athale, C.; Herrmann, H.; Eils, R. 4-D Single Particle Tracking of Synthetic and Proteinaceous Microspheres Reveals Preferential Movement of Nuclear Particles Along Chromatin-Poor Tracks. *BMC Cell Biol.* 2004, 5, 45.

(53) Genovesio, A.; Liedl, T.; Emiliani, V.; Parak, W. J.; Coppey-Moisan, M.; Olivo-Marin, J. C. Multiple Particle Tracking in 3-D+T Microscopy: Method and Application to the Tracking of Endocytosed Quantum Dots. *IEEE Trans. Image Process.* 2006, 15, 1062−1070.

(54) Ram, S.; Kim, D.; Ward, E. S.; Ober, R. J. Fast 3D Single Molecule Tracking with Multifocal Plane Microscopy in Polarized Epithelia Reveals a Novel Cellular Process of Intercellular Transfer. *Biophys. J.* 2013, 104, 535a.

(55) Ram, S.; Kim, D.; Ober, R. J.; Ward, E. S. 3D Single Molecule Tracking with Multifocal Plane Microscopy Reveals Rapid Intercellular Transferrin Transport at Epithelial Cell Barriers. *Biophys. J.* 2012, 103, 1594−1603.

(56) Ram, S.; Prabhat, P.; Chao, J.; Ward, E. S.; Ober, R. J. High Accuracy 3D Quantum Dot Tracking with Multifocal Plane Microscopy for the Study of Fast Intracellular Dynamics in Live Cells. *Biophys. J.* 2008, 95, 6025−6043.

(57) Levi, V.; Ruan, Q.; Kis-Petikova, K.; Gratton, E. Scanning FCS, a Novel Method for Three-Dimensional Particle Tracking. *Biochem. Soc. Trans.* 2003, 31, 997−1000.

(58) Dupont, A.; Lamb, D. C. Nanoscale Three-Dimensional Single Particle Tracking. *Nanoscale* 2011, 3, 4532−4541.

(59) Ruthardt, N.; Lamb, D. C.; Brauchle, C. Single-Particle Tracking as a Quantitative Microscopy-Based Approach to Unravel Cell Entry Mechanisms of Viruses and Pharmaceutical Nanoparticles. *Mol. Ther.* 2011, 19, 1199−1211.

(60) Hou, S.; Johnson, C.; Welsher, K. Real-Time 3D Single Particle Tracking: Towards Active Feedback Single Molecule Spectroscopy in Live Cells. *Molecules* 2019, 24, 2826.

(61) Montiel, D.; Yang, H. Real-Time Three-Dimensional Single-Particle Tracking Spectroscopy for Complex Systems. *Laser Photonics Rev.* 2010, 4, 374−385.

(62) Walsh, E. E.; Hruska, J. Monoclonal Antibodies to Respiratory Syncytial Virus Proteins: Identification of the Fusion Protein. *J. Virol.* 1983, 47, 171−177.

(63) Matlin, K. S.; Reggio, H.; Helenius, A.; Simons, K. Infectious Entry Pathway of Influenza Virus in a Canine Kidney Cell Line. *J. Cell Biol.* 1981, 91, 601−613.

(64) Bächi, T. Direct Observation of the Budding and Fusion of an Enveloped Virus by Video Microscopy of Viable Cells. *J. Cell Biol.* 1988, 107, 1689−1695.

(65) Lowy, R. J.; Sarkar, D. P.; Chen, Y.; Blumenthal, R. Observation of Single Influenza Virus-Cell Fusion and Measurement by Fluorescence Video Microscopy. *Proc. Natl. Acad. Sci. U. S. A.* 1990, 87, 1850−1854.

(66) Georgi, A.; Mottola-Hartshorn, C.; Warner, A.; Fields, B.; Chen, L. B. Detection of Individual Fluorescently Labeled Reovirions in Living Cells. *Proc. Natl. Acad. Sci. U. S. A.* 1990, 87, 6579−6583.

(67) Pelkmans, L.; Kartenbeck, J.; Helenius, A. Caveolar Endocytosis of Simian Virus 40 Reveals a New Two-Step Vesicular-Transport Pathway to the ER. *Nat. Cell Biol.* 2001, 3, 473−483.

(68) Lakadamyali, M.; Rust, M. J.; Babcock, H. P.; Zhuang, X. Visualizing Infection of Individual Influenza Viruses. *Proc. Natl. Acad. Sci. U. S. A.* 2003, 100, 9280−9285.

(69) Seisenberger, G.; Ried, M. U.; Endress, T.; Buning, H.; Hallek, M.; Brauchle, C. Real-Time Single-Molecule Imaging of the Infection Pathway of an Adeno-Associated Virus. *Science* 2001, 294, 1929−1932.

(70) Suomalainen, M.; Nakano, M. Y.; Keller, S.; Boucke, K.; Stidwill, R. P.; Greber, U. F. Microtubule-Dependent Plus- and Minus End-Directed Motilities Are Competing Processes for Nuclear Targeting of Adenovirus. *J. Cell Biol.* 1999, 144, 657−672.

(71) Coller, K. E.; Berger, K. L.; Heaton, N. S.; Cooper, J. D.; Yoon, R.; Randall, G. RNA Interference and Single Particle Tracking Analysis of Hepatitis C Virus Endocytosis. *PLoS Pathog.* 2009, 5, No. e1000702.

(72) Rust, M. J.; Lakadamyali, M.; Zhang, F.; Zhuang, X. Assembly of Endocytic Machinery around Individual Influenza Viruses During Viral Entry. *Nat. Struct. Mol. Biol.* 2004, 11, 567−573.

(73) van der Schaar, H. M.; Rust, M. J.; Waarts, B. L.; van der Ende-Metselaar, H.; Kuhn, R. J.; Wilschut, J.; Zhuang, X.; Smit, J. M. Characterization of the Early Events in Dengue Virus Cell Entry by Biochemical Assays and Single-Virus Tracking. *J. Virol.* 2007, 81, 12019−12028.

(74) Chen, C.; Zhuang, X. Epsin 1 Is a Cargo-Specific Adaptor for the Clathrin-Mediated Endocytosis of the Influenza Virus. *Proc. Natl. Acad. Sci. U. S. A.* 2008, 105, 11790−11795.

(75) van der Schaar, H. M.; Rust, M. J.; Chen, C.; van der Ende-Metselaar, H.; Wilschut, J.; Zhuang, X.; Smit, J. M. Dissecting the Cell Entry Pathway of Dengue Virus by Single-Particle Tracking in Living Cells. *PLoS Pathog.* 2008, 4, No. e1000244.

(76) Tsien, R. Y. The Green Fluorescent Protein. *Annu. Rev. Biochem.* 1998, 67, 509−544.

(77) Baulcombe, D. C.; Chapman, S.; Santa Cruz, S. Jellyfish Green Fluorescent Protein as a Reporter for Virus Infections. *Plant J.* 1995, 7, 1045−1053.

(78) Elliott, G.; O'Hare, P. Live-Cell Analysis of a Green Fluorescent Protein-Tagged Herpes Simplex Virus Infection. *J. Virol.* 1999, 73, 4110−4119.

(79) Cruz, S. S.; Chapman, S.; Roberts, A. G.; Roberts, I. M.; Prior, D.; Oparka, K. J. Assembly and Movement of a Plant Virus Carrying a Green Fluorescent Protein Overcoat. *Proc. Natl. Acad. Sci. U. S. A.* 1996, 93, 6286−6290.

(80) Desai, P.; Person, S. Incorporation of the Green Fluorescent Protein into the Herpes Simplex Virus Type 1 Capsid. *J. Virol.* **1998**, *72*, 7563–7568.

(81) Moradpour, D.; Evans, M. J.; Gosert, R.; Yuan, Z.; Blum, H. E.; Goff, S. P.; Lindenbach, B. D.; Rice, C. M. Insertion of Green Fluorescent Protein into Nonstructural Protein 5A Allows Direct Visualization of Functional Hepatitis C Virus Replication Complexes. *J. Virol.* **2004**, *78*, 7400–7409.

(82) McDonald, D.; Vodicka, M. A.; Lucero, G.; Svitkina, T. M.; Borisy, G. G.; Emerman, M.; Hope, T. J. Visualization of the Intracellular Behavior of HIV in Living Cells. *J. Cell Biol.* **2002**, *159*, 441–452.

(83) Miyauchi, K.; Kim, Y.; Latinovic, O.; Morozov, V.; Melikyan, G. B. HIV Enters Cells via Endocytosis and Dynamin-Dependent Fusion with Endosomes. *Cell* **2009**, *137*, 433–444.

(84) Koch, P.; Lampe, M.; Godinez, W. J.; Müller, B.; Rohr, K.; Kräusslich, H.-G.; Lehmann, M. J. Visualizing Fusion of Pseudotyped HIV-1 Particles in Real Time by Live Cell Microscopy. *Retrovirology* **2009**, *6*, 84.

(85) Endreß, T.; Lampe, M.; Briggs, J. A. G.; Kräusslich, H.-G.; Bräuchle, C.; Müller, B.; Lamb, D. C. HIV-1−Cellular Interactions Analyzed by Single Virus Tracing. *Eur. Biophys. J.* **2008**, *37*, 1291–1301.

(86) Jolly, C.; Kashefi, K.; Hollinshead, M.; Sattentau, Q. J. HIV-1 Cell to Cell Transfer Across an Env-Induced, Actin-Dependent Synapse. *J. Exp. Med.* **2004**, *199*, 283–293.

(87) Arhel, N.; Genovesio, A.; Kim, K. A.; Miko, S.; Perret, E.; Olivo-Marin, J. C.; Shorte, S.; Charneau, P. Quantitative Four-Dimensional Tracking of Cytoplasmic and Nuclear HIV-1 Complexes. *Nat. Methods* **2006**, *3*, 817–824.

(88) Hubner, W.; McNerney, G. P.; Chen, P.; Dale, B. M.; Gordon, R. E.; Chuang, F. Y.; Li, X. D.; Asmuth, D. M.; Huser, T.; Chen, B. K. Quantitative 3D Video Microscopy of HIV Transfer Across T Cell Virological Synapses. *Science* **2009**, *323*, 1743–1747.

(89) Dahan, M.; Levi, S.; Luccardini, C.; Rostaing, P.; Riveau, B.; Triller, A. Diffusion Dynamics of Glycine Receptors Revealed by Single-Quantum Dot Tracking. *Science* **2003**, *302*, 442–445.

(90) Bonneau, S.; Dahan, M.; Cohen, L. D. Single Quantum Dot Tracking Based on Perceptual Grouping Using Minimal Paths in a Spatiotemporal Volume. *IEEE T. Image Process* **2005**, *14*, 1384–1395.

(91) Bachir, A. I.; Durisic, N.; Hebert, B.; Grütter, P.; Wiseman, P. W. Characterization of Blinking Dynamics in Quantum Dot Ensembles Using Image Correlation Spectroscopy. *J. Appl. Phys.* **2006**, *99*, No. 064503.

(92) Durisic, N.; Bachir, A. I.; Kolin, D. L.; Hebert, B.; Lagerholm, B. C.; Grutter, P.; Wiseman, P. W. Detection and Correction of Blinking Bias in Image Correlation Transport Measurements of Quantum Dot Tagged Macromolecules. *Biophys. J.* **2007**, *93*, 1338–1346.

(93) He, K.; Luo, W.; Zhang, Y.; Liu, F.; Liu, D.; Xu, L.; Qin, L.; Xiong, C.; Lu, Z.; Fang, X. Intercellular Transportation of Quantum Dots Mediated by Membrane Nanotubes. *ACS Nano* **2010**, *4*, 3015–3022.

(94) Chang, Y.-P.; Pinaud, F.; Antelman, J.; Weiss, S. Tracking Bio-Molecules in Live Cells Using Quantum Dots. *J. Biophotonics* **2008**, *1*, 287–298.

(95) Pinaud, F.; Clarke, S.; Sittner, A.; Dahan, M. Probing Cellular Events, One Quantum Dot at a Time. *Nat. Methods* **2010**, *7*, 275–285.

(96) Wang, Z. G.; Liu, S. L.; Tian, Z. Q.; Zhang, Z. L.; Tang, H. W.; Pang, D. W. Myosin-Driven Intercellular Transportation of Wheat Germ Agglutinin Mediated by Membrane Nanotubes between Human Lung Cancer Cells. *ACS Nano* **2012**, *6*, 10033–10041.

(97) Liu, S. L.; Zhang, Z. L.; Sun, E. Z.; Peng, J.; Xie, M.; Tian, Z. Q.; Lin, Y.; Pang, D. W. Visualizing the Endocytic and Exocytic Processes of Wheat Germ Agglutinin by Quantum Dot-Based Single-Particle Tracking. *Biomaterials* **2011**, *32*, 7616–7624.

(98) Joo, K.-I.; Lei, Y.; Lee, C.-L.; Lo, J.; Xie, J.; Hamm-Alvarez, S. F.; Wang, P. Site-Specific Labeling of Enveloped Viruses with Quantum Dots for Single Virus Tracking. *ACS Nano* **2008**, *2*, 1553–1562.

(99) Liu, S. L.; Tian, Z. Q.; Zhang, Z. L.; Wu, Q. M.; Zhao, H. S.; Ren, B.; Pang, D. W. High-Efficiency Dual Labeling of Influenza Virus for Single-Virus Imaging. *Biomaterials* **2012**, *33*, 7828–7833.

(100) Lv, C.; Lin, Y.; Liu, A. A.; Hong, Z. Y.; Wen, L.; Zhang, Z.; Zhang, Z. L.; Wang, H.; Pang, D. W. Labeling Viral Envelope Lipids with Quantum Dots by Harnessing the Biotinylated Lipid-Self-Inserted Cellular Membrane. *Biomaterials* **2016**, *106*, 69–77.

(101) Hong, Z. Y.; Lv, C.; Liu, A. A.; Liu, S. L.; Sun, E. Z.; Zhang, Z. L.; Lei, A. W.; Pang, D. W. Clicking Hydrazine and Aldehyde: The Way to Labeling of Viruses with Quantum Dots. *ACS Nano* **2015**, *9*, 11750–11760.

(102) Wen, L.; Lin, Y.; Zheng, Z. H.; Zhang, Z. L.; Zhang, L. J.; Wang, L. Y.; Wang, H. Z.; Pang, D. W. Labeling the Nucleocapsid of Enveloped Baculovirus with Quantum Dots for Single-Virus Tracking. *Biomaterials* **2014**, *35*, 2295–2301.

(103) Xie, M.; Luo, K.; Huang, B.-H.; Liu, S.-L.; Hu, J.; Cui, D.; Zhang, Z.-L.; Xiao, G.-F.; Pang, D.-W. PEG-Interspersed Nitrilotri-acetic Acid-Functionalized Quantum Dots for Site-Specific Labeling of Prion Proteins Expressed on Cell Surfaces. *Biomaterials* **2010**, *31*, 8362–8370.

(104) Wen, L.; Zheng, Z. H.; Liu, A. A.; Lv, C.; Zhang, L. J.; Ao, J.; Zhang, Z. L.; Wang, H. Z.; Lin, Y.; Pang, D. W. Tracking Single Baculovirus Retrograde Transportation in Host Cell via Quantum Dot-Labeling of Virus Internal Component. *J. Nanobiotechnol.* **2017**, *15*, 37.

(105) Hao, J.; Huang, L. L.; Zhang, R.; Wang, H. Z.; Xie, H. Y. A Mild and Reliable Method to Label Enveloped Virus with Quantum Dots by Copper-Free Click Chemistry. *Anal. Chem.* **2012**, *84*, 8364–8370.

(106) Zhang, P.; Liu, S.; Gao, D.; Hu, D.; Gong, P.; Sheng, Z.; Deng, J.; Ma, Y.; Cai, L. Click-Functionalized Compact Quantum Dots Protected by Multidentate-Imidazole Ligands: Conjugation-Ready Nanotags for Living-Virus Labeling and Imaging. *J. Am. Chem. Soc.* **2012**, *134*, 8388–8391.

(107) Liu, H.; Liu, Y.; Liu, S.; Pang, D. W.; Xiao, G. Clathrin-Mediated Endocytosis in Living Host Cells Visualized through Quantum Dot Labeling of Infectious Hematopoietic Necrosis virus. *J. Virol.* **2011**, *85*, 6252–6262.

(108) Liu, S. L.; Zhang, Z. L.; Tian, Z. Q.; Zhao, H. S.; Liu, H.; Sun, E. Z.; Xiao, G. F.; Zhang, W.; Wang, H. Z.; Pang, D. W. Effectively and Efficiently Dissecting the Infection of Influenza Virus by Quantum-Dot-Based Single-Particle Tracking. *ACS Nano* **2012**, *6*, 141–150.

(109) Luo, K.; Li, S.; Xie, M.; Wu, D.; Wang, W.; Chen, R.; Huang, L.; Huang, T.; Pang, D.; Xiao, G. Real-Time Visualization of Prion Transport in Single Live Cells Using Quantum Dots. *Biochem. Biophys. Res. Commun.* **2010**, *394*, 493–497.

(110) Liu, S. L.; Zhang, L. J.; Wang, Z. G.; Zhang, Z. L.; Wu, Q. M.; Sun, E. Z.; Shi, Y. B.; Pang, D. W. Globally Visualizing the Microtubule-Dependent Transport Behaviors of Influenza Virus in Live Cells. *Anal. Chem.* **2014**, *86*, 3902–3908.

(111) Liu, S. L.; Wu, Q. M.; Zhang, L. J.; Wang, Z. G.; Sun, E. Z.; Zhang, Z. L.; Pang, D. W. Three-Dimensional Tracking of Rab5- and Rab7-Associated Infection Process of Influenza Virus. *Small* **2014**, *10*, 4746–4753.

(112) Wang, Z. G.; Liu, S. L.; Zhang, Z. L.; Tian, Z. Q.; Tang, H. W.; Pang, D. W. Exploring Sialic Acid Receptors-Related Infection Behavior of Avian Influenza Virus in Human Bronchial Epithelial Cells by Single-Particle Tracking. *Small* **2014**, *10*, 2712–2720.

(113) Qin, C.; Li, W.; Li, Q.; Yin, W.; Zhang, X.; Zhang, Z.; Zhang, X. E.; Cui, Z. Real-Time Dissection of Dynamic Uncoating of Individual Influenza Viruses. *Proc. Natl. Acad. Sci. U. S. A.* **2019**, *116*, 2577–2582.

(114) Sun, E. Z.; Liu, A. A.; Zhang, Z. L.; Liu, S. L.; Tian, Z. Q.; Pang, D. W. Real-Time Dissection of Distinct Dynamin-Dependent Endocytic Routes of Influenza A Virus by Quantum Dot-Based Single-Virus Tracking. *ACS Nano* **2017**, *11*, 4395–4406.

(115) Wu, Q. M.; Liu, S. L.; Chen, G.; Zhang, W.; Sun, E. Z.; Xiao, G. F.; Zhang, Z. L.; Pang, D. W. Uncovering the Rab5-Independent Autophagic Trafficking of Influenza A Virus by Quantum-Dot-Based Single-Virus Tracking. *Small* **2018**, *14*, No. e1702841.

(116) Ma, Y.; Wang, M.; Li, W.; Zhang, Z.; Zhang, X.; Tan, T.; Zhang, X. E.; Cui, Z. Live Cell Imaging of Single Genomic Loci with Quantum Dot-Labeled TALEs. *Nat. Commun.* **2017**, *8*, 15318.

(117) Li, Q.; Yin, W.; Li, W.; Zhang, Z.; Zhang, X.; Zhang, X. E.; Cui, Z. Encapsulating Quantum Dots within HIV-1 Virions through Site-Specific Decoration of the Matrix Protein Enables Single Virus Tracking in Live Primary Macrophages. *Nano Lett.* **2018**, *18*, 7457−7468.

(118) Zhang, L. J.; Xia, L.; Liu, S. L.; Sun, E. Z.; Wu, Q. M.; Wen, L.; Zhang, Z. L.; Pang, D. W. A ″Driver Switchover″ Mechanism of Influenza Virus Transport from Microfilaments to Microtubules. *ACS Nano* **2018**, *12*, 474−484.

(119) Muller, B.; Daecke, J.; Fackler, O. T.; Dittmar, M. T.; Zentgraf, H.; Krausslich, H. G. Construction and Characterization of a Fluorescently Labeled Infectious Human Immunodeficiency Virus Type 1 Derivative. *J. Virol.* **2004**, *78*, 10803−10813.

(120) Carlson, L. A.; Briggs, J. A. G.; Glass, B.; Riches, J. D.; Simon, M. N.; Johnson, M. C.; Muller, B.; Grunewald, K.; Krausslich, H. G. Three-Dimensional Analysis of Budding Sites and Released Virus Suggests a Revised Model for HIV-1 Morphogenesis. *Cell Host Microbe* **2008**, *4*, 592−599.

(121) Sakin, V.; Paci, G.; Lemke, E. A.; Muller, B. Labeling of Virus Components for Advanced, Quantitative Imaging Analyses. *FEBS Lett.* **2016**, *590*, 1896−1914.

(122) Goncalves, M. S. Fluorescent Labeling of Biomolecules with Organic Probes. *Chem. Rev.* **2009**, *109*, 190−212.

(123) Resch-Genger, U.; Grabolle, M.; Cavaliere-Jaricot, S.; Nitschke, R.; Nann, T. Quantum Dots versus Organic Dyes as Fluorescent Labels. *Nat. Methods* **2008**, *5*, 763−775.

(124) Miyawaki, A.; Sawano, A.; Kogure, T. Lighting Up Cells: Labelling Proteins with Fluorophores. *Nat. Cell Biol.* **2003**, S1−S7.

(125) Sivaraman, D.; Biswas, P.; Cella, L. N.; Yates, M. V.; Chen, W. Detecting RNA Viruses in Living Mammalian Cells by Fluorescence Microscopy. *Trends Biotechnol.* **2011**, *29*, 307−313.

(126) Wang, I. H.; Burckhardt, C. J.; Yakimovich, A.; Greber, U. F. Imaging, Tracking and Computational Analyses of Virus Entry and Egress with the Cytoskeleton. *Viruses* **2018**, *10*, 166.

(127) Rao, J.; Dragulescu-Andrasi, A.; Yao, H. Fluorescence Imaging in Vivo: Recent Advances. *Curr. Opin. Biotechnol.* **2007**, *18*, 17−25.

(128) Lakadamyali, M.; Rust, M. J.; Zhuang, X. Ligands for Clathrin-Mediated Endocytosis Are Differentially Sorted into Distinct Populations of Early Endosomes. *Cell* **2006**, *124*, 997−1009.

(129) Babcock, H. P.; Chen, C.; Zhuang, X. Using Single-Particle Tracking to Study Nuclear Trafficking of Viral Genes. *Biophys. J.* **2004**, *87*, 2749−2758.

(130) Vaughan, J. C.; Brandenburg, B.; Hogle, J. M.; Zhuang, X. Rapid Actin-Dependent Viral Motility in Live Cells. *Biophys. J.* **2009**, *97*, 1647−1656.

(131) Brandenburg, B.; Lee, L. Y.; Lakadamyali, M.; Rust, M. J.; Zhuang, X.; Hogle, J. M. Imaging Poliovirus Entry in Live Cells. *PLoS Biol.* **2007**, *5*, No. e183.

(132) Xu, H.; Hao, X.; Wang, S.; Wang, Z.; Cai, M.; Jiang, J.; Qin, Q.; Zhang, M.; Wang, H. Real-Time Imaging of Rabies Virus Entry into Living Vero Cells. *Sci. Rep.* **2015**, *5*, 11753.

(133) Vonderheit, A.; Helenius, A. Rab7 Associates with Early Endosomes to Mediate Sorting and Transport of Semliki Forest Virus to Late Endosomes. *PLoS Biol.* **2005**, *3*, No. e233.

(134) Johannsdottir, H. K.; Mancini, R.; Kartenbeck, J.; Amato, L.; Helenius, A. Host Cell Factors and Functions Involved in Vesicular Stomatitis Virus Entry. *J. Virol.* **2009**, *83*, 440−453.

(135) Engel, S.; Heger, T.; Mancini, R.; Herzog, F.; Kartenbeck, J.; Hayer, A.; Helenius, A. Role of Endosomes in Simian Virus 40 Entry and Infection. *J. Virol.* **2011**, *85*, 4198−4211.

(136) Joo, K. I.; Fang, Y.; Liu, Y.; Xiao, L.; Gu, Z.; Tai, A.; Lee, C. L.; Tang, Y.; Wang, P. Enhanced Real-Time Monitoring of Adeno-Associated Virus Trafficking by Virus-Quantum Dot Conjugates. *ACS Nano* **2011**, *5*, 3523−3535.

(137) Schelhaas, M.; Ewers, H.; Rajamaki, M. L.; Day, P. M.; Schiller, J. T.; Helenius, A. Human Papillomavirus Type 16 Entry: Retrograde Cell Surface Transport along Actin-Rich Protrusions. *PLoS Pathog.* **2008**, *4*, No. e1000148.

(138) Martin-Acebes, M. A.; Vazquez-Calvo, A.; Gonzalez-Magaldi, M.; Sobrino, F. Foot-and-Mouth Disease Virus Particles Inactivated with Binary Ethylenimine Are Efficiently Internalized into Cultured Cells. *Vaccine* **2011**, *29*, 9655−9662.

(139) Ewers, H.; Smith, A. E.; Sbalzarini, I. F.; Lilie, H.; Koumoutsakos, P.; Helenius, A. Single-Particle Tracking of Murine Polyoma Virus-Like Particles on Live Cells and Artificial Membranes. *Proc. Natl. Acad. Sci. U. S. A.* **2005**, *102*, 15110−15115.

(140) Cureton, D. K.; Massol, R. H.; Whelan, S. P.; Kirchhausen, T. The Length of Vesicular Stomatitis Virus Particles Dictates a Need for Actin Assembly During Clathrin-Dependent Endocytosis. *PLoS Pathog.* **2010**, *6*, No. e1001127.

(141) Pelkmans, L.; Puntener, D.; Helenius, A. Local Actin Polymerization and Dynamin Recruitment in SV40-Induced Internalization of Caveolae. *Science* **2002**, *296*, 535−539.

(142) Cureton, D. K.; Harbison, C. E.; Cocucci, E.; Parrish, C. R.; Kirchhausen, T. Limited Transferrin Receptor Clustering Allows Rapid Diffusion of Canine Parvovirus into Clathrin Endocytic Structures. *J. Virol.* **2012**, *86*, 5330−5340.

(143) Ehrlich, M.; Boll, W.; Van Oijen, A.; Hariharan, R.; Chandran, K.; Nibert, M. L.; Kirchhausen, T. Endocytosis by Random Initiation and Stabilization of Clathrin-Coated Pits. *Cell* **2004**, *118*, 591−605.

(144) Damm, E. M.; Pelkmans, L.; Kartenbeck, J.; Mezzacasa, A.; Kurzchalia, T.; Helenius, A. Clathrin- and Caveolin-1-Independent Endocytosis: Entry of Simian Virus 40 into Cells Devoid of Caveolae. *J. Cell Biol.* **2005**, *168*, 477−488.

(145) Meier, R.; Franceschini, A.; Horvath, P.; Tetard, M.; Mancini, R.; Von Mering, C.; Helenius, A.; Lozach, P.-Y. Genome-Wide Small Interfering RNA Screens Reveal VAMP3 as a Novel Host Factor Required for Uukuniemi Virus Late Penetration. *J. Virol.* **2014**, *88*, 8565−8578.

(146) Kalin, S.; Amstutz, B.; Gastaldelli, M.; Wolfrum, N.; Boucke, K.; Havenga, M.; DiGennaro, F.; Liska, N.; Hemmi, S.; Greber, U. F. Macropinocytotic Uptake and Infection of Human Epithelial Cells with Species B2 Adenovirus Type 35. *J. Virol.* **2010**, *84*, 5336−5350.

(147) Mishra, A.; Behera, R. K.; Behera, P. K.; Mishra, B. K.; Behera, G. B. Cyanines During the 1990s: A Review. *Chem. Rev.* **2000**, *100*, 1973−2011.

(148) Kvach, M. V.; Ustinov, A. V.; Stepanova, I. A.; Malakhov, A. D.; Skorobogatyi, M. V.; Shmanai, V. V.; Korshun, V. A. A Convenient Synthesis of Cyanine Dyes: Reagents for the Labeling of Biomolecules. *Eur. J. Org. Chem.* **2008**, *2008*, 2107−2117.

(149) Yang, X.; Shi, C.; Tong, R.; Qian, W.; Zhau, H. E.; Wang, R.; Zhu, G.; Cheng, J.; Yang, V. W.; Cheng, T.; et al. Near IR Heptamethine Cyanine Dye-Mediated Cancer Imaging. *Clin. Cancer Res.* **2010**, *16*, 2833−2844.

(150) Brauchle, C.; Seisenberger, G.; Endress, T.; Ried, M. U.; Buning, H.; Hallek, M. Single Virus Tracing: Visualization of the Infection Pathway of a Virus into a Living Cell. *ChemPhysChem* **2002**, *3*, 299−303.

(151) Berlier, J. E.; Rothe, A.; Buller, G.; Bradford, J.; Gray, D. R.; Filanoski, B. J.; Telford, W. G.; Yue, S.; Liu, J. X.; Cheung, C. Y.; et al. Quantitative Comparison of Long-Wavelength Alexa Fluor Dyes to Cy Dyes: Fluorescence of the Dyes and Their Bioconjugates. *J. Histochem. Cytochem.* **2003**, *51*, 1699−1712.

(152) Mahmoudian, J.; Hadavi, R.; Jeddi-Tehrani, M.; Mahmoudi, A. R.; Bayat, A. A.; Shaban, E.; Vafakhah, M.; Darzi, M.; Tarahomi, M.; Ghods, R. Comparison of the Photobleaching and Photostability Traits of Alexa Fluor 568-and Fluorescein Isothiocyanate- Conjugated Antibody. *Cell J.* **2011**, *13*, 169−172.

(153) Hoekstra, D.; de Boer, T.; Klappe, K.; Wilschut, J. Fluorescence Method for Measuring the Kinetics of Fusion between Biological Membranes. *Biochemistry* **1984**, *23*, 5675−5681.

(154) Floyd, D. L.; Ragains, J. R.; Skehel, J. J.; Harrison, S. C.; van Oijen, A. M. Single-Particle Kinetics of Influenza Virus Membrane Fusion. *Proc. Natl. Acad. Sci. U. S. A.* **2008**, *105*, 15382−15387.

(155) Jha, N. K.; Latinovic, O.; Martin, E.; Novitskiy, G.; Marin, M.; Miyauchi, K.; Naughton, J.; Young, J. A.; Melikyan, G. B. Imaging Single Retrovirus Entry through Alternative Receptor Isoforms and Intermediates of Virus-Endosome Fusion. *PLoS Pathog.* **2011**, *7*, No. e1001260.

(156) Hoornweg, T. E.; van Duijl-Richter, M. K. S.; Ayala Nunez, N. V.; Albulescu, I. C.; van Hemert, M. J.; Smit, J. M. Dynamics of Chikungunya Virus Cell Entry Unraveled by Single-Virus Tracking in Living Cells. *J. Virol.* **2016**, *90*, 4745−4756.

(157) Li, Q.; Li, W.; Yin, W.; Guo, J.; Zhang, Z. P.; Zeng, D.; Zhang, X.; Wu, Y.; Zhang, X. E.; Cui, Z. Single-Particle Tracking of Human Immunodeficiency Virus Type 1 Productive Entry into Human Primary Macrophages. *ACS Nano* **2017**, *11*, 3890−3903.

(158) Nanbo, A.; Imai, M.; Watanabe, S.; Noda, T.; Takahashi, K.; Neumann, G.; Halfmann, P.; Kawaoka, Y. Ebolavirus Is Internalized into Host Cells via Macropinocytosis in a Viral Glycoprotein-Dependent Manner. *PLoS Pathog.* **2010**, *6*, No. e1001121.

(159) Hao, X.; Shang, X.; Wu, J. Z.; Shan, Y. P.; Cai, M. J.; Jiang, J. G.; Huang, Z.; Tang, Z. Y.; Wang, H. D. Single-Particle Tracking of Hepatitis B Virus-Like Vesicle Entry into Cells. *Small* **2011**, *7*, 1212−1218.

(160) Le Blanc, I.; Luyet, P. P.; Pons, V.; Ferguson, C.; Emans, N.; Petiot, A.; Mayran, N.; Demaurex, N.; Faure, J.; Sadoul, R.; et al. Endosome-to-Cytosol Transport of Viral Nucleocapsids. *Nat. Cell Biol.* **2005**, *7*, 653−664.

(161) Lozach, P.-Y.; Kühbacher, A.; Meier, R.; Mancini, R.; Bitto, D.; Bouloy, M.; Helenius, A. DC-SIGN as a Receptor for Phleboviruses. *Cell Host Microbe* **2011**, *10*, 75−88.

(162) Ayala-Nuñez, N. V.; Wilschut, J.; Smit, J. M. Monitoring Virus Entry into Living Cells Using DiD-Labeled Dengue Virus Particles. *Methods* **2011**, *55*, 137−143.

(163) Crowther, D.; Melnick, J. L. The Incorporation of Neutral Red and Acridine Orange into Developing Poliovirus Particles Making Them Photosensitive. *Virology* **1961**, *14*, 11−21.

(164) Wilson, J. N.; Cooper, P. D. Aspects of the Growth of Poliovirus as Revealed by the Photodynamic Effects of Neutral Red and Acridine Orange. *Virology* **1963**, *21*, 135−145.

(165) Glynn, T. J.; Power, S.; Ryder, A. G.; Morrison, J. J. Time-Domain Measurement of Fluorescence Lifetime Variation with pH. *Proc. SPIE-Int. Soc. Opt. Eng.*; Society of Photo-optical Instrumentation Engineers: 2001.

(166) Kremser, L.; Okun, V. M.; Nicodemou, A.; Blaas, D.; Kenndler, E. Binding of Fluorescent Dye to Genomic RNA inside Intact Human Rhinovirus after Viral Capsid Penetration Investigated by Capillary Electrophoresis. *Anal. Chem.* **2004**, *76*, 882−887.

(167) Kremser, L.; Petsch, M.; Blaas, D.; Kenndler, E. Labeling of Capsid Proteins and Genomic RNA of Human Rhinovirus with Two Different Fluorescent Dyes for Selective Detection by Capillary Electrophoresis. *Anal. Chem.* **2004**, *76*, 7360−7365.

(168) Jones, L. J.; Yue, S. T.; Cheung, C. Y.; Singer, V. L. RNA Quantitation by Fluorescence-Based Solution Assay: RiboGreen Reagent Characterization. *Anal. Biochem.* **1998**, *265*, 368−374.

(169) Lin, Y.-W.; Chiu, T.-C.; Chang, H.-T. Laser-Induced Fluorescence Technique for DNA and Proteins Separated by Capillary Electrophoresis. *J. Chromatogr. B: Anal. Technol. Biomed. Life Sci.* **2003**, *793*, 37−48.

(170) Wen, L.; Lin, Y.; Zhang, Z. L.; Lu, W.; Lv, C.; Chen, Z. L.; Wang, H. Z.; Pang, D. W. Intracellular Self-Assembly Based Multi-Labeling of Key Viral Components: Envelope, Capsid and Nucleic Acids. *Biomaterials* **2016**, *99*, 24−33.

(171) Zhou, P.; Zheng, Z.; Lu, W.; Zhang, F.; Zhang, Z.; Pang, D.; Hu, B.; He, Z.; Wang, H. Multicolor Labeling of Living-Virus Particles in Live Cells. *Angew. Chem., Int. Ed.* **2012**, *51*, 670−674.

(172) Huang, L. L.; Zhou, P.; Wang, H. Z.; Zhang, R.; Hao, J.; Xie, H. Y.; He, Z. K. A New Stable and Reliable Method for Labeling Nucleic Acids of Fully Replicative Viruses. *Chem. Commun.* **2012**, *48*, 2424−2426.

(173) Shimomura, O.; Johnson, F. H.; Saiga, Y. Extraction, Purification and Properties of Aequorin, a Bioluminescent Protein from the Luminous Hydromedusan, Aequorea. *J. Cell. Comp. Physiol.* **1962**, *59*, 223−239.

(174) Chalfie, M. Green Fluorescent Protein as a Marker for Gene Expression. *Trends Genet.* **1994**, *10*, 151.

(175) Lippincott-Schwartz, J.; Patterson, G. H. Development and Use of Fluorescent Protein Markers in Living Cells. *Science* **2003**, *300*, 87−91.

(176) Day, R. N.; Davidson, M. W. The Fluorescent Protein Palette: Tools for Cellular Imaging. *Chem. Soc. Rev.* **2009**, *38*, 2887−2921.

(177) Wiedenmann, J.; Oswald, F.; Nienhaus, G. U. Fluorescent Proteins for Live Cell Imaging: Opportunities, Limitations, and Challenges. *IUBMB Life* **2009**, *61*, 1029−1042.

(178) Shaner, N. C.; Campbell, R. E.; Steinbach, P. A.; Giepmans, B. N.; Palmer, A. E.; Tsien, R. Y. Improved Monomeric Red, Orange and Yellow Fluorescent Proteins Derived from Discosoma sp. Red Fluorescent Protein. *Nat. Biotechnol.* **2004**, *22*, 1567−1572.

(179) Shkrob, M. A.; Yanushevich, Y. G.; Chudakov, D. M.; Gurskaya, N. G.; Labas, Y. A.; Poponov, S. Y.; Mudrik, N. N.; Lukyanov, S.; Lukyanov, K. A. Far-Red Fluorescent Proteins Evolved From a Blue Chromoprotein from Actinia Equina. *Biochem. J.* **2005**, *392*, 649−654.

(180) Nienhaus, K.; Nienhaus, G. U. Fluorescent Proteins for Live-Cell Imaging with Super-Resolution. *Chem. Soc. Rev.* **2014**, *43*, 1088−1106.

(181) Shcherbakova, D. M.; Verkhusha, V. V. Near-Infrared Fluorescent Proteins for Multicolor in Vivo Imaging. *Nat. Methods* **2013**, *10*, 751−754.

(182) Shcherbakova, D. M.; Subach, O. M.; Verkhusha, V. V. Red Fluorescent Proteins: Advanced Imaging Applications and Future Design. *Angew. Chem., Int. Ed.* **2012**, *51*, 10724−10738.

(183) Tomosugi, W.; Matsuda, T.; Tani, T.; Nemoto, T.; Kotera, I.; Saito, K.; Horikawa, K.; Nagai, T. An Ultramarine Fluorescent Protein with Increased Photostability and pH Insensitivity. *Nat. Methods* **2009**, *6*, 351−353.

(184) Ai, H. W.; Shaner, N. C.; Cheng, Z.; Tsien, R. Y.; Campbell, R. E. Exploration of New Chromophore Structures Leads to the Identification of Improved Blue Fluorescent Proteins. *Biochemistry* **2007**, *46*, 5904−5910.

(185) Subach, O. M.; Gundorov, I. S.; Yoshimura, M.; Subach, F. V.; Zhang, J.; Grüenwald, D.; Souslova, E. A.; Chudakov, D. M.; Verkhusha, V. V. Conversion of Red Fluorescent Protein into a Bright Blue Probe. *Chem. Biol.* **2008**, *15*, 1116−1124.

(186) Goedhart, J.; van Weeren, L.; Hink, M. A.; Vischer, N. O.; Jalink, K.; Gadella, T. W., Jr. Bright Cyan Fluorescent Protein Variants Identified by Fluorescence Lifetime Screening. *Nat. Methods* **2010**, *7*, 137−139.

(187) Ai, H. W.; Henderson, J. N.; Remington, S. J.; Campbell, R. E. Directed Evolution of a Monomeric, Bright and Photostable Version of Clavularia Cyan Fluorescent Protein: Structural Characterization and Applications in Fluorescence Imaging. *Biochem. J.* **2006**, *400*, 531−540.

(188) Samarkina, O. N.; Popova, A. G.; Gvozdik, E. Y.; Chkalina, A. V.; Zvyagin, I. V.; Rylova, Y. V.; Rudenko, N. V.; Lusta, K. A.; Kelmanson, I. V.; Gorokhovatsky, A. Y.; et al. Universal and Rapid Method for Purification of GFP-Like Proteins by the Ethanol Extraction. *Protein Expression Purif.* **2009**, *65*, 108−113.

(189) Ai, H. W.; Olenych, S. G.; Wong, P.; Davidson, M. W.; Campbell, R. E. Hue-Shifted Monomeric Variants of Clavularia Cyan Fluorescent Protein: Identification of the Molecular Determinants of Color and Applications in Fluorescence Imaging. *BMC Biol.* **2008**, *6*, 13.

(190) Shaner, N. C.; Lambert, G. G.; Chammas, A.; Ni, Y.; Cranfill, P. J.; Baird, M. A.; Sell, B. R.; Allen, J. R.; Day, R. N.; Israelsson, M. A Bright Monomeric Green Fluorescent Protein Derived from Branchiostoma Lanceolatum. *Nat. Methods* **2013**, *10*, 407−409.

(191) Miyawaki, A.; Griesbeck, O.; Heim, R.; Tsien, R. Y. Dynamic and Quantitative Ca2+ Measurements Using Improved Cameleons. *Proc. Natl. Acad. Sci. U. S. A.* **1999**, *96*, 2135−2140.

(192) Griesbeck, O.; Baird, G. S.; Campbell, R. E.; Zacharias, D. A.; Tsien, R. Y. Reducing the Environmental Sensitivity of Yellow Fluorescent Protein Mechanism and Applications. *J. Biol. Chem.* **2001**, *276*, 29188−29194.

(193) Sakaue-Sawano, A.; Kurokawa, H.; Morimura, T.; Hanyu, A.; Hama, H.; Osawa, H.; Kashiwagi, S.; Fukami, K.; Miyata, T.; Miyoshi, H. Visualizing Spatiotemporal Dynamics of Multicellular Cell-Cycle Progression. *Cell* **2008**, *132*, 487−498.

(194) Merzlyak, E. M.; Goedhart, J.; Shcherbo, D.; Bulina, M. E.; Shcheglov, A. S.; Fradkov, A. F.; Gaintzeva, A.; Lukyanov, K. A.; Lukyanov, S.; Gadella, T. W.; et al. Bright Monomeric Red Fluorescent Protein with an Extended Fluorescence Lifetime. *Nat. Methods* **2007**, *4*, 555−557.

(195) Lam, A. J.; St-Pierre, F.; Gong, Y.; Marshall, J. D.; Cranfill, P. J.; Baird, M. A.; McKeown, M. R.; Wiedenmann, J.; Davidson, M. W.; Schnitzer, M. J.; et al. Improving FRET Dynamic Range with Bright Green and Red Fluorescent Proteins. *Nat. Methods* **2012**, *9*, 1005−1012.

(196) Shcherbo, D.; Murphy, C. S.; Ermakova, G. V.; Solovieva, E. A.; Chepurnykh, T. V.; Shcheglov, A. S.; Verkhusha, V. V.; Pletnev, V. Z.; Hazelwood, K. L.; Roche, P. M.; et al. Far-Red Fluorescent Tags for Protein Imaging in Living Tissues. *Biochem. J.* **2009**, *418*, 567−574.

(197) Lin, M. Z.; McKeown, M. R.; Ng, H. L.; Aguilera, T. A.; Shaner, N. C.; Campbell, R. E.; Adams, S. R.; Gross, L. A.; Ma, W.; Alber, T.; et al. Autofluorescent Proteins with Excitation in the Optical Window for Intravital Imaging in Mammals. *Chem. Biol.* **2009**, *16*, 1169−1179.

(198) Piatkevich, K. D.; Malashkevich, V. N.; Morozova, K. S.; Nemkovich, N. A.; Almo, S. C.; Verkhusha, V. V. Extended Stokes Shift in Fluorescent Proteins: Chromophore-Protein Interactions in a Near-Infrared TagRFP675 Variant. *Sci. Rep.* **2013**, *3*, 1847.

(199) Sankaranarayanan, S.; De Angelis, D.; Rothman, J. E.; Ryan, T. A. The Use of pHluorins for Optical Measurements of Presynaptic Activity. *Biophys. J.* **2000**, *79*, 2199−2208.

(200) Shen, Y.; Rosendale, M.; Campbell, R. E.; Perrais, D. pHuji, A pH-Sensitive Red Fluorescent Protein for Imaging of Exo- and Endocytosis. *J. Cell Biol.* **2014**, *207*, 419−432.

(201) Rodriguez, E. A.; Campbell, R. E.; Lin, J. Y.; Lin, M. Z.; Miyawaki, A.; Palmer, A. E.; Shu, X.; Zhang, J.; Tsien, R. Y. The Growing and Glowing Toolbox of Fluorescent and Photoactive Proteins. *Trends Biochem. Sci.* **2017**, *42*, 111−129.

(202) Shaner, N. C.; Steinbach, P. A.; Tsien, R. Y. A Guide to Choosing Fluorescent Proteins. *Nat. Methods* **2005**, *2*, 905−909.

(203) Chudakov, D. M.; Matz, M. V.; Lukyanov, S.; Lukyanov, K. A. Fluorescent Proteins and Their Applications in Imaging Living Cells and Tissues. *Physiol. Rev.* **2010**, *90*, 1103−1163.

(204) Foo, Y. H.; Naredi-Rainer, N.; Lamb, D. C.; Ahmed, S.; Wohland, T. Factors Affecting the Quantification of Biomolecular Interactions by Fluorescence Cross-Correlation Spectroscopy. *Biophys. J.* **2012**, *102*, 1174−1183.

(205) McDonald, D.; Wu, L.; Bohks, S. M.; KewalRamani, V. N.; Unutmaz, D.; Hope, T. J. Recruitment of HIV and Its Receptors to Dendritic Cell-T Cell Junctions. *Science* **2003**, *300*, 1295−1297.

(206) Zacharias, D. A.; Tsien, R. Y. Molecular Biology and Mutation of Green Fluorescent Protein. *Methods Biochem. Anal.* **2005**, *47*, 83−120.

(207) Klingen, Y.; Conzelmann, K. K.; Finke, S. Double-Labeled Rabies Virus: Live Tracking of Enveloped Virus Transport. *J. Virol.* **2008**, *82*, 237−245.

(208) Lehmann, M. J.; Sherer, N. M.; Marks, C. B.; Pypaert, M.; Mothes, W. Actin- and Myosin-Driven Movement of Viruses along Filopodia Precedes Their Entry into Cells. *J. Cell Biol.* **2005**, *170*, 317−325.

(209) Sugimoto, K.; Uema, M.; Sagara, H.; Tanaka, M.; Sata, T.; Hashimoto, Y.; Kawaguchi, Y. Simultaneous Tracking of Capsid, Tegument, and Envelope Protein Localization in Living Cells Infected with Triply Fluorescent Herpes Simplex Virus 1. *J. Virol.* **2008**, *82*, 5198−5211.

(210) Liesche, J.; Ziomkiewicz, I.; Schulz, A. Super-Resolution Imaging with Pontamine Fast Scarlet 4BS Enables Direct Visualization of Cellulose Orientation and Cell Connection Architecture in Onion Epidermis Cells. *BMC Plant Biol.* **2013**, *13*, 226.

(211) Melikyan, G. B.; Barnard, R. J.; Abrahamyan, L. G.; Mothes, W.; Young, J. A. Imaging Individual Retroviral Fusion Events: From Hemifusion to Pore Formation and Growth. *Proc. Natl. Acad. Sci. U. S. A.* **2005**, *102*, 8728−8733.

(212) Dixit, R.; Tiwari, V.; Shukla, D. Herpes Simplex Virus Type 1 Induces Filopodia in Differentiated P19 Neural Cells to Facilitate Viral Spread. *Neurosci. Lett.* **2008**, *440*, 113−118.

(213) Adu-Gyamfi, E.; Digman, M. A.; Gratton, E.; Stahelin, R. V. Single-Particle Tracking Demonstrates That Actin Coordinates the Movement of the Ebola Virus Matrix Protein. *Biophys. J.* **2012**, *103*, L41−143.

(214) Miyauchi, K.; Marin, M.; Melikyan, G. B. Visualization of Retrovirus Uptake and Delivery into Acidic Endosomes. *Biochem. J.* **2011**, *434*, 559−569.

(215) Padilla-Parra, S.; Marin, M.; Kondo, N.; Melikyan, G. B. Pinpointing Retrovirus Entry Sites in Cells Expressing Alternatively Spliced Receptor Isoforms by Single Virus Imaging. *Retrovirology* **2014**, *11*, 47.

(216) Mercer, J.; Helenius, A. Vaccinia Virus Uses Macropinocytosis and Apoptotic Mimicry to Enter Host Cells. *Science* **2008**, *320*, 531−535.

(217) Manicassamy, B.; Manicassamy, S.; Belicha-Villanueva, A.; Pisanelli, G.; Pulendran, B.; Garcia-Sastre, A. Analysis of in Vivo Dynamics of Influenza Virus Infection in Mice Using a GFP Reporter Virus. *Proc. Natl. Acad. Sci. U. S. A.* **2010**, *107*, 11531−11536.

(218) Bencina, M. Illumination of the Spatial Order of Intracellular pH by Genetically Encoded pH-Sensitive Sensors. *Sensors* **2013**, *13*, 16736−16758.

(219) Hogue, I. B.; Bosse, J. B.; Engel, E. A.; Scherer, J.; Hu, J. R.; Del Rio, T.; Enquist, L. W. Fluorescent Protein Approaches in Alpha Herpesvirus Research. *Viruses* **2015**, *7*, 5933−5961.

(220) Jouvenet, N.; Bieniasz, P. D.; Simon, S. M. Imaging the Biogenesis of Individual HIV-1 Virions in Live Cells. *Nature* **2008**, *454*, 236−240.

(221) Hogue, I. B.; Bosse, J. B.; Hu, J. R.; Thiberge, S. Y.; Enquist, L. W. Cellular Mechanisms of Alpha Herpesvirus Eegress: Live Cell Fluorescence Microscopy of Pseudorabies Virus Exocytosis. *PLoS Pathog.* **2014**, *10*, No. e1004535.

(222) Adam, V.; Berardozzi, R.; Byrdin, M.; Bourgeois, D. Phototransformable Fluorescent Proteins: Future Challenges. *Curr. Opin. Chem. Biol.* **2014**, *20*, 92−102.

(223) Chudakov, D. M.; Verkhusha, V. V.; Staroverov, D. B.; Souslova, E. A.; Lukyanov, S.; Lukyanov, K. A. Photoswitchable Cyan Fluorescent Protein for Protein Tracking. *Nat. Biotechnol.* **2004**, *22*, 1435−1439.

(224) Nemet, I.; Ropelewski, P.; Imanishi, Y. Applications of Phototransformable Fluorescent Proteins for Tracking the Dynamics of Cellular Components. *Photochem. Photobiol. Sci.* **2015**, *14*, 1787−1806.

(225) Ando, R.; Hama, H.; Yamamoto-Hino, M.; Mizuno, H.; Miyawaki, A. An Optical Marker Based on the UV-Induced Green-to-Red Photoconversion of a Fluorescent Protein. *Proc. Natl. Acad. Sci. U. S. A.* **2002**, *99*, 12651−12656.

(226) Patterson, G. H.; Lippincott-Schwartz, J. A Photoactivatable GFP for Selective Photolabeling of Proteins and Cells. *Science* **2002**, *297*, 1873−1877.

(227) Zhou, X. X.; Lin, M. Z. Photoswitchable Fluorescent Proteins: Ten Years of Colorful Chemistry and Exciting Applications. *Curr. Opin. Chem. Biol.* **2013**, *17*, 682−690.

(228) Shroff, H.; Galbraith, C. G.; Galbraith, J. A.; White, H.; Gillette, J.; Olenych, S.; Davidson, M. W.; Betzig, E. Dual-Color Superresolution Imaging of Genetically Expressed Probes within

Individual Adhesion Complexes. *Proc. Natl. Acad. Sci. U. S. A.* **2007**, *104*, 20308−20313.

(229) Betzig, E.; Patterson, G. H.; Sougrat, R.; Lindwasser, O. W.; Olenych, S.; Bonifacino, J. S.; Davidson, M. W.; Lippincott-Schwartz, J.; Hess, H. F. Imaging Intracellular Fluorescent Proteins at Nanometer Resolution. *Science* **2006**, *313*, 1642−1645.

(230) Fernandez-Suarez, M.; Ting, A. Y. Fluorescent Probes for Super-Resolution Imaging in Living Cells. *Nat. Rev. Mol. Cell Biol.* **2008**, *9*, 929−943.

(231) Bourgeois, D.; Adam, V. Reversible Photoswitching in Fluorescent Proteins: A Mechanistic View. *IUBMB Life* **2012**, *64*, 482−491.

(232) Muranyi, W.; Malkusch, S.; Muller, B.; Heilemann, M.; Krausslich, H. G. Super-Resolution Microscopy Reveals Specific Recruitment of HIV-1 Envelope Proteins to Viral Assembly Sites Dependent on the Envelope C-Terminal Tail. *PLoS Pathog.* **2013**, *9*, No. e1003198.

(233) Muller, B.; Heilemann, M. Shedding New Light on Viruses: Super-Resolution Microscopy for Studying Human Immunodeficiency Virus. *Trends Microbiol.* **2013**, *21*, 522−533.

(234) Grove, J. Super-Resolution Microscopy: A Virus' Eye View of the Cell. *Viruses* **2014**, *6*, 1365−1378.

(235) Manley, S.; Gillette, J. M.; Patterson, G. H.; Shroff, H.; Hess, H. F.; Betzig, E.; Lippincott-Schwartz, J. High-Density Mapping of Single-Molecule Trajectories with Photoactivated Localization Microscopy. *Nat. Methods* **2008**, *5*, 155−157.

(236) Gao, X.; Cui, Y.; Levenson, R. M.; Chung, L. W. K.; Nie, S. In Vivo Cancer Targeting and Imaging with Semiconductor Quantum Dots. *Nat. Biotechnol.* **2004**, *22*, 969−976.

(237) Algar, W. R.; Susumu, K.; Delehanty, J. B.; Medintz, I. L. Semiconductor Quantum Dots in Bioanalysis: Crossing the Valley of Death. *Anal. Chem.* **2011**, *83*, 8826−8837.

(238) Wegner, K. D.; Hildebrandt, N. Quantum Dots: Bright and Versatile in Vitro and in Vivo Fluorescence Imaging Biosensors. *Chem. Soc. Rev.* **2015**, *44*, 4792−4834.

(239) Chen, G.; Zhu, J. Y.; Zhang, Z. L.; Zhang, W.; Ren, J. G.; Wu, M.; Hong, Z. Y.; Lv, C.; Pang, D. W.; Zhao, Y. F. Transformation of Cell-Derived Microparticles into Quantum-Dot-Labeled Nanovectors for Antitumor siRNA Delivery. *Angew. Chem., Int. Ed.* **2015**, *54*, 1036−1040.

(240) Rosenthal, S. J.; Chang, J. C.; Kovtun, O.; McBride, J. R.; Tomlinson, I. D. Biocompatible Quantum Dots for Biological Applications. *Chem. Biol.* **2011**, *18*, 10−24.

(241) Jethi, L.; Mack, T. G.; Kambhampati, P. Extending Semiconductor Nanocrystals from the Quantum Dot Regime to the Molecular Cluster Regime. *J. Phys. Chem. C* **2017**, *121*, 26102−26107.

(242) Zhou, J.; Liu, Y.; Tang, J.; Tang, W. Surface Ligands Engineering of Semiconductor Quantum Dots for Chemosensory and Biological Applications. *Mater. Today* **2017**, *20*, 360−376.

(243) Zhou, J.; Yang, Y.; Zhang, C. Y. Toward Biocompatible Semiconductor Quantum Dots: From Biosynthesis and Bioconjugation to Biomedical Application. *Chem. Rev.* **2015**, *115*, 11669−11717.

(244) Zhang, M.; Yue, J.; Cui, R.; Ma, Z.; Wan, H.; Wang, F.; Zhu, S.; Zhou, Y.; Kuang, Y.; Zhong, Y.; et al. Bright Quantum Dots Emitting at Approximately 1,600 nm in the NIR-IIb Window for Deep Tissue Fluorescence Imaging. *Proc. Natl. Acad. Sci. U. S. A.* **2018**, *115*, 6590−6595.

(245) Zhao, J. Y.; Chen, G.; Gu, Y. P.; Cui, R.; Zhang, Z. L.; Yu, Z. L.; Tang, B.; Zhao, Y. F.; Pang, D. W. Ultrasmall Magnetically Engineered Ag2Se Quantum Dots for Instant Efficient Labeling and Whole-Body High-Resolution Multimodal Real-Time Tracking of Cell-Derived Microvesicles. *J. Am. Chem. Soc.* **2016**, *138*, 1893−1903.

(246) Gu, Y. P.; Cui, R.; Zhang, Z. L.; Xie, Z. X.; Pang, D. W. Ultrasmall Near-Infrared Ag2Se Quantum Dots with Tunable Fluorescence for in Vivo Imaging. *J. Am. Chem. Soc.* **2012**, *134*, 79−82.

(247) Alivisatos, A. P.; Gu, W. W.; Larabell, C. Quantum Dots as Cellular Probes. *Annu. Rev. Biomed. Eng.* **2005**, *7*, 55−76.

(248) Gao, X.; Yang, L.; Petros, J. A.; Marshall, F. F.; Simons, J. W.; Nie, S. In Vivo Molecular and Cellular Imaging with Quantum Dots. *Curr. Opin. Biotechnol.* **2005**, *16*, 63−72.

(249) Bruchez, M.; Moronne, M.; Gin, P.; Weiss, S.; Alivisatos, A. P. Semiconductor Nanocrystals as Fluorescent Biological Labels. *Science* **1998**, *281*, 2013−2016.

(250) Smith, A. M.; Duan, H. W.; Mohs, A. M.; Nie, S. M. Bioconjugated Quantum Dots for in Vivo Molecular and Cellular Imaging. *Adv. Drug Delivery Rev.* **2008**, *60*, 1226−1240.

(251) Lidke, D. S.; Nagy, P.; Heintzmann, R.; Arndt-Jovin, D. J.; Post, J. N.; Grecco, H. E.; Jares-Erijman, E. A.; Jovin, T. M. Quantum Dot Ligands Provide New Insights into erbB/HER Receptor− Mediated Signal Transduction. *Nat. Biotechnol.* **2004**, *22*, 198−203.

(252) Srinivasan, C.; Lee, J.; Papadimitrakopoulos, F.; Silbart, L. K.; Zhao, M.; Burgess, D. J. Labeling and Intracellular Tracking of Functionally Active Plasmid DNA with Semiconductor Quantum Dots. *Mol. Ther.* **2006**, *14*, 192−201.

(253) Wu, X.; Liu, H.; Liu, J.; Haley, K. N.; Treadway, J. A.; Larson, J. P.; Ge, N.; Peale, F.; Bruchez, M. P. Immunofluorescent Labeling of Cancer Marker Her2 and Other Cellular Targets with Semiconductor Quantum Dots. *Nat. Biotechnol.* **2003**, *21*, 41−46.

(254) Chen, C.; Peng, J.; Xia, H.; Wu, Q.; Zeng, L.; Xu, H.; Tang, H.; Zhang, Z.; Zhu, X.; Pang, D.; et al. Quantum-Dot-Based Immunofluorescent Imaging of HER2 and ER Provides New Insights into Breast Cancer Heterogeneity. *Nanotechnology* **2010**, *21*, No. 095101.

(255) Chen, C.; Xia, H. S.; Gong, Y. P.; Peng, J.; Peng, C. W.; Hu, M. B.; Zhu, X. B.; Pang, D. W.; Sun, S. R.; Li, Y. The Quantitative Detection of Total HER2 Load by Quantum Dots and the Identification of a New Subtype of Breast Cancer with Different 5-Year Prognosis. *Biomaterials* **2010**, *31*, 8818−8825.

(256) Chen, C.; Liu, S. L.; Cui, R.; Huang, B. H.; Tian, Z. Q.; Jiang, P.; Pang, D. W.; Zhang, Z. L. Diffusion Behaviors of Water-Soluble CdSe/ZnS Core/Shell Quantum Dots Investigated by Single-Particle Tracking. *J. Phys. Chem. C* **2008**, *112*, 18904−18910.

(257) Gao, X.; Wang, T.; Wu, B.; Chen, J.; Chen, J.; Yue, Y.; Dai, N.; Chen, H.; Jiang, X. Quantum Dots for Tracking Cellular Transport of Lectin-Functionalized Nanoparticles. *Biochem. Biophys. Res. Commun.* **2008**, *377*, 35−40.

(258) Rajan, S. S.; Liu, H. Y.; Vu, T. Q. Ligand-Bound Quantum Dot Probes for Studying the Molecular Scale Dynamics of Receptor Endocytic Trafficking in Live Cells. *ACS Nano* **2008**, *2*, 1153−1166.

(259) Murcia, M. J.; Minner, D. E.; Mustata, G. M.; Ritchie, K.; Naumann, C. A. Design of Quantum Dot-Conjugated Lipids for Long-Term, High-Speed Tracking Experiments on Cell Surfaces. *J. Am. Chem. Soc.* **2008**, *130*, 15054−15062.

(260) Medintz, I. L.; Uyeda, H. T.; Goldman, E. R.; Mattoussi, H. Quantum Dot Bioconjugates for Imaging, Labelling and Sensing. *Nat. Mater.* **2005**, *4*, 435−446.

(261) Michalet, X.; Pinaud, F. F.; Bentolila, L. A.; Tsay, J. M.; Doose, S.; Li, J. J.; Sundaresan, G.; Wu, A. M.; Gambhir, S. S.; Weiss, S. Quantum Dots for Live Cells, in Vivo Imaging, and Diagnostics. *Science* **2005**, *307*, 538−544.

(262) Bentolila, L. A.; Ebenstein, Y.; Weiss, S. Quantum Dots for in Vivo Small-Animal Imaging. *J. Nucl. Med.* **2009**, *50*, 493−496.

(263) Zrazhevskiy, P.; Sena, M.; Gao, X. Designing Multifunctional Quantum Dots for Bioimaging, Detection, and Drug Delivery. *Chem. Soc. Rev.* **2010**, *39*, 4326−4354.

(264) Ruan, G.; Agrawal, A.; Marcus, A. I.; Nie, S. Imaging and Tracking of Tat Peptide-Conjugated Quantum Dots in Living Cells: New Insights into Nanoparticle Uptake, Intracellular Transport, and Vesicle Shedding. *J. Am. Chem. Soc.* **2007**, *129*, 14759−14766.

(265) Bruchez, M. P. Quantum Dots Find Their Stride in Single Molecule Tracking. *Curr. Opin. Chem. Biol.* **2011**, *15*, 775−780.

(266) Tada, H.; Higuchi, H.; Wanatabe, T. M.; Ohuchi, N. In Vivo Real-Time Tracking of Single Quantum Dots Conjugated with Monoclonal Anti-HER2 Antibody in Tumors of Mice. *Cancer Res.* **2007**, *67*, 1138−1144.

(267) Wells, N. P.; Lessard, G. A.; Werner, J. H. Confocal, Three-Dimensional Tracking of Individual Quantum Dots in High-Background Environments. *Anal. Chem.* **2008**, *80*, 9830−9834.

(268) Cui, Z. Q.; Ren, Q.; Wei, H. P.; Chen, Z.; Deng, J. Y.; Zhang, Z. P.; Zhang, X. E. Quantum Dot-Aptamer Nanoprobes for Recognizing and Labeling Influenza A Virus Particles. *Nanoscale* **2011**, *3*, 2454−2457.

(269) Saxton, M. J.; Jacobson, K. Single-Particle Tracking: Applications to Membrane Dynamics. *Annu. Rev. Biophys. Biomol. Struct.* **1997**, *26*, 373−399.

(270) Kusumi, A.; Sako, Y.; Yamamoto, M. Confined Lateral Diffusion of Membrane Receptors as Studied by Single Particle Tracking (Nanovid Microscopy). Effects of Calcium-Induced Differentiation in Cultured Epithelial Cells. *Biophys. J.* **1993**, *65*, 2021−2040.

(271) Wan, X. Y.; Zheng, L. L.; Gao, P. F.; Yang, X. X.; Li, C. M.; Li, Y. F.; Huang, C. Z. Real-Time Light Scattering Tracking of Gold Nanoparticles- Bioconjugated Respiratory Syncytial Virus Infecting HEp-2 Cells. *Sci. Rep.* **2015**, *4*, 4529.

(272) Marjomaki, V.; Lahtinen, T.; Martikainen, M.; Koivisto, J.; Malola, S.; Salorinne, K.; Pettersson, M.; Hakkinen, H. Site-Specific Targeting of Enterovirus Capsid by Functionalized Monodisperse Gold Nanoclusters. *Proc. Natl. Acad. Sci. U. S. A.* **2014**, *111*, 1277−1281.

(273) Wan, X. K.; Xu, W. W.; Yuan, S. F.; Gao, Y.; Zeng, X. C.; Wang, Q. M. A Near-Infrared-Emissive Alkynyl-Protected Au24 Nanocluster. *Angew. Chem., Int. Ed.* **2015**, *54*, 9683−9686.

(274) Jin, R.; Zeng, C.; Zhou, M.; Chen, Y. Atomically Precise Colloidal Metal Nanoclusters and Nanoparticles: Fundamentals and Opportunities. *Chem. Rev.* **2016**, *116*, 10346−10413.

(275) Zhang, L. B.; Wang, E. K. Metal Nanoclusters: New Fluorescent Probes for Sensors and Bioimaging. *Nano Today* **2014**, *9*, 132−157.

(276) Shang, L.; Dong, S. J.; Nienhaus, G. U. Ultra-Small Fluorescent Metal Nanoclusters: Synthesis and Biological Applications. *Nano Today* **2011**, *6*, 401−418.

(277) Draz, M. S.; Fang, B. A.; Li, L. J.; Chen, Z.; Wang, Y. J.; Xu, Y. H.; Yang, J.; Killeen, K.; Chen, F. F. Hybrid Nanocluster Plasmonic Resonator for Lmmunological Detection of Hepatitis B Virus. *ACS Nano* **2012**, *6*, 7634−7643.

(278) Shokri, E.; Hosseini, M.; Faridbod, F.; Rahaie, M. Rapid Pre-Symptomatic Recognition of Tristeza Viral RNA by a Novel Fluorescent Self-Dimerized DNA-Silver Nanocluster probe. *RSC Adv.* **2016**, *6*, 99437−99443.

(279) Tao, Y.; Li, M.; Ren, J.; Qu, X. Metal Nanoclusters: Novel Probes for Diagnostic and Therapeutic Applications. *Chem. Soc. Rev.* **2015**, *44*, 8636−8663.

(280) Basle, E.; Joubert, N.; Pucheault, M. Protein Chemical Modification on Endogenous Amino Acids. *Chem. Biol.* **2010**, *17*, 213−227.

(281) Hong, Z. Y.; Zhang, Z. L.; Tang, B.; Ao, J.; Wang, C.; Yu, C.; Pang, D. W. Equipping Inner Central Components of Influenza A Virus with Quantum Dots. *Anal. Chem.* **2018**, *90*, 14020−14028.

(282) Huisgen, R. 1.3-Dipolare Cycloadditionen Rückschau und Ausblick. *Angew. Chem.* **1963**, *75*, 604−637.

(283) Kolb, H. C.; Finn, M. G.; Sharpless, K. B. Click Chemistry: Diverse Chemical Function from a Few Good Reactions. *Angew. Chem., Int. Ed.* **2001**, *40*, 2004−2021.

(284) Nwe, K.; Brechbiel, M. W. Growing Applications of "Click Chemistry" for Bioconjugation in Contemporary Biomedical Research. *Cancer Biother.Radiopharm.* **2009**, *24*, 289−302.

(285) Codelli, J. A.; Baskin, J. M.; Agard, N. J.; Bertozzi, C. R. Second-Generation Difluorinated Cyclooctynes for Copper-Free Click Chemistry. *J. Am. Chem. Soc.* **2008**, *130*, 11486−11493.

(286) Baskin, J. M.; Prescher, J. A.; Laughlin, S. T.; Agard, N. J.; Chang, P. V.; Miller, I. A.; Lo, A.; Codelli, J. A.; Bertozzi, C. R. Copper-Free Click Chemistry for Dynamic in Vivo Imaging. *Proc. Natl. Acad. Sci. U. S. A.* **2007**, *104*, 16793−16797.

(287) Hoyle, C. E.; Bowman, C. N. Thiol-Ene Click Chemistry. *Angew. Chem., Int. Ed.* **2010**, *49*, 1540−1573.

(288) Nikic, I.; Plass, T.; Schraidt, O.; Szymanski, J.; Briggs, J. A.; Schultz, C.; Lemke, E. A. Minimal Tags for Rapid Dual-Color Live-Cell Labeling and Super-Resolution Microscopy. *Angew. Chem., Int. Ed.* **2014**, *53*, 2245−2249.

(289) Salic, A.; Mitchison, T. J. A Chemical Method for Fast and Sensitive Detection of DNA Synthesis in Vivo. *Proc. Natl. Acad. Sci. U. S. A.* **2008**, *105*, 2415−2420.

(290) Jao, C. Y.; Salic, A. Exploring RNA Transcription and Turnover in Vivo by Using Click Chemistry. *Proc. Natl. Acad. Sci. U. S. A.* **2008**, *105*, 15779−15784.

(291) Jewett, J. C.; Bertozzi, C. R. Cu-Free Click Cycloaddition Reactions in Chemical Biology. *Chem. Soc. Rev.* **2010**, *39*, 1272−1279.

(292) Rubino, F. A.; Oum, Y. H.; Rajaram, L.; Chu, Y.; Carrico, I. S. Chemoselective Modification of Viral Surfaces via Bioorthogonal Click Chemistry. *J. Visualized Exp.* **2012**, No. e4246.

(293) Oum, Y. H.; Desai, T. M.; Marin, M.; Melikyan, G. B. Click Labeling of Unnatural Sugars Metabolically Incorporated into Viral Envelope Glycoproteins Enables Visualization of Single Particle Fusion. *J. Virol. Methods* **2016**, *233*, 62−71.

(294) Huang, L. L.; Lu, G. H.; Hao, J.; Wang, H. Z.; Yin, D. L.; Xie, H. Y. Enveloped Virus Labeling via Both Intrinsic Biosynthesis and Metabolic Incorporation of Phospholipids in Host Cells. *Anal. Chem.* **2013**, *85*, 5263−5270.

(295) Hou, W.; Li, Y.; Kang, W.; Wang, X.; Wu, X.; Wang, S.; Liu, F. Real-Time Analysis of Quantum Dot Labeled Single Porcine Epidemic Diarrhea Virus Moving along the Microtubules Using Single Particle Tracking. *Sci. Rep.* **2019**, *9*, 1307.

(296) Lin, S.; Yan, H.; Li, L.; Yang, M.; Peng, B.; Chen, S.; Li, W.; Chen, P. R. Site-Specific Engineering of Chemical Functionalities on the Surface of Live Hepatitis D Virus. *Angew. Chem., Int. Ed.* **2013**, *52*, 13970−13974.

(297) Huang, L. L.; Liu, K.; Zhang, Q.; Xu, J.; Zhao, D.; Zhu, H.; Xie, H. Y. Integrating Two Efficient and Specific Bioorthogonal Ligation Reactions with Natural Metabolic Incorporation in One Cell for Virus Dual Labeling. *Anal. Chem.* **2017**, *89*, 11620−11627.

(298) Wang, I. H.; Suomalainen, M.; Andriasyan, V.; Kilcher, S.; Mercer, J.; Neef, A.; Luedtke, N. W.; Greber, U. F. Tracking Viral Genomes in Host Cells at Single-Molecule Resolution. *Cell Host Microbe* **2013**, *14*, 468−480.

(299) Green, N. M. Avidin and Streptavidin. *Methods Enzymol*; Elsevier: 1990; Vol. *184*, pp 51−67.

(300) Zhang, F.; Zheng, Z.; Liu, S. L.; Lu, W.; Zhang, Z.; Zhang, C.; Zhou, P.; Zhang, Y.; Long, G.; He, Z.; et al. Self-Biotinylation and Site-Specific Double Labeling of Baculovirus Using Quantum Dots for Single-Virus in-Situ Tracking. *Biomaterials* **2013**, *34*, 7506−7518.

(301) Liu, J.; Xu, M.; Tang, B.; Hu, L.; Deng, F.; Wang, H.; Pang, D. W.; Hu, Z.; Wang, M.; Zhou, Y. Single-Particle Tracking Reveals the Sequential Entry Process of the Bunyavirus Severe Fever with Thrombocytopenia Syndrome Virus. *Small* **2019**, *15*, No. e1803788.

(302) Liu, J.; Yu, C.; Gui, J. F.; Pang, D. W.; Zhang, Q. Y. Real-Time Dissecting the Entry and Intracellular Dynamics of Single Reovirus Particle. *Front. Microbiol.* **2018**, *9*, 2797.

(303) Dixit, S. K.; Goicochea, N. L.; Daniel, M. C.; Murali, A.; Bronstein, L.; De, M.; Stein, B.; Rotello, V. M.; Kao, C. C.; Dragnea, B. Quantum Dot Encapsulation in Viral Capsids. *Nano Lett.* **2006**, *6*, 1993−1999.

(304) Huang, B. H.; Lin, Y.; Zhang, Z. L.; Zhuan, F.; Liu, A. A.; Xie, M.; Tian, Z. Q.; Zhang, Z.; Wang, H.; Pang, D. W. Surface Labeling of Enveloped Viruses Assisted by Host Cells. *ACS Chem. Biol.* **2012**, *7*, 683−688.

(305) You, J. O.; Liu, Y. S.; Liu, Y. C.; Joo, K. I.; Peng, C. A. Incorporation of Quantum Dots on Virus in Polycationic Solution. *Int. J. Nanomedicine* **2006**, *1*, 59−64.

(306) Chen, Y. H.; Wang, C. H.; Chang, C. W.; Peng, C. A. In Situ Formation of Viruses Tagged with Quantum Dots. *Integr. Biol.* **2010**, *2*, 258−264.

(307) Li, F.; Zhang, Z. P.; Peng, J.; Cui, Z. Q.; Pang, D. W.; Li, K.; Wei, H. P.; Zhou, Y. F.; Wen, J. K.; Zhang, X. E. Imaging Viral Behavior in Mammalian Cells with Self-Assembled Capsid-Quantum-Dot Hybrid Particles. *Small* **2009**, *5*, 718−726.

(308) Johnson, H. E.; Haugh, J. M. Quantitative Analysis of Phosphoinositide 3-Kinase (PI3K) Signaling Using Live-Cell Total Internal Reflection Fluorescence (TIRF) Microscopy. *Curr. Protoc. Cell Biol.* **2013**, *61*, 14.14.1−14.14.24.

(309) Chen, I.; Ting, A. Y. Site-Specific Labeling of Proteins with Small Molecules in Live Cells. *Curr. Opin. Biotechnol.* **2005**, *16*, 35−40.

(310) Gong, Y. K.; Pan, L. F. Recent Advances in Bioorthogonal Reactions for Site-Specific Protein Labeling and Engineering. *Tetrahedron Lett.* **2015**, *56*, 2123−2132.

(311) Zhang, G.; Zheng, S. Q.; Liu, H. P.; Chen, P. R. Illuminating Biological Processes through Site-Specific Protein Labeling. *Chem. Soc. Rev.* **2015**, *44*, 3405−3417.

(312) Jing, C.; Cornish, V. W. Chemical Tags for Labeling Proteins inside Living Cells. *Acc. Chem. Res.* **2011**, *44*, 784−792.

(313) Klein, T.; Loschberger, A.; Proppert, S.; Wolter, S.; van de Linde, S.; Sauer, M. Live-Cell dSTORM with SNAP-Tag Fusion Proteins. *Nat. Methods* **2011**, *8*, 7−9.

(314) Chen, Z.; Cornish, V. W.; Min, W. Chemical Tags: Inspiration for Advanced Imaging Techniques. *Curr. Opin. Chem. Biol.* **2013**, *17*, 637−643.

(315) Wombacher, R.; Cornish, V. W. Chemical Tags: Applications in Live Cell Fluorescence Imaging. *J. Biophotonics* **2011**, *4*, 391−402.

(316) Specht, E. A.; Braselmann, E.; Palmer, A. E. A Critical and Comparative Review of Fluorescent Tools for Live-Cell Imaging. *Annu. Rev. Physiol.* **2017**, *79*, 93−117.

(317) Eckhardt, M.; Anders, M.; Muranyi, W.; Heilemann, M.; Krijnse-Locker, J.; Muller, B. A SNAP-Tagged Derivative of HIV-1−A Versatile Tool to Study Virus-Cell Interactions. *PLoS One* **2011**, *6*, No. e22007.

(318) Hanne, J.; Gottfert, F.; Schimer, J.; Anders-Osswein, M.; Konvalinka, J.; Engelhardt, J.; Muller, B.; Hell, S. W.; Krausslich, H. G. Stimulated Emission Depletion Nanoscopy Reveals Time-Course of Human Immunodeficiency Virus Proteolytic Maturation. *ACS Nano* **2016**, *10*, 8215−8222.

(319) Sun, X.; Zhang, A.; Baker, B.; Sun, L.; Howard, A.; Buswell, J.; Maurel, D.; Masharina, A.; Johnsson, K.; Noren, C. J.; et al. Development of SNAP-Tag Fluorogenic Probes for Wash-Free Fluorescence Imaging. *ChemBioChem* **2011**, *12*, 2217−2226.

(320) Keppler, A.; Pick, H.; Arrivoli, C.; Vogel, H.; Johnsson, K. Labeling of Fusion Proteins with Synthetic Fluorophores in Live Cells. *Proc. Natl. Acad. Sci. U. S. A.* **2004**, *101*, 9955−9959.

(321) Lavis, L. D. Teaching Old Dyes New Tricks: Biological Probes Built from Fluoresceins and Rhodamines. *Annu. Rev. Biochem.* **2017**, *86*, 825−843.

(322) Ross-Thriepland, D.; Mankouri, J.; Harris, M. Serine Phosphorylation of the Hepatitis C Virus NS5A Protein Controls the Establishment of Replication Complexes. *J. Virol.* **2015**, *89*, 3123−3135.

(323) Gautier, A.; Juillerat, A.; Heinis, C.; Correa, I. R., Jr.; Kindermann, M.; Beaufils, F.; Johnsson, K. An Engineered Protein Tag for Multiprotein Labeling in Living Cells. *Chem. Biol.* **2008**, *15*, 128−136.

(324) Liu, A. A.; Zhang, Z.; Sun, E. Z.; Zheng, Z.; Zhang, Z. L.; Hu, Q.; Wang, H.; Pang, D. W. Simultaneous Visualization of Parental and Progeny Viruses by a Capsid-Specific HaloTag Labeling Strategy. *ACS Nano* **2016**, *10*, 1147−1155.

(325) Los, G. V.; Encell, L. P.; McDougall, M. G.; Hartzell, D. D.; Karassina, N.; Zimprich, C.; Wood, M. G.; Learish, R.; Ohana, R. F.; Urh, M.; et al. HaloTag: A Novel Protein Labeling Technology for Cell Imaging and Protein Analysis. *ACS Chem. Biol.* **2008**, *3*, 373−382.

(326) Chen, Z.; Jing, C.; Gallagher, S. S.; Sheetz, M. P.; Cornish, V. W. Second-Generation Covalent TMP-Tag for Live Cell Imaging. *J. Am. Chem. Soc.* **2012**, *134*, 13692−13699.

(327) Gallagher, S. S.; Jing, C.; Peterka, D. S.; Konate, M.; Wombacher, R.; Kaufman, L. J.; Yuste, R.; Cornish, V. W. A Trimethoprim-Based Chemical Tag for Live Cell Two-Photon Imaging. *ChemBioChem* **2010**, *11*, 782−784.

(328) Wombacher, R.; Heidbreder, M.; van de Linde, S.; Sheetz, M. P.; Heilemann, M.; Cornish, V. W.; Sauer, M. Live-Cell Super-Resolution Imaging with Trimethoprim Conjugates. *Nat. Methods* **2010**, *7*, 717−719.

(329) Miller, L. W.; Cai, Y.; Sheetz, M. P.; Cornish, V. W. In Vivo Protein Labeling with Trimethoprim Conjugates: A Flexible Chemical Tag. *Nat. Methods* **2005**, *2*, 255−257.

(330) Rudner, L.; Nydegger, S.; Coren, L. V.; Nagashima, K.; Thali, M.; Ott, D. E. Dynamic Fluorescent Imaging of Human Immunodeficiency Virus Type 1 Gag in Live Cells by Biarsenical Labeling. *J. Virol.* **2005**, *79*, 4055−4065.

(331) Das, S. C.; Panda, D.; Nayak, D.; Pattnaik, A. K. Biarsenical Labeling of Vesicular Stomatitis Virus Encoding Tetracysteine-Tagged M Protein Allows Dynamic Imaging of M Protein and Virus Uncoating in Infected Cells. *J. Virol.* **2009**, *83*, 2611−2622.

(332) Li, Y.; Lu, X.; Li, J.; Berube, N.; Giest, K. L.; Liu, Q.; Anderson, D. H.; Zhou, Y. Genetically Engineered, Biarsenically Labeled Influenza Virus Allows Visualization of Viral NS1 Protein in Living Cells. *J. Virol.* **2010**, *84*, 7204−7213.

(333) Martin, B. R.; Giepmans, B. N.; Adams, S. R.; Tsien, R. Y. Mammalian Cell-Based Optimization of the Biarsenical-Binding Tetracysteine Motif for Improved Fluorescence and Affinity. *Nat. Biotechnol.* **2005**, *23*, 1308−1314.

(334) Adams, S. R.; Campbell, R. E.; Gross, L. A.; Martin, B. R.; Walkup, G. K.; Yao, Y.; Llopis, J.; Tsien, R. Y. New Biarsenical Ligands and Tetracysteine Motifs for Protein Labeling in Vitro and in Vivo: Synthesis and Biological Applications. *J. Am. Chem. Soc.* **2002**, *124*, 6063−6076.

(335) Zheng, L. L.; Li, C. M.; Zhen, S. J.; Li, Y. F.; Huang, C. Z. His-Tag Based in Situ Labelling of Progeny Viruses for Real-Time Single Virus Tracking in Living Cells. *Nanoscale* **2016**, *8*, 18635−18639.

(336) Guignet, E. G.; Hovius, R.; Vogel, H. Reversible Site-Selective Labeling of Membrane Proteins in Live Cells. *Nat. Biotechnol.* **2004**, *22*, 440−444.

(337) Chen, I.; Howarth, M.; Lin, W.; Ting, A. Y. Site-Specific Labeling of Cell Surface Proteins with Biophysical Probes Using Biotin Ligase. *Nat. Methods* **2005**, *2*, 99−104.

(338) Howarth, M.; Ting, A. Y. Imaging Proteins in Live Mammalian Cells with Biotin Ligase and Monovalent Streptavidin. *Nat. Protoc.* **2008**, *3*, 534−545.

(339) Uttamapinant, C.; White, K. A.; Baruah, H.; Thompson, S.; Fernandez-Suarez, M.; Puthenveetil, S.; Ting, A. Y. A Fluorophore Ligase for Site-Specific Protein Labeling inside Living Cells. *Proc. Natl. Acad. Sci. U. S. A.* **2010**, *107*, 10914−10919.

(340) Fernandez-Suarez, M.; Baruah, H.; Martinez-Hernandez, L.; Xie, K. T.; Baskin, J. M.; Bertozzi, C. R.; Ting, A. Y. Redirecting Lipoic Acid Ligase for Cell Surface Protein Labeling with Small-Molecule Probes. *Nat. Biotechnol.* **2007**, *25*, 1483−1487.

(341) Schumacher, D.; Helma, J.; Mann, F. A.; Pichler, G.; Natale, F.; Krause, E.; Cardoso, M. C.; Hackenberger, C. P.; Leonhardt, H. Versatile and Efficient Site-Specific Protein Functionalization by Tubulin Tyrosine Ligase. *Angew. Chem., Int. Ed.* **2015**, *54*, 13787−13791.

(342) Schumacher, D.; Lemke, O.; Helma, J.; Gerszonowicz, L.; Waller, V.; Stoschek, T.; Durkin, P. M.; Budisa, N.; Leonhardt, H.; Keller, B. G.; et al. Broad Substrate Tolerance of Tubulin Tyrosine Ligase Enables One-Step Site-Specific Enzymatic Protein Labeling. *Chem. Sci.* **2017**, *8*, 3471−3478.

(343) Zhou, Z.; Cironi, P.; Lin, A. J.; Xu, Y.; Hrvatin, S.; Golan, D. E.; Silver, P. A.; Walsh, C. T.; Yin, J. Genetically Encoded Short Peptide Tags for Orthogonal Protein Labeling by Sfp and AcpS Phosphopantetheinyl Transferases. *ACS Chem. Biol.* **2007**, *2*, 337−346.

(344) Yin, J.; Straight, P. D.; McLoughlin, S. M.; Zhou, Z.; Lin, A. J.; Golan, D. E.; Kelleher, N. L.; Kolter, R.; Walsh, C. T. Genetically

Encoded Short Peptide Tag for Versatile Protein Labeling by Sfp Phosphopantetheinyl Transferase. *Proc. Natl. Acad. Sci. U. S. A.* **2005**, *102*, 15815−15820.

(345) Crivat, G.; Taraska, J. W. Imaging Proteins inside Cells with Fluorescent Tags. *Trends Biotechnol.* **2012**, *30*, 8−16.

(346) Hoehnel, S.; Lutolf, M. P. Capturing Cell-Cell Interactions via SNAP-tag and CLIP-tag Technology. *Bioconjugate Chem.* **2015**, *26*, 1678−1686.

(347) Liss, V.; Barlag, B.; Nietschke, M.; Hensel, M. Self-Labelling Enzymes as Universal Tags for Fluorescence Microscopy, Super-Resolution Microscopy and Rectron Microscopy. *Sci. Rep.* **2016**, *5*, 17740.

(348) Jing, C.; Cornish, V. W. A Fluorogenic TMP-Tag for High Signal-to-Background Intracellular Live Cell Imaging. *ACS Chem. Biol.* **2013**, *8*, 1704−1712.

(349) Lai, Y. T.; Chang, Y. Y.; Hu, L.; Yang, Y.; Chao, A.; Du, Z. Y.; Tanner, J. A.; Chye, M. L.; Qian, C.; Ng, K. M.; et al. Rapid Labeling of Intracellular His-Tagged Proteins in Living Cells. *Proc. Natl. Acad. Sci. U. S. A.* **2015**, *112*, 2948−2953.

(350) Stephanopoulos, N.; Francis, M. B. Choosing an Effective Protein Bioconjugation Strategy. *Nat. Chem. Biol.* **2011**, *7*, 876−884.

(351) Howarth, M.; Takao, K.; Hayashi, Y.; Ting, A. Y. Targeting Quantum Dots to Surface Proteins in Living Cells with Biotin Ligase. *Proc. Natl. Acad. Sci. U. S. A.* **2005**, *102*, 7583−7588.

(352) Cohen, J. D.; Zou, P.; Ting, A. Y. Site-Specific Protein Modification Using Lipoic Acid Ligase and Bis-Aryl Hydrazone Formation. *ChemBioChem* **2012**, *13*, 888−894.

(353) Lotze, J.; Reinhardt, U.; Seitz, O.; Beck-Sickinger, A. G. Peptide-Tags for Site-Specific Protein Labelling in Vitro and in Vivo. *Mol. BioSyst.* **2016**, *12*, 1731−1745.

(354) Sunbul, M.; Yen, M.; Zou, Y.; Yin, J. Enzyme Catalyzed Site-Specific Protein Labeling and Cell Imaging with Quantum Dots. *Chem. Commun.* **2008**, 5927−5929.

(355) Zhang, Y.; Ke, X.; Zheng, Z.; Zhang, C.; Zhang, Z.; Zhang, F.; Hu, Q.; He, Z.; Wang, H. Encapsulating Quantum Dots into Enveloped Virus in Living Cells for Tracking Virus Infection. *ACS Nano* **2013**, *7*, 3896−3904.

(356) Molenaar, C.; Marras, S. A.; Slats, J. C.; Truffert, J. C.; Lemaitre, M.; Raap, A. K.; Dirks, R. W.; Tanke, H. J. Linear 2' O-Methyl RNA Probes for the Visualization of RNA in Living Cells. *Nucleic Acids Res.* **2001**, *29*, E89−9.

(357) Ma, Y.; Mao, G.; Huang, W.; Wu, G.; Yin, W.; Ji, X.; Deng, Z.; Cai, Z.; Zhang, X. E.; He, Z.; et al. Quantum Dot Nanobeacons for Single RNA Labeling and Imaging. *J. Am. Chem. Soc.* **2019**, *141*, 13454−13458.

(358) Ortega-Arroyo, J.; Kukura, P. Interferometric Scattering Microscopy (iSCAT): New Frontiers in Ultrafast and Ultrasensitive Optical Microscopy. *Phys. Chem. Chem. Phys.* **2012**, *14*, 15625−15636.

(359) Kukura, P.; Ewers, H.; Muller, C.; Renn, A.; Helenius, A.; Sandoghdar, V. High-Speed Nanoscopic Tracking of the Position and Orientation of a Single Virus. *Nat. Methods* **2009**, *6*, 923−927.

(360) Renz, M. Fluorescence Microscopy-A Historical and Technical Perspective. *Cytometry, Part A* **2013**, *83*, 767−779.

(361) Lorenz, K. S.; Salama, P.; Dunn, K. W.; Delp, E. J. Digital Correction of Motion Artefacts in Microscopy Image Sequences Collected from Living Animals Using Rigid and Nonrigid Registration. *J. Microsc.* **2012**, *245*, 148−160.

(362) Combs, C. A.; Shroff, H. Fluorescence Microscopy: A Concise Guide to Current Imaging Methods. *Curr. Protoc. Neurosci.* **2017**, *79*, 2.1.1−2.1.25.

(363) Masters, B. R. Fluorescence Microscopy: from Principles to Biological Applications. *J. Biomed. Opt.* **2014**, *19*, No. 049901.

(364) Ma, Y. Y.; Wang, X.; Liu, H.; Wei, L.; Xiao, L. H. Recent Advances in Optical Microscopic Methods for Single-Particle Tracking in Biological Samples. *Anal. Bioanal. Chem.* **2019**, *411*, 4445−4463.

(365) Deschout, H.; Cella Zanacchi, F.; Mlodzianoski, M.; Diaspro, A.; Bewersdorf, J.; Hess, S. T.; Braeckmans, K. Precisely and Accurately Localizing Single Emitters in Fluorescence Microscopy. *Nat. Methods* **2014**, *11*, 253−266.

(366) Lichtman, J. W.; Conchello, J. A. Fluorescence Microscopy. *Nat. Methods* **2005**, *2*, 910−919.

(367) Beier, H. T.; Ibey, B. L. Experimental Comparison of the High-Speed Imaging Performance of an EM-CCD and sCMOS Camera in a Dynamic Live-Cell Imaging Test Case. *PLoS One* **2014**, *9*, No. e84614.

(368) Long, F.; Zeng, S.; Huang, Z. L. Localization-Based Super-Resolution Microscopy with an sCMOS Camera Part II: Experimental Methodology for Comparing sCMOS with EMCCD Cameras. *Opt. Express* **2012**, *20*, 17741−17759.

(369) Fullerton, S. A Guide to Choosing and Using Scientific Imaging Cameras. *Laser Focus World* **2014**, *50*, 37−40.

(370) Ivanchenko, S.; Godinez, W. J.; Lampe, M.; Krausslich, H. G.; Eils, R.; Rohr, K.; Brauchle, C.; Muller, B.; Lamb, D. C. Dynamics of HIV-1 Assembly and Release. *PLoS Pathog.* **2009**, *5*, No. e1000652.

(371) Axelrod, D. Cell-Substrate Contacts Illuminated by Total Internal Reflection Fluorescence. *J. Cell Biol.* **1981**, *89*, 141−145.

(372) Axelrod, D. Total Internal Reflection Fluorescence Microscopy in Cell Biology. *Traffic* **2001**, *2*, 764−774.

(373) Reichert, W. M.; Truskey, G. A. Total Internal Reflection Fluorescence (TIRF) Microscopy. I. Modelling Cell Contact Region Fluorescence. *J. Cell Sci.* **1990**, *96*, 219−230.

(374) Johnson, C. *Spectroscopy and Dynamics of Single Molecules: Methods and Applications*; Elsevier: 2019.

(375) Tokunaga, M.; Kitamura, K.; Saito, K.; Iwane, A. H.; Yanagida, T. Single Molecule Imaging of Fluorophores and Enzymatic Reactions Achieved by Objective-Type Total Internal Reflection Fluorescence Microscopy. *Biochem. Biophys. Res. Commun.* **1997**, *235*, 47−53.

(376) Parhamifar, L.; Moghimi, S. M. Total Internal Reflection Fluorescence (TIRF) Microscopy for Real-Time Imaging of Nano-particle-Cell Plasma Membrane Interaction. *Methods Mol. Biol.* **2012**, *906*, 473−482.

(377) Fish, K. N. Total Internal Reflection Fluorescence (TIRF) Microscopy. *Curr. Protoc. Cytom.* **2009**, *12*, 12−18.

(378) Mattheyses, A. L.; Simon, S. M.; Rappoport, J. Z. Imaging with Total Internal Reflection Fluorescence Microscopy for the Cell Biologist. *J. Cell Sci.* **2010**, *123*, 3621−3628.

(379) Johnson, D. S.; Jaiswal, J. K.; Simon, S. Total Internal Reflection Fluorescence (TIRF) Microscopy Illuminator for Improved Imaging of Cell Surface Events. *Curr. Protoc. Cytom.* **2012**, *12*, 12−29.

(380) Ewers, H.; Schelhaas, M. Analysis of Virus Entry and Cellular Membrane Dynamics by Single Particle Tracking. *Methods Enzymol.* **2012**, *506*, 63−80.

(381) Tokunaga, M.; Imamoto, N.; Sakata-Sogawa, K. Highly Inclined Thin Illumination Enables Clear Single-Molecule Imaging in Cells. *Nat. Methods* **2008**, *5*, 159−161.

(382) Schmidt, F. I.; Kuhn, P.; Robinson, T.; Mercer, J.; Dittrich, P. S. Single-Virus Fusion Experiments Reveal Proton Influx into Vaccinia Virions and Hemifusion Lag Times. *Biophys. J.* **2013**, *105*, 420−431.

(383) Naredi-Rainer, N.; Prescher, J.; Hartschuh, A.; Lamb, D. C. Confocal Microscopy. *Fluorescence Microscopy* **2013**, *107S*, 175−213.

(384) Minsky, M. Memoir on Inventing the Confocal Scanning Microscope. *Scanning* **1988**, *10*, 128−138.

(385) Graf, R.; Rietdorf, J.; Zimmermann, T. Live Cell Spinning Disk Microscopy. *Adv. Biochem. Eng./Biotechnol.* **2005**, *95*, 57−75.

(386) Egger, M. D.; Petran, M. New Reflected-Light Microscope for Viewing Unstained Brain and Ganglion Cells. *Science* **1967**, *157*, 305−307.

(387) Andersson, S. B. Tracking a Single Fluorescent Molecule with a Confocal Microscope. *Appl. Phys. B: Lasers Opt.* **2005**, *80*, 809−816.

(388) Han, J. J.; Kiss, C.; Bradbury, A. R. M.; Werner, J. H. Time-Resolved, Confocal Single-Molecule Tracking of Individual Organic Dyes and Fluorescent Proteins in Three Dimensions. *ACS Nano* **2012**, *6*, 8922−8932.

(389) Krzic, U.; Gunther, S.; Saunders, T. E.; Streichan, S. J.; Hufnagel, L. Multiview Light-Sheet Microscope for Rapid in toto Imaging. *Nat. Methods* **2012**, *9*, 730−733.

(390) Vettenburg, T.; Dalgarno, H. I. C.; Nylk, J.; Coll-Llado, C.; Ferrier, D. E. K.; Cizmar, T.; Gunn-Moore, F. J.; Dholakia, K. Light-Sheet Microscopy Using An Airy Beam. *Nat. Methods* **2014**, *11*, 541−544.

(391) Pitrone, P. G.; Schindelin, J.; Stuyvenberg, L.; Preibisch, S.; Weber, M.; Eliceiri, K. W.; Huisken, J.; Tomancak, P. OpenSPIM: An Open-Access Light-Sheet Microscopy Platform. *Nat. Methods* **2013**, *10*, 598−599.

(392) Li, Y.; Hu, Y.; Cang, H. Light Sheet Microscopy for Tracking Single Molecules on the Apical Surface of Living Cells. *J. Phys. Chem. B* **2013**, *117*, 15503−15511.

(393) Keller, P. J.; Schmidt, A. D.; Wittbrodt, J.; Stelzer, E. H. Reconstruction of Zebrafish Early Embryonic Development by Scanned Light Sheet Microscopy. *Science* **2008**, *322*, 1065−1069.

(394) Ritter, J. G.; Veith, R.; Veenendaal, A.; Siebrasse, J. P.; Kubitscheck, U. Light Sheet Microscopy for Single Molecule Tracking in Living Tissue. *PLoS One* **2010**, *5*, No. e11639.

(395) Wan, Y.; McDole, K.; Keller, P. J. Light-Sheet Microscopy and Its Potential for Understanding Developmental Processes. *Annu. Rev. Cell Dev. Biol.* **2019**, *35*, 655−681.

(396) Hillman, E. M. C.; Voleti, V.; Li, W.; Yu, H. Light-Sheet Microscopy in Neuroscience. *Annu. Rev. Neurosci.* **2019**, *42*, 295−313.

(397) Stelzer, E. H. K. Light-Sheet Fluorescence Microscopy for Quantitative Biology. *Nat. Methods* **2015**, *12*, 23−26.

(398) Bosse, J. B.; Hogue, I. B.; Feric, M.; Thiberge, S. Y.; Sodeik, B.; Brangwynne, C. P.; Enquist, L. W. Remodeling Nuclear Architecture Allows Efficient Transport of Herpesvirus Capsids by Diffusion. *Proc. Natl. Acad. Sci. U. S. A.* **2015**, *112*, E5725−E5733.

(399) Hoyer, P.; de Medeiros, G.; Balazs, B.; Norlin, N.; Besir, C.; Hanne, J.; Krausslich, H. G.; Engelhardt, J.; Sahl, S. J.; Hell, S. W.; et al. Breaking the Diffraction Limit of Light-Sheet Fluorescence Microscopy by RESOLFT. *Proc. Natl. Acad. Sci. U. S. A.* **2016**, *113*, 3442−3446.

(400) Rust, M. J.; Bates, M.; Zhuang, X. Sub-Diffraction-Limit Imaging by Stochastic Optical Reconstruction Microscopy (STORM). *Nat. Methods* **2006**, *3*, 793−795.

(401) Malkusch, S.; Muranyi, W.; Muller, B.; Krausslich, H. G.; Heilemann, M. Single-Molecule Coordinate-Based Analysis of the Morphology of HIV-1 Assembly Sites with Near-Molecular Spatial Resolution. *Histochem. Cell Biol.* **2013**, *139*, 173−179.

(402) Lehmann, M.; Rocha, S.; Mangeat, B.; Blanchet, F.; Uji, I. H.; Hofkens, J.; Piguet, V. Quantitative Multicolor Super-Resolution Microscopy Reveals Tetherin HIV-1 Interaction. *PLoS Pathog.* **2011**, *7*, No. e1002456.

(403) Inamdar, K.; Floderer, C.; Favard, C.; Muriaux, D. Monitoring HIV-1 Assembly in Living Cells: Insights from Dynamic and Single Molecule Microscopy. *Viruses* **2019**, *11*, 72.

(404) Bleck, M.; Itano, M. S.; Johnson, D. S.; Thomas, V. K.; North, A. J.; Bieniasz, P. D.; Simon, S. M. Temporal and Spatial Organization of ESCRT Protein Recruitment During HIV-1 Budding. *Proc. Natl. Acad. Sci. U. S. A.* **2014**, *111*, 12211−12216.

(405) Prescher, J.; Baumgartel, V.; Ivanchenko, S.; Torrano, A. A.; Brauchle, C.; Muller, B.; Lamb, D. C. Super-Resolution Imaging of ESCRT-Proteins at HIV-1 Assembly Sites. *PLoS Pathog.* **2015**, *11*, No. e1004677.

(406) Shao, L.; Kner, P.; Rego, E. H.; Gustafsson, M. G. Super-Resolution 3D Microscopy of Live Whole Cells Using Structured Illumination. *Nat. Methods* **2011**, *8*, 1044−1046.

(407) Jones, S. A.; Shim, S. H.; He, J.; Zhuang, X. Fast, Three-Dimensional Super-Resolution Imaging of Live Cells. *Nat. Methods* **2011**, *8*, 499−508.

(408) Nair, D.; Hosy, E.; Petersen, J. D.; Constals, A.; Giannone, G.; Choquet, D.; Sibarita, J. B. Super-Resolution Imaging Reveals That AMPA Receptors Inside Synapses Are Dynamically Organized in Nanodomains Regulated by PSD95. *J. Neurosci.* **2013**, *33*, 13204−13224.

(409) Izeddin, I.; Recamier, V.; Bosanac, L.; Cisse, I. I.; Boudarene, L.; Dugast-Darzacq, C.; Proux, F.; Benichou, O.; Voituriez, R.; Bensaude, O.; et al. Single-Molecule Tracking in Live Cells Reveals Distinct Target-Search Strategies of Transcription Factors in the Nucleus. *eLife* **2014**, *3*, No. e02230.

(410) Yang, L.; Dun, A. R.; Martin, K. J.; Qiu, Z.; Dunn, A.; Lord, G. J.; Lu, W.; Duncan, R. R.; Rickman, C. Secretory Vesicles Are Preferentially Targeted to Areas of Low Molecular SNARE Density. *PLoS One* **2012**, *7*, No. e49514.

(411) Juette, M. F.; Gould, T. J.; Lessard, M. D.; Mlodzianoski, M. J.; Nagpure, B. S.; Bennett, B. T.; Hess, S. T.; Bewersdorf, J. Three-Dimensional Sub-100 nm Resolution Fluorescence Microscopy of Thick Samples. *Nat. Methods* **2008**, *5*, 527−529.

(412) Pavani, S. R.; Thompson, M. A.; Biteen, J. S.; Lord, S. J.; Liu, N.; Twieg, R. J.; Piestun, R.; Moerner, W. E. Three-Dimensional, Single-Molecule Fluorescence Imaging Beyond the Diffraction Limit by Using a Double-Helix Point Spread Function. *Proc. Natl. Acad. Sci. U. S. A.* **2009**, *106*, 2995−2999.

(413) Thompson, M. A.; Lew, M. D.; Badieirostami, M.; Moerner, W. E. Localizing and Tracking Single Nanoscale Emitters in Three Dimensions with High Spatiotemporal Resolution Using a Double-Helix Point Spread Function. *Nano Lett.* **2010**, *10*, 211−218.

(414) Yu, B.; Yu, J.; Li, W.; Cao, B.; Li, H.; Chen, D.; Niu, H. Nanoscale Three-Dimensional Single Particle Tracking by Light-Sheet-Based Double-Helix Point Spread Function Microscopy. *Appl. Opt.* **2016**, *55*, 449−453.

(415) Holtzer, L.; Meckel, T.; Schmidt, T. Nanometric Three-Dimensional Tracking of Individual Quantum Dots in Cells. *Appl. Phys. Lett.* **2007**, *90*, No. 053902.

(416) Huang, B.; Wang, W.; Bates, M.; Zhuang, X. Three-Dimensional Super-Resolution Imaging by Stochastic Optical Reconstruction Microscopy. *Science* **2008**, *319*, 810−813.

(417) Lange, S.; Katayama, Y.; Schmid, M.; Burkacky, O.; Brauchle, C.; Lamb, D. C.; Jansen, R. P. Simultaneous Transport of Different Localized mRNA Species Revealed by Live-Cell Imaging. *Traffic* **2008**, *9*, 1256−1267.

(418) Wells, N. P.; Lessard, G. A.; Goodwin, P. M.; Phipps, M. E.; Cutler, P. J.; Lidke, D. S.; Wilson, B. S.; Werner, J. H. Time-Resolved Three-Dimensional Molecular Tracking in Live Cells. *Nano Lett.* **2010**, *10*, 4732−4737.

(419) Cang, H.; Xu, C. S.; Montiel, D.; Yang, H. Guiding a Confocal Microscope by Single Fluorescent Nanoparticles. *Opt. Lett.* **2007**, *32*, 2729−2731.

(420) Balzarotti, F.; Eilers, Y.; Gwosch, K. C.; Gynna, A. H.; Westphal, V.; Stefani, F. D.; Elf, J.; Hell, S. W. Nanometer Resolution Imaging and Tracking of Fluorescent Molecules with Minimal Photon Fluxes. *Science* **2017**, *355*, 606−612.

(421) Enderlein, J. Tracking of Fluorescent Molecules Diffusing within Membranes. *Appl. Phys. B: Lasers Opt.* **2000**, *71*, 773−777.

(422) Kis-Petikova, K.; Gratton, E. Distance Measurement by Circular Scanning of the Excitation Beam in the Two-Photon Microscope. *Microsc. Res. Tech.* **2004**, *63*, 34−49.

(423) Lessard, G. A.; Goodwin, P. M.; Werner, J. H. Three-Dimensional Tracking of Individual Quantum Dots. *Appl. Phys. Lett.* **2007**, *91*, 224106.

(424) Verdeny-Vilanova, I.; Wehnekamp, F.; Mohan, N.; Alvarez, A. S.; Borbely, J. S.; Otterstrom, J. J.; Lamb, D. C.; Lakadamyali, M. 3D Motion of Vesicles along Microtubules Helps Them to Circumvent Obstacles in Cells. *J. Cell Sci.* **2017**, *130*, 1904−1916.

(425) Wehnekamp, F.; Plucinska, G.; Thong, R.; Misgeld, T.; Lamb, D. C. Nanoresolution Real-Time 3D Orbital Tracking for Studying Mitochondrial Trafficking in Vertebrate Axons in Vivo. *eLife* **2019**, *8*, No. e46059.

(426) Katayama, Y.; Burkacky, O.; Meyer, M.; Brauchle, C.; Gratton, E.; Lamb, D. C. Real-Time Nanomicroscopy via Three-Dimensional Single-Particle Tracking. *ChemPhysChem* **2009**, *10*, 2458−2464.

(427) Hellriegel, C.; Gratton, E. Real-Time Multi-Parameter Spectroscopy and Localization in Three-Dimensional Single-Particle Tracking. *J. R. Soc., Interface* **2009**, *6*, S3−S14.

(428) Liu, Z.; Lavis, L. D.; Betzig, E. Imaging Live-Cell Dynamics and Structure at the Single-Molecule Level. *Mol. Cell* **2015**, *58*, 644−659.

(429) Saxton, M. J. Single-Particle Tracking: Connecting the Dots. *Nat. Methods* **2008**, *5*, 671−672.

(430) Carter, B. C.; Shubeita, G. T.; Gross, S. P. Tracking Single Particles: A User-Friendly Quantitative Evaluation. *Phys. Biol.* **2005**, *2*, 60−72.

(431) Thompson, R. E.; Larson, D. R.; Webb, W. W. Precise Nanometer Localization Analysis for Individual Fluorescent Probes. *Biophys. J.* **2002**, *82*, 2775−2783.

(432) Small, A.; Stahlheber, S. Fluorophore Localization Algorithms for Super-Resolution Microscopy. *Nat. Methods* **2014**, *11*, 267−279.

(433) Ernst, D.; Kohler, J. How the Number of Fitting Points for the Slope of the Mean-Square Displacement Influences the Experimentally Determined Particle Size Distribution from Single-Particle Tracking. *Phys. Chem. Chem. Phys.* **2013**, *15*, 3429−3432.

(434) Born, M.; Wolf, E. *Principles of Optics: Electromagnetic Theory of Propagation, Interference and Diffraction of Light*; Elsevier: 2013.

(435) Liu, S. L.; Li, J.; Zhang, Z. L.; Wang, Z. G.; Tian, Z. Q.; Wang, G. P.; Pang, D. W. Fast and High-Accuracy Localization for Three-Dimensional Single-Particle Tracking. *Sci. Rep.* **2013**, *3*, 2462.

(436) Qu, X. H.; Wu, D.; Mets, L.; Scherer, N. F. Nanometer-Localized Multiple Single-Molecule Fluorescence Microscopy. *Proc. Natl. Acad. Sci. U. S. A.* **2004**, *101*, 11298−11303.

(437) Hess, S. T.; Girirajan, T. P.; Mason, M. D. Ultra-High Resolution Imaging by Fluorescence Photoactivation Localization Microscopy. *Biophys. J.* **2006**, *91*, 4258−4272.

(438) Parthasarathy, R. Rapid, Accurate Particle Tracking by Calculation of Radial Symmetry Centers. *Nat. Methods* **2012**, *9*, 724−726.

(439) Sage, D.; Neumann, F. R.; Hediger, F.; Gasser, S. M.; Unser, M. Automatic Tracking of Individual Fluorescence Particles: Application to the Study of Chromosome Dynamics. *IEEE Trans. Image Process.* **2005**, *14*, 1372−1383.

(440) Godinez, W. J.; Lampe, M.; Worz, S.; Muller, B.; Eils, R.; Rohr, K. Deterministic and Probabilistic Approaches for Tracking Virus Particles in Time-Lapse Fluorescence Microscopy Image Sequences. *Med. Image Anal.* **2009**, *13*, 325−342.

(441) Chenouard, N.; Smal, I.; de Chaumont, F.; Maska, M.; Sbalzarini, I. F.; Gong, Y.; Cardinale, J.; Carthel, C.; Coraluppi, S.; Winter, M.; et al. Objective Comparison of Particle Tracking Methods. *Nat. Methods* **2014**, *11*, 281−289.

(442) Reid, D. An Algorithm for Tracking Multiple Targets. *IEEE Trans. Autom. Control* **1979**, *24*, 843−854.

(443) Veenman, C. J.; Reinders, M. J.; Backer, E. Resolving Motion Correspondence for Densely Moving Points. *IEEE T. Pattern Anal.* **2001**, *23*, 54−72.

(444) Jiang, S.; Zhou, X.; Kirchhausen, T.; Wong, S. T. Tracking Molecular Particles in Live Cells Using Fuzzy Rule-Based System. *Cytometry, Part A* **2007**, *71*, 576−584.

(445) Shafique, K.; Shah, M. A Noniterative Greedy Algorithm for Multiframe Point Correspondence. *IEEE Trans. Pattern Anal. Mach. Intell.* **2005**, *27*, 51−65.

(446) Jaqaman, K.; Loerke, D.; Mettlen, M.; Kuwata, H.; Grinstein, S.; Schmid, S. L.; Danuser, G. Robust Single-Particle Tracking in Live-Cell Time-Lapse Sequences. *Nat. Methods* **2008**, *5*, 695−702.

(447) Saxton, M. J. Single-Particle Tracking: The Distribution of Diffusion Coefficients. *Biophys. J.* **1997**, *72*, 1744−1753.

(448) Dahan, M. From Analog to Digital: Exploring Cell Dynamics with Single Quantum Dots. *Histochem. Cell Biol.* **2006**, *125*, 451−456.

(449) Dupont, A.; Gorelashvili, M.; Schuller, V.; Wehnekamp, F.; Arcizet, D.; Katayama, Y.; Lamb, D. C.; Heinrich, D. Three-Dimensional Single-Particle Tracking in Live Cells: News from the Third Dimension. *New J. Phys.* **2013**, *15*, No. 075008.

(450) Bannai, H.; Lévi, S.; Schweizer, C.; Dahan, M.; Triller, A. Imaging the Lateral Diffusion of Membrane Molecules with Quantum Dots. *Nat. Protoc.* **2006**, *1*, 2628−2634.

(451) Saxton, M. J. Single-Particle Tracking: Effects of Corrals. *Biophys. J.* **1995**, *69*, 389−398.

(452) Rock, R. S. Myosin VI Is a Processive Motor with a Large Step Size. *Proc. Natl. Acad. Sci. U. S. A.* **2001**, *98*, 13655−13659.

(453) Ma, S.; Chisholm, R. L. Cytoplasmic Dynein-Associated Structures Move Bidirectionally in Vivo. *J. Cell Sci.* **2002**, *115*, 1453−1460.

(454) Sieczkarski, S. B.; Whittaker, G. R. Dissecting Virus Entry via Endocytosis. *J. Gen. Virol.* **2002**, *83*, 1535−1545.

(455) Boulant, S.; Stanifer, M.; Lozach, P. Y. Dynamics of Virus-Receptor Interactions in Virus Binding, Signaling, and Endocytosis. *Viruses* **2015**, *7*, 2794−2815.

(456) Mudhakir, D.; Harashima, H. Learning from the Viral Journey: How to Enter Cells and How to Overcome Intracellular Barriers to Reach the Nucleus. *AAPS J.* **2009**, *11*, 65−77.

(457) Damm, E. M.; Pelkmans, L. Systems Biology of Virus Entry in Mammalian Cells. *Cell. Microbiol.* **2006**, *8*, 1219−1227.

(458) Chang, K.; Baginski, J.; Hassan, S. F.; Volin, M.; Shukla, D.; Tiwari, V. Filopodia and Vruses: An Analysis of Membrane Processes in Entry Mechanisms. *Front. Microbiol.* **2016**, *7*, 300.

(459) Shinya, K.; Ebina, M.; Yamada, S.; Ono, M.; Kasai, N.; Kawaoka, Y. Avian Flu: Influenza Virus Receptors in the Human Airway. *Nature* **2006**, *440*, 435−436.

(460) Ibricevic, A.; Pekosz, A.; Walter, M. J.; Newby, C.; Battaile, J. T.; Brown, E. G.; Holtzman, M. J.; Brody, S. L. Influenza Virus Receptor Specificity and Cell Tropism in Mouse and Human Airway Epithelial Cells. *J. Virol.* **2006**, *80*, 7469−7480.

(461) Lakadamyali, M.; Rust, M. J.; Zhuang, X. Endocytosis of Influenza Viruses. *Microbes Infect.* **2004**, *6*, 929−936.

(462) Mercer, J.; Schelhaas, M.; Helenius, A. Virus Entry by Endocytosis. *Annu. Rev. Biochem.* **2010**, *79*, 803−833.

(463) Nisole, S.; Saib, A. Early Steps of Retrovirus Replicative Cycle. *Retrovirology* **2004**, *1*, 9.

(464) Spear, P. G.; Eisenberg, R. J.; Cohen, G. H. Three Classes of Cell Surface Receptors for Alphaherpesvirus Entry. *Virology* **2000**, *275*, 1−8.

(465) Bailey, C. J.; Crystal, R. G.; Leopold, P. L. Association of Adenovirus with the Microtubule Organizing Center. *J. Virol.* **2003**, *77*, 13275−13287.

(466) Kielian, M.; Rey, F. A. Virus Membrane-Fusion Proteins: More Than One Way to Make a Hairpin. *Nat. Rev. Microbiol.* **2006**, *4*, 67−76.

(467) Dupont, A.; Stirnnagel, K.; Lindemann, D.; Lamb, D. C. Tracking Image Correlation: Combining Single-Particle Tracking and Image Correlation. *Biophys. J.* **2013**, *104*, 2373−2382.

(468) Alenquer, M.; Vale-Costa, S.; Etibor, T. A.; Ferreira, F.; Sousa, A. L.; Amorim, M. J. Influenza A Virus Ribonucleoproteins Form Liquid Organelles at Endoplasmic Reticulum Exit Sites. *Nat. Commun.* **2019**, *10*, 1629.

(469) Jo, S.; Kawaguchi, A.; Takizawa, N.; Morikawa, Y.; Momose, F.; Nagata, K. Involvement of Vesicular Trafficking System in Membrane Targeting of the Progeny Influenza Virus Genome. *Microbes Infect.* **2010**, *12*, 1079−1084.

(470) Avilov, S. V.; Moisy, D.; Naffakh, N.; Cusack, S. Influenza A Virus Progeny vRNP Trafficking in Live Infected Cells Studied with the Virus-Encoded Fluorescently Tagged PB2 Protein. *Vaccine* **2012**, *30*, 7411−7417.

(471) Amorim, M. J.; Bruce, E. A.; Read, E. K. C.; Foeglein, A.; Mahen, R.; Stuart, A. D.; Digard, P. A Rab11-and Microtubule-Dependent Mechanism for Cytoplasmic Transport of Influenza A Virus Viral RNA. *J. Virol.* **2011**, *85*, 4143−4156.

(472) Hendrix, J.; Baumgartel, V.; Schrimpf, W.; Ivanchenko, S.; Digman, M. A.; Gratton, E.; Krausslich, H. G.; Muller, B.; Lamb, D. C. Live-Cell Observation of Cytosolic HIV-1 Assembly onset Reveals RNA-Interacting Gag Oligomers. *J. Cell Biol.* **2015**, *210*, 629−646.

(473) Jose, J.; Tang, J.; Taylor, A. B.; Baker, T. S.; Kuhn, R. J. Fluorescent Protein-Tagged Sindbis Virus E2 Glycoprotein Allows Single Particle Analysis of Virus Budding from Live Cells. *Viruses* **2015**, *7*, 6182−6199.

(474) Baumgartel, V.; Muller, B.; Lamb, D. C. Quantitative Live-Cell Imaging of Human Immunodeficiency Virus (HIV-1) Assembly. *Viruses* **2012**, *4*, 777−799.

(475) Perlman, M.; Resh, M. D. Identification of an Intracellular Trafficking and Assembly Pathway for HIV-1 Gag. *Traffic* **2006**, *7*, 731−745.

(476) Gunzenhauser, J.; Olivier, N.; Pengo, T.; Manley, S. Quantitative Super-Resolution Imaging Reveals Protein Stoichiometry and Nanoscale Morphology of Assembling HIV-Gag Virions. *Nano Lett.* **2012**, *12*, 4705−4710.

(477) Fogarty, K. H.; Chen, Y.; Grigsby, I. F.; Macdonald, P. J.; Smith, E. M.; Johnson, J. L.; Rawson, J. M.; Mansky, L. M.; Mueller, J. D. Characterization of Cytoplasmic Gag-Gag Interactions by Dual-Color z-Scan Fluorescence Fluctuation Spectroscopy. *Biophys. J.* **2011**, *100*, 1587−1595.

(478) Chen, Y.; Wu, B.; Musier-Forsyth, K.; Mansky, L. M.; Mueller, J. D. Fluorescence Fluctuation Spectroscopy on Viral-Like Particles Reveals Variable Gag Stoichiometry. *Biophys. J.* **2009**, *96*, 1961−1969.

(479) Sardo, L.; Hatch, S. C.; Chen, J.; Nikolaitchik, O.; Burdick, R. C.; Chen, D.; Westlake, C. J.; Lockett, S.; Pathak, V. K.; Hu, W. S. Dynamics of HIV-1 RNA Near the Plasma Membrane during Virus Assembly. *J. Virol.* **2015**, *89*, 10832−10840.

(480) Rahman, S. A.; Koch, P.; Weichsel, J.; Godinez, W. J.; Schwarz, U.; Rohr, K.; Lamb, D. C.; Krausslich, H. G.; Muller, B. Investigating the Role of F-Actin in Human Immunodeficiency Virus Assembly by Live-Cell Microscopy. *J. Virol.* **2014**, *88*, 7904−7914.

(481) Baumgartel, V.; Ivanchenko, S.; Dupont, A.; Sergeev, M.; Wiseman, P. W.; Krausslich, H. G.; Brauchle, C.; Muller, B.; Lamb, D. C. Live-Cell Visualization of Dynamics of HIV Budding Site Interactions with an ESCRT Component. *Nat. Cell Biol.* **2011**, *13*, 469−474.

(482) Dimitrov, D. S.; Willey, R. L.; Sato, H.; Chang, L. J.; Blumenthal, R.; Martin, M. A. Quantitation of Human Immunodeficiency Virus Type 1 Infection Kinetics. *J. Virol.* **1993**, *67*, 2182−2190.

(483) Johnson, D. C.; Huber, M. T. Directed Egress of Animal Viruses Promotes Cell-to-Cell Spread. *J. Virol.* **2002**, *76*, 1−8.

(484) Sattentau, Q. Avoiding the Void: Cell-to-Cell Spread of Human Viruses. *Nat. Rev. Microbiol.* **2008**, *6*, 815−826.

(485) Sherer, N. M.; Lehmann, M. J.; Jimenez-Soto, L. F.; Horensavitz, C.; Pypaert, M.; Mothes, W. Retroviruses Can Establish Filopodial Bridges for Efficient Cell-to-Cell Transmission. *Nat. Cell Biol.* **2007**, *9*, 310−315.

(486) Mothes, W.; Sherer, N. M.; Jin, J.; Zhong, P. Virus Cell-to-Cell Transmission. *J. Virol.* **2010**, *84*, 8360−8368.

(487) Eugenin, E. A.; Gaskill, P. J.; Berman, J. W. Tunneling Nanotubes (TNT) Are Induced by HIV-Infection of Macrophages: A Potential Mechanism for Intercellular HIV Trafficking. *Cell. Immunol.* **2009**, *254*, 142−148.

(488) Gousset, K.; Schiff, E.; Langevin, C.; Marijanovic, Z.; Caputo, A.; Browman, D. T.; Chenouard, N.; de Chaumont, F.; Martino, A.; Enninga, J.; et al. Prions Hijack Tunnelling Nanotubes for Intercellular Spread. *Nat. Cell Biol.* **2009**, *11*, 328−336.

(489) Sowinski, S.; Jolly, C.; Berninghausen, O.; Purbhoo, M. A.; Chauveau, A.; Köhler, K.; Oddos, S.; Eissmann, P.; Brodsky, F. M.; Hopkins, C. Membrane Nanotubes Physically Connect T Cells over Long Distances Presenting a Novel Route for HIV-1 Transmission. *Nat. Cell Biol.* **2008**, *10*, 211−219.

(490) Kumar, A.; Kim, J. H.; Ranjan, P.; Metcalfe, M. G.; Cao, W.; Mishina, M.; Gangappa, S.; Guo, Z.; Boyden, E. S.; Zaki, S.; et al. Influenza Virus Exploits Tunneling Nanotubes for Cell-to-Cell Spread. *Sci. Rep.* **2017**, *7*, 40360.

(491) Nzounza, P.; Chazal, M.; Guedj, C.; Schmitt, A.; Masse, J. M.; Randriamampita, C.; Pique, C.; Ramirez, B. C. The Scaffolding Protein Dlg1 Is a Negative Regulator of Cell-Free Virus Infectivity but Not of Cell-to-Cell HIV-1 Transmission in T Cells. *PLoS One* **2012**, *7*, No. e30130.

(492) Igakura, T.; Stinchcombe, J. C.; Goon, P. K.; Taylor, G. P.; Weber, J. N.; Griffiths, G. M.; Tanaka, Y.; Osame, M.; Bangham, C. R.

Spread of HTLV-I between Lymphocytes by Virus-Induced Polarization of the Cytoskeleton. *Science* **2003**, *299*, 1713−1716.

(493) Barnard, A. L.; Igakura, T.; Tanaka, Y.; Taylor, G. P.; Bangham, C. R. Engagement of Specific T-Cell Surface Molecules Regulates Cytoskeletal Polarization in HTLV-1−Infected Lymphocytes. *Blood* **2005**, *106*, 988−995.

(494) Johnson, D. C.; Webb, M.; Wisner, T. W.; Brunetti, C. Herpes Simplex Virus gE/gI Sorts Nascent Virions to Epithelial Cell Junctions, Promoting Virus Spread. *J. Virol.* **2001**, *75*, 821−833.

(495) Rustom, A.; Saffrich, R.; Markovic, I.; Walther, P.; Gerdes, H. H. Nanotubular Highways for Intercellular Organelle Transport. *Science* **2004**, *303*, 1007−1010.

(496) Davis, D. M.; Sowinski, S. Membrane Nanotubes: Dynamic Long-Distance Connections between Animal Cells. *Nat. Rev. Mol. Cell Biol.* **2008**, *9*, 431−436.

(497) Efros, A. L.; Nesbitt, D. J. Origin and Control of Blinking in Quantum Dots. *Nat. Nanotechnol.* **2016**, *11*, 661−671.

(498) Marchuk, K.; Guo, Y.; Sun, W.; Vela, J.; Fang, N. High-Precision Tracking with Non-Blinking Quantum Dots Resolves Nanoscale Vertical Displacement. *J. Am. Chem. Soc.* **2012**, *134*, 6108−6111.

(499) Keller, A. M.; Ghosh, Y.; DeVore, M. S.; Phipps, M. E.; Stewart, M. H.; Wilson, B. S.; Lidke, D. S.; Hollingsworth, J. A.; Werner, J. H. 3-Dimensional Tracking of Non-blinking 'Giant' Quantum Dots in Live Cells. *Adv. Funct. Mater.* **2014**, *24*, 4796−4803.

(500) Patterson, G.; Davidson, M.; Manley, S.; Lippincott-Schwartz, J. Superresolution Imaging Using Single-Molecule Localization. *Annu. Rev. Phys. Chem.* **2010**, *61*, 345−367.

(501) Lee, A.; Tsekouras, K.; Calderon, C.; Bustamante, C.; Presse, S. Unraveling the Thousand Word Picture: An Introduction to Super-Resolution Data Analysis. *Chem. Rev.* **2017**, *117*, 7276−7330.

(502) Huang, B.; Bates, M.; Zhuang, X. Super-Resolution Fluorescence Microscopy. *Annu. Rev. Biochem.* **2009**, *78*, 993−1016.

(503) Pan, W.; Dong, Z.; Li, F.; Meng, W.; Feng, L.; Niu, X.; Li, C.; Luo, Q.; Li, Z.; Sun, C.; et al. Visualizing Influenza Virus Infection in Living Mice. *Nat. Commun.* **2013**, *4*, 2369.

(504) Pan, H.; Zhang, P.; Gao, D.; Zhang, Y.; Li, P.; Liu, L.; Wang, C.; Wang, H.; Ma, Y.; Cai, L. Noninvasive Visualization of Respiratory Viral Infection Using Bioorthogonal Conjugated Near-Infrared-Emitting Quantum Dots. *ACS Nano* **2014**, *8*, 5468−5477.

(505) Zong, W.; Wu, R.; Li, M.; Hu, Y.; Li, Y.; Li, J.; Rong, H.; Wu, H.; Xu, Y.; Lu, Y.; et al. Fast High-Resolution Miniature Two-Photon Microscopy for Brain Imaging in Freely Behaving Mice. *Nat. Methods* **2017**, *14*, 713−719.

(506) Wang, K.; Sun, W.; Richie, C. T.; Harvey, B. K.; Betzig, E.; Ji, N. Direct Wavefront Sensing for High-Resolution in Vivo Imaging in Scattering Tissue. *Nat. Commun.* **2015**, *6*, 7276.

(507) Hong, G.; Antaris, A. L.; Dai, H. Near-Infrared Fluorophores for Biomedical Imaging. *Nat. Biomed. Eng.* **2017**, *1*, No. 0010.

(508) Ding, F.; Zhan, Y. B.; Lu, X. J.; Sun, Y. Recent Advances in Near-Infrared II Fluorophores for Multifunctional Biomedical Imaging. *Chem. Sci.* **2018**, *9*, 4370−4380.

(509) Smith, A. M.; Mancini, M. C.; Nie, S. Bioimaging: Second Window for in Vivo Imaging. *Nat. Nanotechnol.* **2009**, *4*, 710.

(510) Zhang, J. J.; Lin, Y.; Zhou, H.; He, H.; Ma, J. J.; Luo, M. Y.; Zhang, Z. L.; Pang, D. W. Cell Membrane-Camouflaged NIR II Fluorescent Ag_2Te Quantum Dots-Based Nanobioprobes for Enhanced in Vivo Homotypic Tumor Imaging. *Adv. Healthcare Mater.* **2019**, *8*, No. e1900341.

(511) Hong, G.; Robinson, J. T.; Zhang, Y.; Diao, S.; Antaris, A. L.; Wang, Q.; Dai, H. In Vivo Fluorescence Imaging with Ag_2S Quantum Dots in the Second Near-Infrared Region. *Angew. Chem., Int. Ed.* **2012**, *51*, 9818−9821.

(512) Jiang, P.; Zhu, C. N.; Zhang, Z. L.; Tian, Z. Q.; Pang, D. W. Water-Soluble Ag_2S Quantum Dots for Near-Infrared Fluorescence Imaging in Vivo. *Biomaterials* **2012**, *33*, 5130−5135.